Load Shedding and Voltage Management Strategies for Enhancing Resilience in Remote DC Microgrids

PhD Thesis

Abdulrahman Babagana

A thesis submitted for the degree of Doctor of Philosophy to

Department of Electronics and Electrical Engineering

University of Strathclyde, Glasgow

August 14, 2025

This thesis is the result of the author's original research. It has been composed by the author and has not been previously submitted for examination, which has led to the award of a degree.

Acknowledgement

I am grateful to Allah (SWT) for the gift of life, and I want to thank my family, friends, and colleagues for their prayers and moral support during my PhD research journey.

I am deeply thankful to my Ph.D. supervisor, Prof Graeme Burt, for his academic guidance, moral support, and psychological assistance in navigating the hurdles and challenges of doctoral degree studies. I also want to thank Dr Mazheruddin Syed for his guidance, support, and motivation, especially during the early and critical stage of my studies, particularly during the COVID era. I will always appreciate his help in making me a better and more effective researcher.

I extend my gratitude to Dr Yljon Seferi, who, despite his busy schedule, always gave me a listening ear and guided me throughout my PhD journey. I also want to mention the members of the Dynamic Power System Laboratory team: Isa Jimoh, Zhiwang Feng, Taimur Zaman, Maria Robowska, Mayesha Azim, and Richard Munro. Their contributions made this PhD research possible.

I owe much to the Petroleum Technology Development Fund (PTDF), Nigeria, and the Federal Republic of Nigeria for funding this research.

Finally, I thank my wife, Aisha Mohammed Jere, and our children for their constant support and encouragement. I am also thankful to my Family, Friends, Colleagues, and Well-wishers.

Abstract

Reliable and efficient power systems are crucial in areas with limited access to electricity, such as sub-Saharan Africa. Over 50% of rural areas in this region remain disconnected from the national grid due to high transmission and distribution costs. Direct Current (DC) microgrids have emerged as a promising solution, offering advantages such as lower investment costs, improved flexibility, and direct integration of renewable energy sources such as solar power, which is abundant in Africa. The successful operation of DC microgrids requires robust control to regulate DC bus voltages, efficient power sharing between the distributed energy resources (DERs), and a dynamic response to disturbances. However, when the power demand of the loads exceeds the power generation from the DERs in the DC microgrid, voltage control alone cannot maintain the power balance. In such cases, it is necessary to shed some of the noncritical loads to prevent power shortages and enhance the system's resilience against disruptions.

This thesis addresses key challenges in voltage regulation and load management in DC microgrids through the development of enhanced DC bus voltage control and load-shedding strategies aimed at improving voltage stability and overall system resilience. First, it introduces a disturbance identification technique based on the rate of change of voltage (dv/dt), enabling rapid detection, localisation, and quantification of disturbances. This fast and accurate response is crucial in minimising system disruption and facilitating timely corrective actions.

Second, an adaptive DC bus signalling (DBS) control strategy is proposed,

which dynamically adjusts voltage thresholds according to load demand and generation levels. This approach improves system stability by preventing excessive voltage fluctuations and improving responsiveness during disturbances. Furthermore, when the system experiences a power deficit, the control scheme activates a load-shedding mechanism to maintain operational balance.

Third, to Further strengthen system resilience, a novel load-shedding scheme is developed by integrating timer-based control with a mixed-integer linear programming (MILP) algorithm. This approach optimises the load shedding of non-critical loads during severe disturbances, effectively restoring power balance, reducing voltage sags, and minimising reliance on costly communication-based infrastructure.

Simulation results demonstrate that the enhanced DBS control strategy effectively maintains power balance, limits DC bus voltage deviations to within +/-10% based on IEC standard, prevents voltage collapse, and enables smooth transitions between operational states without inducing power oscillations among DERs. Furthermore, the proposed MILP timer-based load-shedding scheme demonstrates superior performance over conventional and adaptive methods by delivering faster and more accurate load-shedding actions. This leads to better protection of critical loads and strengthens the overall integrity and resilience of the DC microgrids.

The findings of this research make a significant contribution to improving the reliability, efficiency and resilience of DC microgrids. These positions DC microgrids as a viable energy solution: particularly well suited for remote areas, improved energy storage coordination, and the integration of renewable energy systems for electrification efforts in sub-Saharan Africa and other disaster-prone or underserved regions around the world.

Contents

List of Figures

List of Figures

List of Tables

Nomenclature

AC	Alternating Current
ANN	Artificial Neural Network
BESS	Battery Energy Storage System
CB	Circuit Breaker
CCL	Constant Current Load
CPL	Constant Power Load
CRL	Constant Resistant Load
DARE	Discrete-time Algebraic Riccati Equation
DBS	DC Bus Signaling
DCCB	Direct Current Circuit Breaker
DC	Direct Current
DER	Distributed Energy Resources
EMS	Energy Management System
ESS	Energy Storage System
EV	Electric Vehicle

Nomenclature

FL	Fuzzy Logic
GA	Genetic Algorithms
GTC	Grid Tied Converter
IEEE	Institute of Electrical Electronics Engineering
IET	Institute of Engineering and Technology
LP	Linear programming
LVDC	Low Voltage Direct Current
LV	Low Voltage
MADC	Mode Adaptive Direct Current
MILP	Mixed Integer Linear Programming
MPPT	Maximum Power Point Tracker
NN	Neural Network
PD	Proportional-Derivative
PMSG	Permanent Magnet Synchronous Generator
PSO	Particle Swarm Optimisation
PV	Photovoltaic
RES	Renewable Energy System
ROCOF	Rate of Change of Frequency
ROCOV	Rate of Change of Voltage
SOC	State of Charge

VSC	Voltage Source Converter
WT	Wind Turbine

Chapter 1

Introduction

1.1 Research Context

Microgrid is an emerging technology that helps integrate distributed energy resources like wind, solar, small hydropower plants, tidal energy, and fuel cell technology. These resources are abundant and eco-friendly, emission-free, making them ideal for sustainable electricity generation in distribution networks [5]. Microgrids enhance energy efficiency by reducing losses and so improve the overall quality and reliability of power delivery to consumers [6], [7]. In regions like Sub-Saharan Africa, where nearly 1 billion people lack access to electricity, adopting innovative solutions, such as DC microgrids, is crucial for providing reliable energy access [8]. The urgent need for energy solutions drives the increasing focus on DC microgrids in this region, their seamless integration with renewable energy sources, and the flexibility of decentralised systems, which collectively address challenges such as energy poverty, transmission costs, reactive power management, and infrastructure limitations in rural areas [9].

A significant shift toward DC microgrids has emerged, driven by their compatibility with modern electrical loads that predominantly operate on DC power, such as electric vehicles (EVs), consumer electronics, LED lighting systems, lap-

tops, and mobile phones [10], [11]. Compared to traditional alternating current (AC) power systems, DC microgrids offer several key advantages. These include reduced power conversion losses by eliminating unnecessary AC/DC conversion stages, lower cable losses due to the absence of the skin effect, and improved reliability and resilience against disturbances originating from the utility grid. Unlike AC systems, DC microgrids do not require complex frequency, phase, or reactive power control mechanisms, leading to lower capital investment and reduced operational costs [12], [13], [14], [15]. This makes the DC microgrid a popular solution for many applications, including data centres, telecommunication stations, shipboard systems, EV charging stations, smart homes, commercial buildings, and renewable energy parks [10].

Robust control strategies are essential for the reliable operation of DC microgrids, as they ensure stable DC bus voltages, facilitate coordinated power sharing among distributed energy resources (DERs), and maintain energy balance within storage systems. These strategies must also demonstrate strong resilience in response to system disturbances [16], [17], [18]. To address power imbalances between generation and demand, various methods have been proposed, including the integration of energy storage systems, backup generators, and interconnection with the utility grid [19], [20]. However, in islanded DC microgrids where external grid support is unavailable, the available DERs may not always meet the system's load demand, particularly during peak load conditions or sudden disturbances. Under such circumstances, conventional control mechanisms such as droop control and bus signalling may become inadequate to maintain power balance and system stability.

In these situations, load-shedding becomes a necessary and effective strategy to preserve the operational integrity of the microgrid [21], [22], [23], [24].A well-designed load-shedding scheme is crucial for maintaining system stability by rapidly disconnecting non-critical loads, protecting critical loads from severe

voltage deviations, and ensuring the continuous and reliable supply of power [21], [22], [23], [24], [15].

In this context, the focus of this thesis is to develop an adaptive control strategy combined with an optimised load-shedding scheme aimed at enhancing the reliability, resilience, and operational efficiency of DC microgrids. The proposed approach seeks to address the limitations of existing load-shedding methods and provide a practical, communication-independent solution for maintaining system stability under dynamic and fault-prone operating conditions commonly encountered in remote or resource-constrained environments.

1.2 Research Motivation

The persistent energy deficit in sub-Saharan Africa, where nearly 50% of the population lacks reliable access to electricity, underscores the urgent need for innovative, decentralized energy solutions. Extending conventional power grids to rural and remote areas remains economically and logistically challenging due to high infrastructure costs, difficult terrain, and the complexity of managing reactive power in traditional AC systems [9]. In response to these limitations, DC microgrids have emerged as a viable and sustainable alternative, offering a flexible and cost-effective approach to rural electrification.

DC microgrids are particularly well-suited to off-grid applications, as they enable efficient integration of renewable energy sources such as solar and wind. Their inherent advantages, such as reduced transmission losses, simplified control, and compatibility with modern DC-based loads, make them an attractive option for addressing energy poverty in underserved regions [10]. However, despite these benefits, the reliable operation of DC microgrids remains a technical challenge, especially under varying load conditions and power disturbances. Ensuring stability, resilience, and uninterrupted power supply requires the implementation of

robust control and load-shedding strategies.

Current communication-based control and load-shedding methods, although effective, are costly and prone to failure in environments where communication infrastructure is limited or unreliable [25]. These limitations can compromise the reliability and scalability of DC microgrids. On the other hand, existing non-communication-based strategies are often hindered by issues such as voltage instability, poor power-sharing among distributed energy resources (DERs), and inadequate disturbance response. Additionally, many non-communication-based load-shedding schemes suffer from trade-offs between voltage regulation and power supply reliability [26].

Motivated by these challenges, this PhD research aims to develop advanced, non-communication-based control and load-shedding strategies that enhance the reliability and operational efficiency of DC microgrids, particularly in remote and energy-scarce regions. The flowchart illustrating the process of disturbance identification, voltage control, and load shedding strategies where demand exceeds the microgrid's generation capacity is presented in Fig. 1.1.

The proposed strategies are designed to operate autonomously, minimising dependence on communication networks and centralised controllers. The key objectives of this research are to:

- **Maintain Power Balance:** Ensure system equilibrium under various disturbance scenarios.
- **Optimise Power Sharing:** Enable effective and fair distribution of power among DERs.
- **Regulate DC Bus Voltage:** Prevent excessive voltage deviations during both transient and steady-state conditions.
- **Enhance Power Supply Reliability:** Improve the overall dependability of power delivery by initiating load-shedding only when necessary and

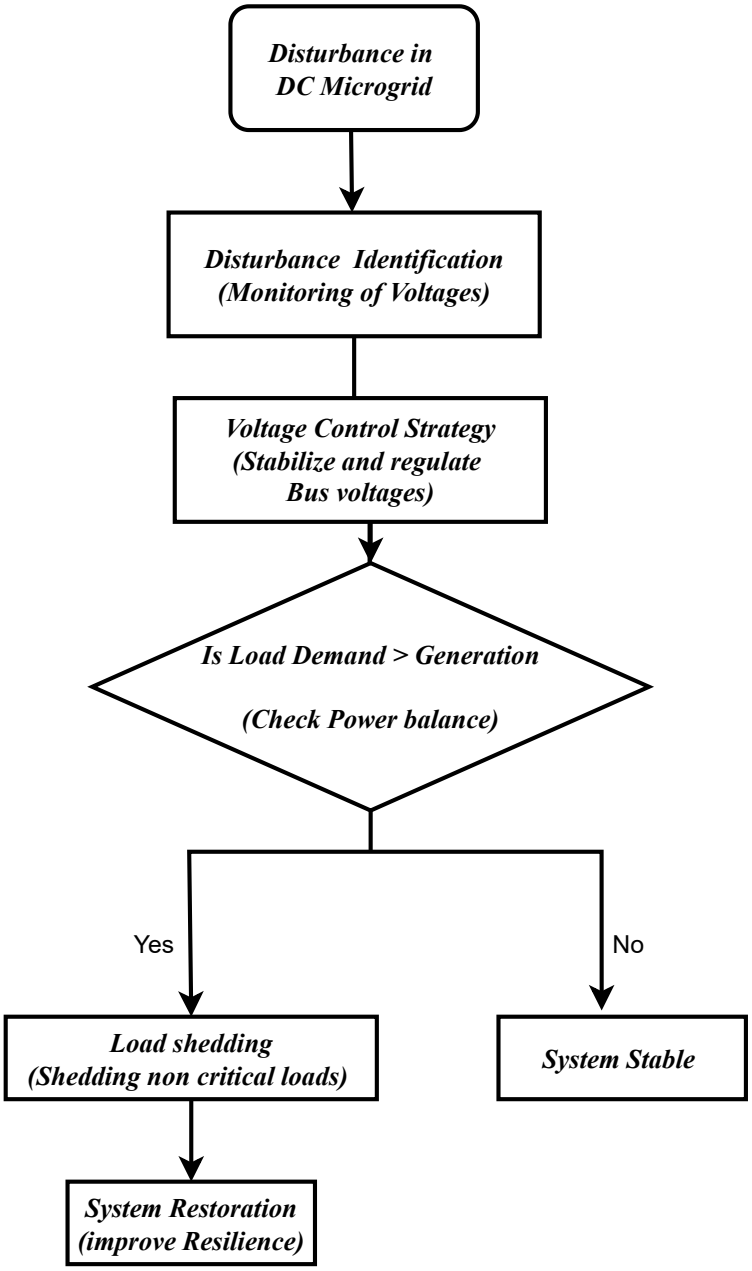

Figure 1.1: Thesis Flowchart

minimising unnecessary disconnections.

Ultimately, this research seeks to contribute toward the development of resilient, scalable, and economically viable DC microgrid solutions that can meet the critical energy needs of underserved communities, especially across sub-Saharan Africa. By addressing the limitations of existing methods, the work aims to pave the way for more reliable and efficient electrification strategies in remote and off-grid areas.

1.3 Contribution to Knowledge

This thesis provides the following main contributions to knowledge:

- Development of a Timer-Based and Mixed-Integer Linear Programming (MILP) Load Shedding Scheme for DC Microgrids that optimises load shedding and enhances system resilience. The proposed technique minimises voltage transients, reduces regulation time during disturbances, and improves system reliability compared to existing schemes.

- Application of a disturbance identification technique in a non-communication-based DC microgrid using voltage differential (dv/dt) to detect and manage disturbances. By applying defined threshold values, it accurately identifies disturbances, pinpoints affected areas and assesses their magnitude. This enables targeted control responses, supporting effective mitigation and enhancing the reliability of DC microgrids under dynamic operating conditions.

- Development and implementation of an improved DC bus signalling control strategy that utilizes a defined voltage threshold to enhance control and reliability in non-communication DC microgrids. The strategy helps to

mitigate the adverse effects of bus voltage deviations during events such as load fluctuations or power disturbances. By continuously monitoring bus voltages and applying corrective actions based on predefined thresholds, the system ensures stable operation and improves reliability.

In addition, the work provides an investigation and comparison of the existing non-communication-based DC load-shedding schemes to highlight their performance under various disturbances and limitations. This analysis shows the need for more advanced load-shedding strategies to enhance system resilience and reliability in DC microgrids.

1.4 Thesis Overview

Chapter 2: This chapter offers an introduction to microgrid concepts, components, and advantages. It explores microgrid architecture, encompassing control systems, energy storage, and the incorporation of renewable energy sources. It also addresses the primary challenges of microgrids and outlines protection strategies to guarantee their safe and dependable operation. This fundamental information lays the groundwork for more in-depth discussions in the following chapters.

Chapter 3: This chapter builds upon the foundational concepts of microgrids by examining key control strategies and load-shedding schemes tailored to DC microgrids. It comprehensively reviews existing approaches, highlighting their limitations and underscoring the need for improved solutions. The insights gained from this review serve as the basis for developing advanced control strategies and evaluating load-shedding techniques in subsequent chapters.

The chapter further focuses on modelling the IEEE 37-bus DC microgrid test system. Detailed models are developed for essential LVDC components, including wind turbines, photovoltaic systems, battery energy storage systems, grid-tied

converters, load models, and DC cables. The objective is to create a simulation environment that accurately reflects real-world operational behaviour and performance, thereby enabling precise analysis and supporting practical implementation as well as future research in the field.

Chapter 4: This chapter presents a performance evaluation and comparative analysis of existing non-communication-based load-shedding schemes in DC microgrids, as introduced in Chapter 3. These schemes are classified into two main categories: conventional approaches (voltage-based, timer-based, and combined methods) and adaptive approaches (adaptive voltage-based and adaptive timer-based methods). The analysis highlights the respective strengths and shortcomings of each scheme, ultimately demonstrating the need for more advanced and efficient load-shedding strategies. This identified gap forms the foundation for the development of improved approaches aimed at enhancing system resilience, which is the central focus of this thesis.

Chapter 5: This chapter presents the design and implementation of a novel disturbance detection technique and an advanced control strategy for a DC microgrid. The proposed detection method utilises the rate of change of voltage (dv/dt) to rapidly identify, localise, and quantify disturbances across the microgrid, enabling timely control actions. The chapter also introduces an enhanced DC Bus Signalling (DBS) control strategy that utilises predefined voltage thresholds to maintain system bus voltage levels. By eliminating the need for costly, high-bandwidth communication infrastructure, this approach enhances voltage stability while reducing overall operational expenses.

Chapter 6: This chapter presents a novel MILP timer-based load-shedding scheme designed for DC microgrids. The proposed strategy integrates a short delay mechanism with a Mixed-Integer Linear Programming (MILP) algorithm to optimise the shedding of non-critical loads while maintaining power balance within the microgrid. Load shedding is initiated when bus voltages fall below a

specified threshold for a predefined duration. The scheme is evaluated through simulation and compared against the performance of an adaptive timer-based approach based on the response time, voltage stabilisation and load-shedding efficiency. Results demonstrate that the proposed method effectively maintains DC bus voltages within acceptable limits, thereby safeguarding critical loads from exposure to excessively low voltage conditions and enhancing overall system reliability.

Chapter 7: This chapter concludes the thesis by summarising the key findings and contributions of the research, particularly in developing advanced control and load-shedding strategies for DC microgrids. It also outlines recommendations for future research, with an emphasis on further improving the resilience, operational efficiency, and scalability of DC microgrids in practical and evolving energy environments.

1.5 List of Publications

The following publications have resulted from the work reported in this thesis:

List of Journal Papers

- A. Babagana, I. A. Jimoh, Y. Seferi and G. Burt, "A Timer and Mixed Integer Linear Programming Load Shedding Scheme for Resilient DC Microgrids," in IEEE Access, vol. 13, pp. 6632-6642, 2025, doi: 10.1109/ACCESS.2025.3525975.

- A. Babagana, Y. Seferi and G.Burt, "Adaptive DC Bus Signalling Control for Voltage Regulation and Load Management in Disturbance-Prone Microgrids". (In Preparation)

Conference Proceedings

- A. Babagana, T. Zaman, Y. Seferi, M. Syed and G. Burt, "Comparison of Non-Communication based DC Load Shedding Schemes," 2022 57th International Universities Power Engineering Conference (UPEC), Istanbul, Turkey, 2022, pp. 1-6, doi: 10.1109/UPEC55022.2022.9917898.

- A. Babagana, Y. Seferi, R. Pena-Alzola and G.Burt, "Adaptive Voltage Derivative Algorithm for Fast Disturbance Detection and Localisation in DC Microgrids," 2025 10th IEEE Workshop on Electronic Grid (eGrid 2025), Glasgow, Submitted.

Chapter 2

Fundamentals of Microgrids: Understanding the Architecture and Components

This chapter provides a general overview of the key concepts, components, and advantages of microgrids. It explores microgrid architecture, control systems, energy storage solutions, and renewable energy sources. By presenting these foundational elements, the chapter serves as an essential guide for understanding the core principles necessary for modelling and simulating microgrid systems effectively.

2.1 Introduction

Microgrids represent a key innovation in modern electricity distribution systems. They integrate various distributed energy resources (DERs) such as storage devices, controllable loads, and distributed generators. The Microgrid Exchange Group (MEG) of the U.S. Department of Energy (DOE) defines a microgrid as "a group of interconnected loads and distributed energy resources within clearly

defined electrical boundaries that act as a single controllable entity for the grid. A microgrid can connect and disconnect from the grid to enable grid-connected and island modes of operation" [27]. They are designed to function in grid-connected or islanded (autonomous operation) modes.

Microgrids typically operate at low to medium voltage levels, ranging from 400 V to 69 kV [28], and vary in size. Some microgrids are relatively small, serving only a few customers and generating hundreds of kilowatts. Others are larger, more complex systems capable of producing tens of megawatts. This flexibility allows microgrids to meet diverse energy needs, making them crucial to improving energy distribution and grid resilience in modern networks [29].

2.1.1 Applications and Benefits of Microgrid

Microgrids have broad applications across various sectors, offering solutions to energy challenges in remote and off-grid communities, industrial complexes, military bases, and emergency response centres. Their versatility and resilience make them a reliable power source in areas with limited access to centralized grids, helping to power homes, schools, healthcare facilities, and other essential services. Microgrids enhance energy efficiency in industrial settings, reducing operational costs through optimized energy usage. Maintaining uninterrupted power during grid failures is critical for military bases and emergency centres, making microgrids a preferred solution for ensuring operational continuity in crises [29].

Key Benefits of Microgrids

The advantages of the microgrid can be categorized as follows;

- Enhanced Power Generation Capacity: Microgrids enable localized generation at the customer end level, improving energy efficiency and security by reducing dependence on centralized power systems. Sub-Saharan Africa

serves as a compelling example where the centralized grid is unable to extend its reach to rural areas, underscoring the vital role of microgrids in delivering power to these underserved regions.

- Lower Carbon Emissions and Fuel Costs: Microgrids encourage the use of renewable energy sources such as solar and wind, which significantly reduce CO2 emissions and lower fuel costs compared to conventional fossil-fueled sources.

- Improved Reliability and Flexibility: Microgrids increase consumer reliability by providing a backup power source and can flexibly switch between grid-connected and islanded operation modes to ensure a continuous supply during outages.

- Reduced Load Congestion: By offloading demand from the traditional power grid, microgrids alleviate load congestion and reduce stress on existing transmission and distribution infrastructure.

- Ancillary Services: Microgrids can provide supplementary services such as demand response, voltage support, and frequency regulation, enhancing the stability and performance of the larger power system [30].

2.2 Components of Microgrid

A microgrid has multiple components that work together to form a reliable and environmentally friendly energy system. These components include distributed energy resources (DERs) such as distributed generators (DGs) and distributed storage (DS) systems, as well as various end-users like residential, commercial, and industrial loads [31]. A simple depiction of a microgrid with its components is shown in 2.1.

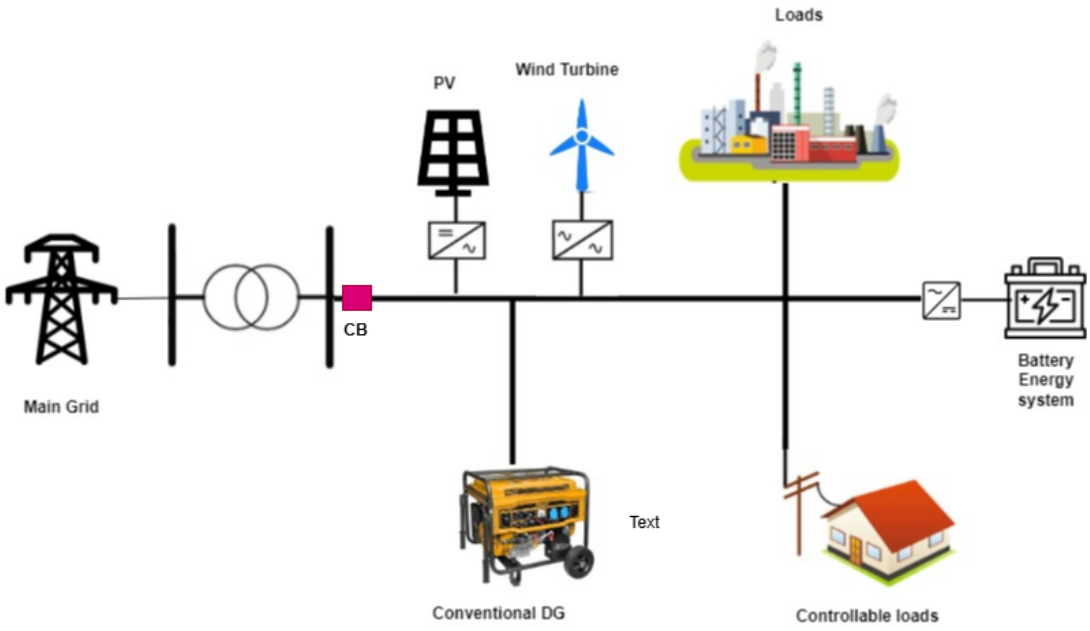

Figure 2.1: Components of a Microgrid

2.2.1 Distributed Generators

Distributed generators (DGs) are small-scale power generation units that can operate independently or in conjunction with larger grid networks. In DC microgrids, DGs play a critical role in supplying power, often relying on two main categories of technologies: renewable and non-renewable. Renewable DGs include solar thermal, photovoltaic (PV), wind, biomass, biogas, and hydroelectric power. In contrast, non-renewable DGs primarily use conventional methods such as diesel engines, steam turbines, gas engines, and induction and synchronous generators [32]. Renewable energy sources have gained considerable traction globally, especially in distributed generation. Wind energy has experienced rapid expansion, growing by approximately 12% per year, while solar energy usage has grown around 4% annually. Solar power has become particularly significant in regions like Sub-Saharan Africa, where access to centralized energy grids is limited. Solar DGs have increasingly powered microgrids, helping reduce reliance on fossil fuels

and improving energy access for remote or off-grid communities [33]. For example, in Africa, solar PV capacity is rising rapidly, making it one of the primary resources in microgrid installations. On a global scale, renewable distributed generation sources now contribute to around 29% of total power generation, with wind energy accounting for 12% and solar for 7%, as shown in Figure 2.2. These percentages are expected to continue growing as technological advancements, policy incentives, and the need for sustainable energy solutions drive further adoption. Additionally, microgrids that connect renewable energy DGs to utility grids help stabilize the grid by eliminating the need for complex frequency regulation. This increases energy security, reduces fuel import dependence, and lowers carbon footprints [1].

Integrating DGs in both AC and DC microgrids introduces a range of challenges; however, the nature and severity of these challenges often differ between the two. In DC microgrids, key issues include maintaining voltage stability without the benefit of system inertia, managing bidirectional power flows from converters and storage units, and ensuring efficient coordination of energy storage, which plays a more central role in balancing supply and demand [34]. Additionally, DC systems lack mature and standardised protection schemes, as the absence of natural current zero-crossings makes fault detection and isolation more complex than in AC systems. The inherently low inertia in DC microgrids also increases their vulnerability to fast transients and disturbances, necessitating rapid and accurate control strategies [34]. In contrast, AC microgrids face their challenges, such as frequency regulation, reactive power management, and synchronisation among sources, issues that are less relevant in DC systems. Furthermore, in both types of microgrids, the integration of intermittent renewable energy sources introduces significant uncertainties in power generation, complicating load forecasting, power modelling, and real-time control [32]. Thus, while AC and DC microgrids share some overarching goals, the technical requirements and control

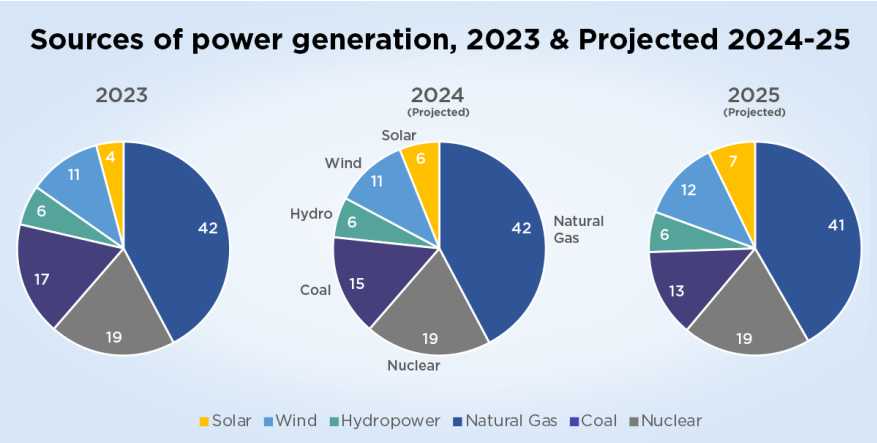

Figure 2.2: World's sources of power generation 2023 and Projected 2024-25 [1]

priorities diverge, particularly in how they handle stability, protection, and energy flow, making tailored solutions essential for each architecture.

2.2.2 Distributed Storage

Energy storage is essential in DC microgrids for integrating renewable energy sources and ensuring grid reliability. Distributed energy storage systems (ESS) balance power generation and demand, contributing to grid stability. They play a crucial role in managing power fluctuations and peak loads and ensuring a consistent energy supply during mode shifts [35], [36].

Types of Energy Storage in DC Microgrids

Distributed energy storage technologies are diverse, offering flexibility and adaptability to meet the specific requirements of microgrids. These technologies are broadly classified into three categories:

- Electrochemical Storage: This category includes batteries (such as lithium-ion, lead-acid, and flow batteries) and flow cells. Batteries are the most widely used storage technology in microgrids due to their scalability, ease

of deployment, and fast response times. Lithium-ion batteries are prevalent, making up approximately 90% of the global microgrid battery storage market [34].

- Kinetic Energy Storage: Flywheel energy storage systems store energy through rotational kinetic energy. Flywheels are valuable for their rapid charge and discharge capabilities, making them suitable for applications requiring short-term energy storage and frequency regulation. While flywheels represent a small portion of the global storage market (less than 1%), their quick response potential in DC microgrids makes them a promising technology.

- Potential Energy Storage: This category includes technologies like pumped hydroelectric and compressed air energy storage (CAES). Pumped hydro storage accounts for approximately 94% of the world's energy storage capacity, though its use in microgrids is limited due to its dependence on geographic features [34].

In microgrid applications, electrochemical storage (mainly batteries) and kinetic storage technologies (like flywheels) are most common due to their versatility and ability to handle the dynamic energy needs of distributed systems [36].

Energy storage technologies have grown rapidly to meet the increasing demand for reliable and flexible energy systems. Lithium-ion batteries dominate the global distributed storage market, accounting for around 7% of total capacity by 2022, with widespread use in microgrids [37]. Flywheels and supercapacitors, though less common, are gaining attention for their fast response times, ideal for short-term stabilization. While pumped hydro storage leads globally, it is rarely used in DC microgrids due to size and geographic constraints [38]. Advances in battery technology are driving growth, particularly in renewable-powered microgrids. Though not yet cost-effective at scale, flywheels are emerging as solutions

for rapid energy balancing. Continued innovations in storage will further enhance the reliability and sustainability of microgrids [36], [39].

2.2.3 Microgrid Loads

In a microgrid, loads can be categorised into critical and non-critical, each serving a distinct role in maintaining the system's functionality and reliability.

Critical loads are essential for continuously operating vital infrastructure and must receive an uninterrupted power supply, even during grid disturbances or faults. These loads are often found in hospitals, emergency shelters, schools, and critical infrastructure like telecommunications systems. Power interruptions to these loads could have severe consequences, so they are typically supported by reliable distributed energy sources (DERs) or storage solutions, ensuring seamless operation in grid-tied or islanded modes [40].

On the other hand, non-critical loads can be temporarily disconnected without significantly affecting the essential services. These may include non-essential lighting, air conditioning, or various appliances in commercial or residential buildings. Non-critical loads play a significant role in optimising grid operation by being flexible to disconnection, especially during peak demand or when energy resources are limited. Such loads can be shed during emergencies or periods of instability to prioritise power for critical systems [41].

Microgrids often implement demand response strategies to manage both critical and non-critical loads effectively, adjusting the consumption patterns of non-essential loads to match system conditions. These strategies help shift or reduce power demand during peak periods or align load consumption with the intermittent availability of renewable energy sources such as solar or wind. The non-critical, controllable portion of these loads is managed through energy management systems to smooth out demand curves, while the non-controllable portion is typically the first to be shed during power imbalances [42].

However, critical loads, which must remain uninterrupted, significantly influence the design and execution of load shedding strategies. To maintain uninterrupted operation, especially in remote or isolated DC microgrids, battery energy storage systems must be considered in these decisions. Specifically, the state of charge (SoC) of the batteries must be carefully monitored and managed to ensure that it can support critical loads for up to 24 hours of continuous operation if needed. This introduces a further layer of complexity, requiring load shedding mechanisms to dynamically adapt based not only on load priority but also on real-time SoC constraints. By effectively coordinating load shedding, demand response, and storage management, microgrids can optimise energy use, enhance efficiency, and ensure system resilience, even under high renewable penetration and fluctuating generation conditions.

2.3 Microgrid Types

Microgrids can be classified into several types based on various factors such as operation modes, distribution systems, geography and ownership models. Each type is tailored to specific energy needs and operational environments.

2.3.1 Based on Operation Modes

A microgrid has two modes of operation, namely, grid-connected and island (stand-alone) modes as shown in 2.3 [43].

2.3.1.1 Grid Connected Microgrids

In grid-connected mode, the microgrid is connected to the main utility grid and operates in parallel with it, as illustrated by the upper selector position in Figure 2.3. In this mode, the microgrid draws power from the grid when needed and can export excess energy to the grid when local generation exceeds demand. The

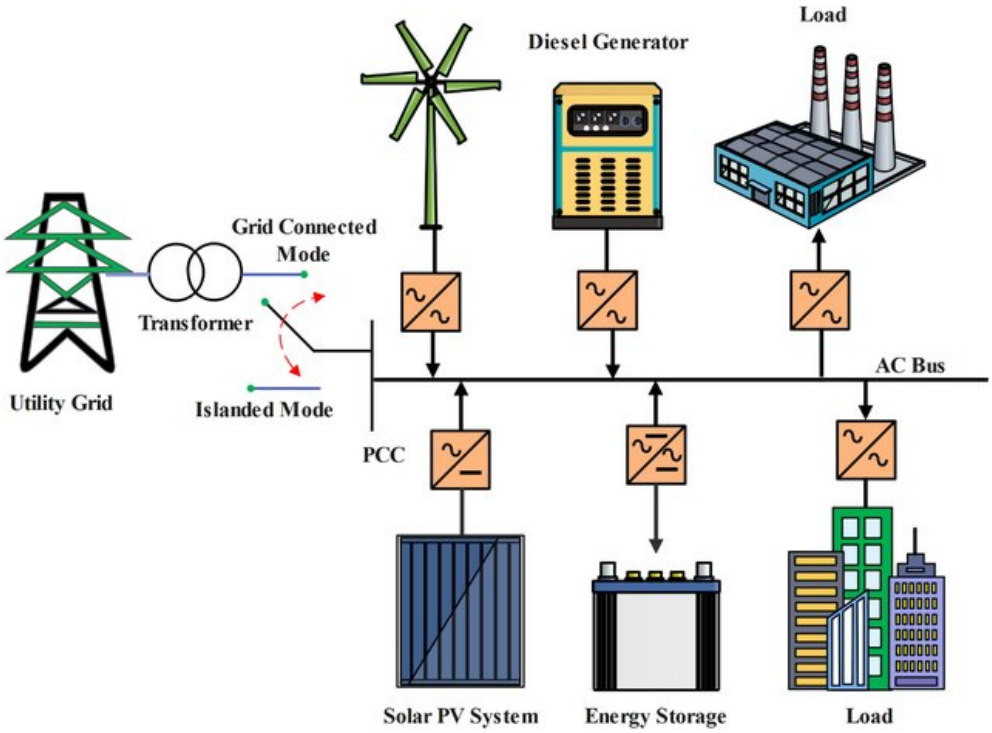

Figure 2.3: Operations of Microgrid [2]

grid provides frequency and voltage regulation, and distributed generation (DG) units operate in a grid-following mode [44].

2.3.1.2 Islanded (stand-alone) Microgrids

Stand-alone or islanded microgrids operate independently of the primary grid. They are common in remote areas where access to the grid is unavailable or scarce. The microgrid must regulate its voltage and frequency in this mode, and DG units operate in grid-forming mode. Islanded microgrids provide power autonomously, often relying on renewable energy sources and storage systems to maintain stability [45] as shown in the lower part of 2.3.

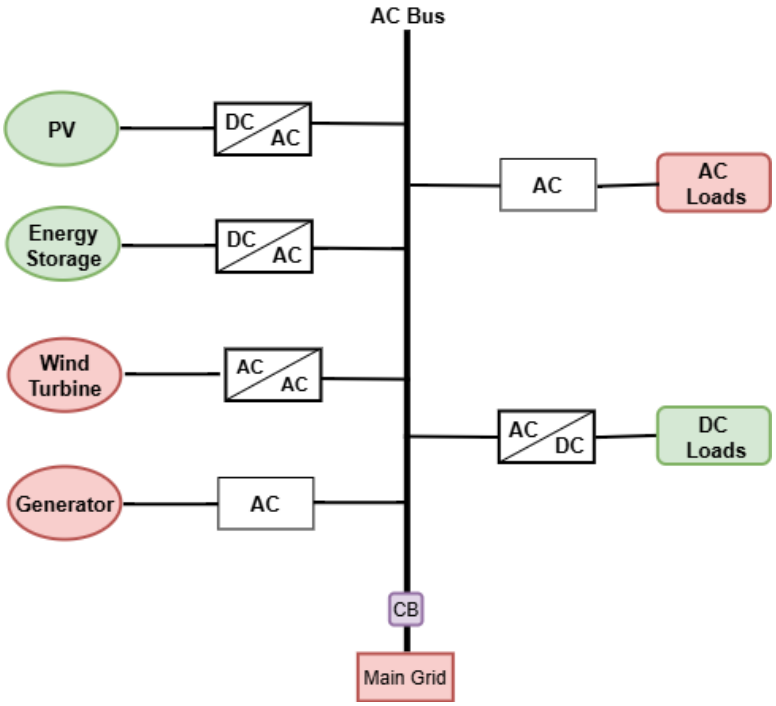

Figure 2.4: Structure of AC Microgrid

2.3.2 Based on Distribution

Microgrids can be categorised based on their distribution characteristics, which are crucial for their operational purpose. They can be classified as either alternating current (AC) or direct current (DC) power systems.

2.3.2.1 AC Microgrid

AC microgrids distribute electricity using Alternating Current (AC), which is compatible with most existing power systems and appliances. These microgrids usually consist of both conventional and renewable energy sources. However, energy storage and DC-generating renewable sources like solar photovoltaics (PV) need power converters to be integrated into an AC microgrid [46], [47].

2.3.2.2 Advantages of AC Microgrid

- Seamless Integration with the Grid: AC microgrids are more easily integrated into the existing AC power grid infrastructure, the global standard for electricity distribution. Most generation sources and loads (such as household appliances and industrial equipment) are designed for AC, making AC microgrids more compatible without complex conversions [48].

- Established Standards: AC technology is well-established, with clear implementation standards and regulations. This leads to more straightforward design, construction, and maintenance of AC microgrids.

- Interconnection of Distributed Energy Resources (DERs): AC microgrids can support a variety of renewable and conventional energy sources, including solar, wind, and gas generators, with minimal adjustments, making them more flexible in handling mixed energy sources [49].

- Advanced Protection Schemes: AC grids benefit from decades of development in protection schemes, ensuring quick and effective responses to faults, load imbalances, and disturbances. The ability to detect and isolate faults in AC microgrids is more advanced, reducing the risk of widespread outages or equipment damage [50].

- Handling Reactive Power: AC microgrids can manage both active and reactive power, essential for maintaining voltage levels in power systems. This ability is necessary for applications with inductive loads, such as motors and transformers, which are common in industrial settings [29].

2.3.2.3 DC Microgrid

DC microgrids distribute power using a DC network, making them highly efficient for integrating renewable energy sources such as solar photovoltaic (PV) systems

and energy storage systems, which naturally generate or store DC power. By avoiding the need for DC-AC conversions, DC microgrids reduce conversion losses and are particularly advantageous in systems with predominantly DC loads, such as data centres and telecommunications infrastructure [46].

Structurally, DC microgrids are similar to their AC counterparts but differ in their use of a DC bus for connecting distributed generators and loads rather than an AC bus. This is illustrated in Figure 2.5. This distinction eliminates the need for synchronisation, reactive power management, and frequency control common challenges in AC systems. The typical operational voltage range for a DC microgrid is between 350 and 400 Volts, which allows it to cater to various load types while minimising energy loss efficiently [51].

The DC bus can be split into low-voltage branches to power electronics-based loads. Solar modules, operating between 20-45V, are connected to the DC bus via high-voltage gain DC-DC converters, which boost the voltage to match the higher voltage levels of the main DC bus, improving system efficiency. DC-DC converters are classified based on their voltage gain and power handling capacity, ensuring they are suitable for the diverse power needs of a DC microgrid [47].

DC microgrids offer a simplified, more efficient architecture for integrating renewable energy sources and storage, especially in applications with heavy DC load usage.

2.3.2.4 Advantages of DC Microgrid

Although AC microgrids have historically dominated the energy landscape, recent advancements reveal several key advantages of DC microgrids, which are driving their growing adoption:

- Higher Efficiency: DC microgrids offer superior energy efficiency, with studies showing up to a 15% increase in performance compared to AC systems due to the elimination of conversion losses between DC and AC [13].

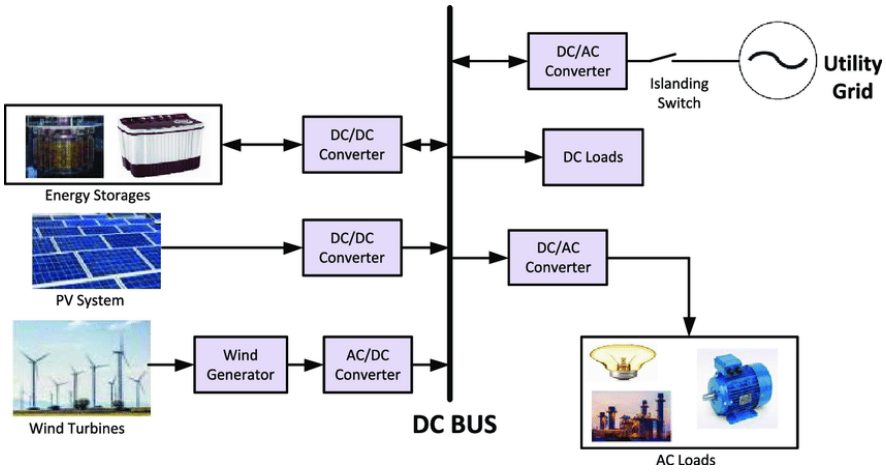

Figure 2.5: Structure of DC Microgrid [2]

- Simplified Control: DC microgrids avoid issues related to reactive power and frequency synchronisation, leading to simpler control systems and easier power flow management.

- Direct Integration: DC microgrids align seamlessly with renewable energy sources such as solar photovoltaics (PV) and energy storage systems (ESS), both of which inherently operate on DC power. This allows for direct DC/DC conversion, enabling more efficient integration compared to traditional AC-based systems. In contrast, connecting PV and ESS through AC/DC or DC/AC conversion stages introduces additional power conversion steps, each of which results in energy losses, increased system complexity, and higher costs. By using dedicated DC/DC converters, PV and ESS units can be more efficiently coupled to the DC bus, significantly reducing conversion losses and improving the overall efficiency, reliability, and responsiveness of the microgrid. This streamlined architecture not only minimises energy wastage but also supports faster and more flexible control of power flow, making DC microgrids especially well-suited for high-penetration renewable applications. [50].

- Tailored for Specialised Applications: DC microgrids are particularly advantageous in applications like rural electrification, where efficiency, reliability, and the use of renewable energy are critical. Additionally, they are ideal for institutional buildings, telecommunications infrastructure, and other facilities with significant DC loads [47].

- Support for Emerging Technologies: As the demand for DC-powered devices increases (e.g., electric vehicles, data centres), DC microgrids are becoming increasingly relevant for modern energy systems.

- They have a convenient controllability system that suffices without causing complexities such as synchronization, harmonics, reactive power control, and frequency control [49].

DC microgrids face challenges such as technical complexity and regulatory hurdles, despite offering improved efficiency and better integration with renewable energy sources. Unlike AC systems, DC microgrids lack a natural zero-crossing point, which makes interrupting fault currents more difficult. Protection devices like circuit breakers and fuses are more complex and expensive for DC systems. This thesis aims to address protection issues such as disturbance detection, control, and load shedding to enhance the resilience and stability of DC microgrids, promoting their widespread adoption by overcoming these barriers.

2.4 Microgrid Control

Microgrid control is the system or set of technologies responsible for managing energy generation, distribution, and storage within a microgrid. It also aims to optimise the balance between energy supply and demand within the microgrid, ensuring reliable, efficient, and sustainable operation. Effective control is essential to maintain power quality, handle energy fluctuations, and seamlessly

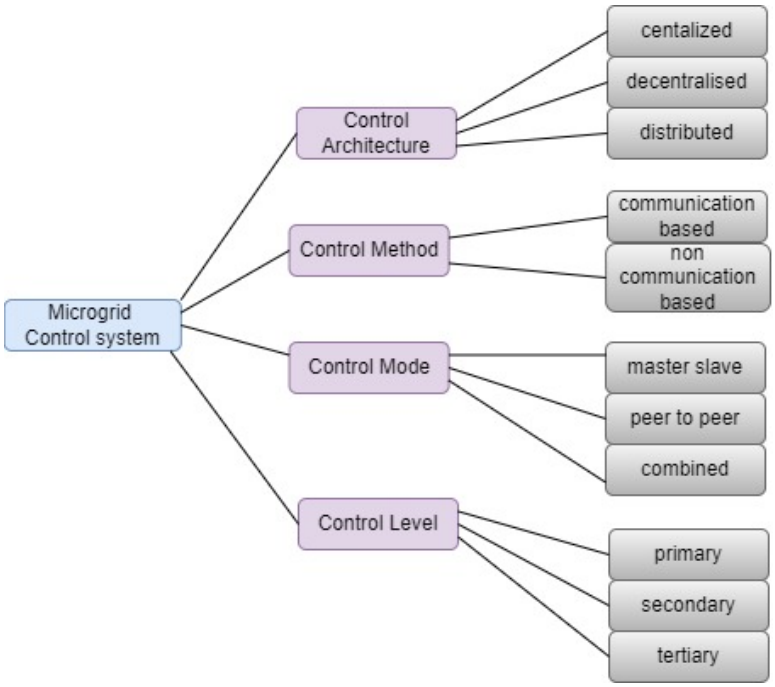

Figure 2.6: Structure of Control Systems in Microgrid

transition between grid-connected and islanded modes of operation [52]. Figure 2.6 illustrates the general structure of the microgrid control system, demonstrating the placement of non-communication-based systems, which is the control implemented in this thesis.

2.4.1 Control Architecture

Microgrid control architectures are hierarchical structures designed to manage microgrid operations efficiently. These architectures typically consist of multiple layers, including steady-state and dynamic control layers [53]. Different control strategies, decentralized, centralized, and distributed control, are employed to manage overall system performance and communication [54]. In centralised control, a central processing unit gathers measurements and makes decisions for coordinated operations across the microgrid. Decentralised control, on the other hand, relies on local measurements and predefined algorithms at individual nodes, with

decisions made at the component level [55]. Distributed control is an enhanced version of decentralised control, where each local controller communicates with its neighbours, combining the advantages of both decentralised and centralised architectures [53].

2.4.2 Control Mode

Microgrids can operate in different control modes, including master-slave, peer-to-peer, and combined modes [53]. Master-slave control is typically employed in smaller microgrids, where a centralised master unit governs the operation of other units. Peer-to-peer control, a decentralised method, eliminates hierarchy among controllers, improving system reliability and reducing operational costs. This approach enables controllers to share information about grid conditions. A multilayer architecture can achieve peer-to-peer control for networked microgrids, enhancing overall system communication and efficiency [56]. The choice of control mode depends on the size, components, and operational requirements of the microgrid.

2.4.3 Control Level

Microgrid control is typically divided into three hierarchical levels: primary, secondary, and tertiary control [57]. The primary control operates at the level of distributed generators, responding to immediate changes in power generation and consumption. Secondary control, which functions at the microgrid level, focuses on stability by managing power flows, restoring voltage and frequency, and compensating for reactive power. At the highest level, tertiary control ensures grid-wide stability and coordinates the microgrid with external grids, optimising the system's overall performance [58]. These multilayer control strategies are essential for addressing the challenges posed by renewable energy sources, energy

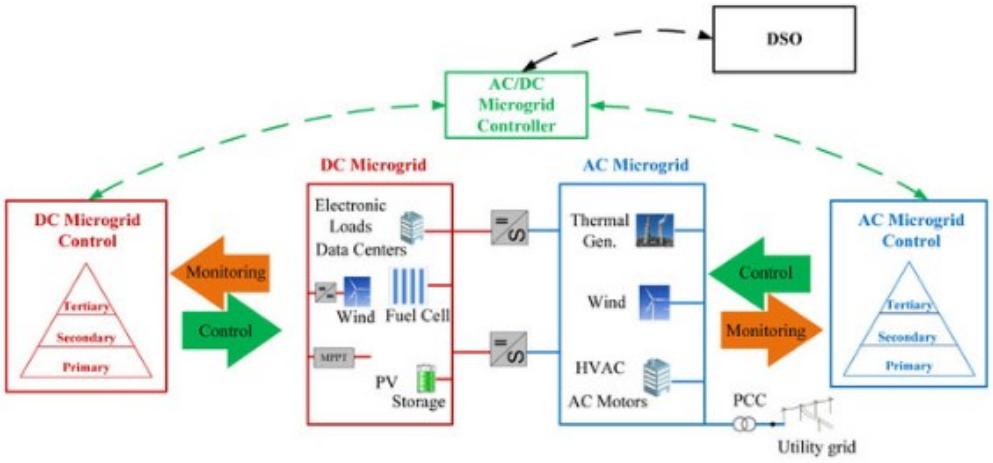

Figure 2.7: Hierachical Control of Microgrid [3]

storage systems, and fluctuating load demands, thus enhancing the microgrid's operational efficiency, stability, and autonomy [57].

2.5 Microgrid Protection

Microgrid protection is a crucial aspect that faces challenges due to fault currents and varying operating scenarios. Modern protection schemes have been proposed to address this issue, such as using Magneto-Resistive sensors for fault detection and localisation and impedance-based methods for line protection in microgrids [59] [60]. Integrating distributed energy resources (DERs) into microgrids has introduced new challenges requiring reliable, selective, and fast protection techniques [61]. Protecting microgrids is essential for grid resilience, particularly during microgrid disturbances, where existing protective devices may not be sufficient. To achieve this, strategies for microgrid protection should consider the impacts on distribution network relay protection and configure protection

schemes for microgrids connected to distribution networks [60]. Microgrid protection through detection and load shedding ensures the stability and reliability of the system in the face of disturbances like power imbalances, faults, or overloads, especially in the DC microgrid, which is the basis of this thesis.

2.6 Microgrid Optimisation

Many optimisation techniques, like linear programming (LP), non linear programming (NLP), mixed integer linear programming (MILP), dynamic programming (DP), and heuristics such as genetic algorithm (GA), particle swarm optimisation (PSO), and artificial bee colony (ABC), have been studied to improve DC microgrid efficiency, stability, and cost [62]. LP and NLP suit continuous variables but struggle with binary/logic decisions in load scheduling and switching. Heuristics handle non-linear, complex problems and high uncertainty, but often take longer and risk suboptimal results, limiting their real-time use [63]. Mixed-Integer Linear Programming (MILP) is popular for microgrid optimisation, combining discrete and continuous decisions in a linear model. It manages binary decisions like load shedding, generator commitment, and battery switching, plus continuous variables such as power flows and storage levels [64]. Its structured form includes operational constraints, load management, and renewable uncertainties, while remaining solvable with guaranteed global optimality. In DC microgrids, MILP effectively optimises demand response, energy storage, and real-time control, balancing efficiency and flexibility. In the existing literature, MILP-based optimisation has been used for:

- Economic dispatch of microgrids with renewable and storage integration [63],
- Unit commitment and coordinated scheduling of distributed generators [64],

- Battery energy storage management, optimising charge/discharge cycles for cost reduction and peak shaving [62].

- Demand-side management and prioritised load shedding to maintain reliability during disturbances [14]. While these studies demonstrate MILP's capability for microgrid control, several limitations remain:

- Scalability issues: As the network size and number of decision variables increase, MILP problems become computationally intensive, limiting their applicability for large-scale or fast real-time control.

- Uncertainty handling: Many existing MILP models assume deterministic forecasts for renewable generation and loads, which may not reflect the stochastic nature of real-world conditions. Robust or stochastic MILP formulations have been proposed, but they often increase complexity and computation time.

- Lack of adaptive response: Traditional MILP optimisation is typically performed in fixed scheduling horizons (e.g., hourly), making it less responsive to sudden disturbances unless combined with faster corrective control strategies.

- Simplified modelling: To maintain tractability, many models use linearised representations of power flow and component dynamics, which may overlook non-linearities critical for accurate DC microgrid behaviour.

Addressing these gaps requires approaches that integrate MILP's structured decision-making capabilities with uncertainty modelling and adaptation. In this thesis, MILP is employed as the primary optimisation method, but it is enhanced to specifically address load-shedding optimisation under disturbance conditions in DC microgrids, considering both operational constraints and system resilience.

2.7 Summary

This chapter presented an overview of microgrids, outlining their definitions, classifications, and growing role in modern energy systems. It highlighted how microgrids integrate various loads and distributed energy resources (DERs), including photovoltaic systems, wind turbines, CHP units, and energy storage to support cleaner energy, cost efficiency, and participation in demand response programs.

Microgrids were classified based on structural configuration (AC or DC) and control schemes, such as centralised, decentralised, and distributed methods. The chapter also introduced advanced multilevel control architectures, emphasising their contribution to improving microgrid performance and autonomy. A distinction between communication-based and non-communication-based control methods was discussed, laying the foundation for the control and load-shedding strategies explored throughout this thesis.

Additionally, the chapter addressed protection challenges within microgrids, underlining the need for effective protection mechanisms to ensure resilience against disturbances. Overall, it provided essential insights into the principles of microgrid operation, control, and protection, serving as a foundation for accurate system modelling and further research in the field.

Chapter 3

DC Microgrid Control Strategies and Modelling

3.1 Introduction

This chapter presents a literature review on DC microgrid control strategies, along with the modelling of the test system used in this study. The control strategies consist of voltage regulation and load-shedding strategies applied in both communication-based and non-communication-based DC microgrid systems. Its primary aim is to establish a clear understanding of existing methods designed to improve system stability and efficiency while also identifying gaps and opportunities for further research. The insights drawn from this review form the basis for the research contributions developed in the following chapters.

In addition, the chapter presents the modelling of a DC equivalent of the IEEE 37-bus system, with a focus on simulating key low-voltage direct current (LVDC) components. Detailed models are developed for essential elements such as wind turbines, photovoltaic systems, battery energy storage systems, grid-tied converters and DC cables. This modelling effort is designed to create a robust simulation environment that captures the complex interactions between system

components, accounts for environmental variability and accurately represents dynamic responses to disturbances and load variations in DC microgrid operations

3.2 DC Microgrid Control Strategies

DC control strategies are methods used to regulate and manage the operation of DC microgrids to ensure stable and efficient performance. These strategies focus on controlling key aspects of the microgrid, including voltage regulation, power sharing, load management, protection and energy storage control [65]. As discussed in the previous chapter, the strategies for controlling DC microgrids can be categorised into communication-based and non-communication-based methods.

3.2.1 Communication-based DC Control Strategies

Communication-based control strategies for DC microgrids rely on communication networks to exchange information between components, enabling centralised decision-making and coordinated operation [66]. A central controller collects data such as voltage, current, and state of charge from all devices, including distributed energy resources (DERs), storage systems, and loads, to make system-wide decisions in real-time [65]. This approach provides high precision in control decisions, facilitates global optimisation (e.g., minimising losses and optimising energy use), and is particularly suitable for managing large and complex microgrids. However, it depends on a reliable communication network, making it vulnerable to cyber-attacks and network failures [12]. A prominent example of this strategy is communication-based droop control, where a central controller adjusts the droop coefficients of DERs based on real-time load and generation data.

Communication-based DC control strategies include (i) centralized [25, 67], (ii) master-slave [68, 69], (iii) circular chain [70], (iv) distributed [71, 72], and (v) hierarchical [73–75] approaches. In centralised control, a central controller pro-

cesses data from DERs and sends commands via communication links to maintain power balance and regulate DC bus voltages [25,67]. Master-slave control assigns the regulation of DC voltage to a high-power DER (the master unit), while other DERs (the slaves) operate under the control of the master or other slaves [69]. Circular chain control forms a control loop where the current reference of each DER is obtained from the previous DER, and the first DER derives its reference from the last, creating a continuous control ring [70]. In distributed control, neighbouring DERs communicate to enhance overall performance, promoting better power sharing and system stability [71, 74]. Hierarchical control consists of decentralised primary control for fast dynamic responses, centralised secondary control for voltage restoration, and tertiary control for optimising power flow and economic operation [72–74].

While communication-based strategies excel in achieving precise power sharing and voltage regulation, they come with significant drawbacks. These strategies require expensive communication infrastructure, reducing system reliability, flexibility, modularity, and scalability. They also lack plug-and-play capability for DERs and are susceptible to communication failures. Consequently, large DC microgrids with geographically dispersed DERs often avoid using communication-based control strategies [13, 16].

3.2.2 Non-Communication based DC Control Strategies

Non-communication-based control strategies for DC microgrids operate independently of data exchange between components, relying solely on local measurements and decentralised decision-making [13]. Each element, such as DERs and storage systems, autonomously adjusts its operation based on parameters like voltage and current. Traditional voltage droop control is a prominent example, enabling DERs to proportionally share power and maintain system stability [17]. These strategies are valued for their reliability, low implementation costs, and

resilience to cyberattacks. However, their reliance on localised decision-making limits optimisation potential, making them less effective for managing large or complex systems [76,77]. Consequently, they are particularly suitable for smaller DC microgrids with multiple geographically dispersed DERs [78].

Non-communication-based strategies include conventional droop control [24, 79, 80], improved droop control [81–83], DC bus signaling (DBS) [84–87], mode adaptive droop control (MADC) [78], and improved mode adaptive droop control [78]. Conventional droop-controlled DERs use fixed droop gains for the entire range of DC terminal voltage, directly impacting system stability, voltage regulation, and power-sharing accuracy. Smaller gains improve voltage regulation but compromise power-sharing accuracy, while larger gains achieve the reverse [24,79,80]. Improved droop strategies address these challenges; for instance, nonlinear droop control enhances power-sharing and voltage regulation but introduces complexity [81]. Adaptive droop control reduces circulating currents and mismatches in power-sharing but requires detailed line parameter knowledge, complicating implementation in large systems [78, 82, 83].

DBS and MADC strategies enhance microgrid performance by adapting to operational conditions using locally measured voltages. DBS coordinates DERs and loads without communication, assigning operational modes based on predefined voltage ranges [20, 86–89]. While DBS strategies are effective during communication failures and countable operational states, they often require high-rated grid-tied converters GTCs or BESSs to manage significant power imbalances. Alternatively, some DBS strategies use GTCs as primary controllers and RESs or BESSs as auxiliary controllers, reducing GTC and BESS ratings but curtailing excess renewable generation instead of storing it [20, 88, 89].

MADC switches voltage control between RESs and BESSs based on bus voltage variations, using hysteresis characteristics for seamless transitions [48, 90–94]. However, conventional MADC assumes equal bus voltages across DERs, neglect-

ing voltage drops due to line resistances, leading to suboptimal coordination and degraded power-sharing in islanded DC microgrids. Improved MADC addresses this issue by minimizing the impact of voltage drops, enhancing voltage regulation and power-sharing between DERs [13, 78]. However, implementing MADC introduces delays that slow the responses to disturbances, compromise power-sharing accuracy, and degrade voltage regulation due to corrective droop adjustments. This ultimately compromises the resilience, stability, and performance of DC microgrids.

3.3 DC Load Shedding Schemes

Load shedding in DC microgrids involves the controlled disconnection of non-critical loads to maintain system stability when the supply and demand balance is disrupted, such as during generation shortfalls or faults. The main objective is to ensure that critical loads like medical facilities and emergency services continue to receive power despite insufficient generation [95].

Load shedding is a common practice in AC power systems, but its implementation in DC microgrids presents unique challenges due to the characteristics of DC power networks. One significant difference is that DC systems simplify the calculation process, as they do not involve reactive power. This means that only real power and voltage magnitudes need to be considered, which reduces computational complexity when determining which loads to shed [96].

However, DC microgrids lack a natural frequency response, necessitating faster response times to prevent voltage collapse during supply shortages. Additionally, integrating distributed generation from intermittent sources such as solar PV and battery storage introduces variability that must be managed in real time. This requires the use of predictive algorithms and continuous monitoring to assess grid conditions and adjust loads accordingly [46].

Control strategies for load shedding in DC microgrids can differ. Some systems employ centralized control, where a main controller decides which loads to shed, while others utilize distributed or hierarchical control, allowing local nodes to make shedding decisions based on local generation, load criticality, and battery state of charge.

Effective load-shedding in DC microgrids is crucial, especially in off-grid or islanded applications where available generation is limited and fluctuating. The ability to prioritize and maintain critical loads, such as emergency communications, medical equipment, or industrial processes, is vital for ensuring essential services remain operational [97]. Furthermore, since DC faults clear more quickly than AC faults, operators have less time to take corrective actions, making automated, real-time load-shedding systems even more essential.

With the increasing adoption of DC-based technologies, including telecommunication systems, electric vehicle charging infrastructure, and renewable energy systems, the need for reliable and intelligent load shedding mechanisms will continue to grow, ensuring the stability, resilience, and reliability of modern DC microgrids.

3.3.1 Communication-based Load Shedding Schemes

The DC microgrid load-shedding schemes can be classified into communication-based and non-communication-based categories. Communication-based load-shedding schemes [23, 70, 95, 98–107, 107–109] are used in microgrids to maintain power balance under large disturbances. In this scheme, a microgrid central controller receives data from DERs and controllable loads and sends commands to them via communication links. Effective communication with the load ensures optimal load-shedding while avoiding unnecessary reductions. Centralized load-shedding schemes provide high observability and controllability. However, they also have several disadvantages, including vulnerability to communication failures, high

computational demands, low reliability, limited flexibility, scalability, and expandability, a lack of plug-and-play capability, and increased complexity and cost. Therefore, centralized load-shedding schemes are more appropriate for small DC microgrids with compact configurations, where centralized data acquisition is not difficult or costly [22], [21].

3.3.2 Non-Communication based Load shedding Schemes

The non-communication-based scheme, sometimes called the decentralized scheme, operates solely on locally measured electrical quantities most commonly the DC voltage signals [16,80,89,93,110–113]. Each load controller or protection device is equipped with its own voltage-sensing capability and decision logic, enabling it to determine whether and when to shed its associated load without relying on any supervisory control or data exchange with other devices. In this approach, there is no exchange of data or control commands between different parts of the microgrid, hence the term "non-communication." The only "signal" involved is the electrical voltage on the bus itself, which is a naturally shared physical quantity rather than an intentional communication channel. When a disturbance, such as a generation shortfall, occurs, the bus voltage drops. Each load-shedding device continuously monitors this voltage locally and compares it against predefined thresholds or rates of change. If the voltage falls below its set threshold (or the rate of change exceeds a set limit in adaptive schemes), the device autonomously disconnects the load it controls.

The scheme's advantages are the simplicity of implementation, cost-effectiveness, scalability, expandability, and robustness against communication failures [22]. As a result, these schemes are suitable for a broader range of DC microgrids, including those with geographically dispersed loads that lack access to communication signals [21]. The categories of non-communication-based load-shedding approaches investigated are the conventional and adaptive load-shedding schemes.

The conventional schemes consist of voltage-based [26, 99, 110, 112, 114], timer-based [20, 26, 114] and the combined based schemes [26, 89, 114], while the adaptive adaptive consist of adaptive voltage scheme [114], [97] and adaptive timer-based scheme [114], [115]. The conventional voltage-based load shedding scheme [26, 89, 99, 114] utilizes different voltage thresholds to prioritize the shedding of non-critical loads. This method instantaneously sheds some load whenever its bus voltage exceeds the corresponding voltage threshold. The voltage-based scheme sheds load in steps. However, the scheme causes unnecessary load shedding due to significant voltage deviations when the difference between the voltage thresholds is large. Thus, power supply reliability and bus voltage regulation performance must be traded off in this scheme. The conventional timer-based strategy [20], [26], [114] prioritizes non-critical loads and sheds them whenever the voltage falls below a common threshold for some time longer than expected preset time delay. This scheme sheds non-critical loads in a specific order, using different preset delays for each load. The timer scheme uses short delays of 0.01s, 0.02s, and 0.03s and long delays of 50s, 100s, and 150s. However, there are some drawbacks to this scheme. When short delays are used, there is a risk of over-shedding, and significant voltage sags can occur when long delays are used. Therefore, the timer-based strategy can compromise the reliability of the power supply and bus voltage regulation. The conventional combined scheme [89], [26], [114] employs both timer-based and voltage-based algorithms and thus operates whenever one of the conditions for load shedding is satisfied. This scheme enjoys the merits of both voltage and timer-based schemes. However, the combined scheme is more likely to cause unnecessary load shedding due to the combination of predetermined voltage thresholds and timer delays. The adaptive voltage-based load-shedding scheme [114], [97] employs automatically adjustable voltage thresholds to manage load-shedding steps. Each voltage threshold is continuously determined based on the locally measured rate of change of voltage (ROCOV). This load-shedding

scheme ensures high reliability and speed [97]. However, this scheme exposes the critical loads to low voltage due to a lower voltage threshold that sheds loads with lower priorities. As a result, it is mostly suitable for microgrids with few load-shedding steps. If many load-shedding steps need to be coordinated, the final step occurs at a significantly lower voltage. Therefore, it is advisable to use the strategy proposed in [97] for microgrids with a relatively small number of load shedding. The adaptive timer-based load-shedding scheme [114], [115] uses automatically adjusted time delays to coordinate the load-shedding. This scheme sheds non-critical loads using a time delay that adapts to the locally measured rate of change of voltage (ROCOV) and a common voltage threshold [115]. This scheme prevents unnecessary shedding of loads when ROCOV is insignificant and performs better than the adaptive voltage-based scheme regarding time regulation. However, similar to the adaptive voltage-based strategy [97] and timer-based scheme [26], the adaptive timer-based strategy utilizes a successively lower threshold, thereby exposing the critical loads to a lower voltage. The paper [114] has thoroughly analyzed and compared all current non-communication-based DC load-shedding schemes. These schemes rely on fixed voltage/time thresholds and ROCOV, which can lead to excessive bus voltage deviations or over-shedding of loads. To overcome the shortcomings of these existing schemes, there is a need for more advanced load-shedding schemes that can optimally shed loads in future DC microgrids. Chapter 4 of the paper comprehensively compares all the existing DC load-shedding schemes.

3.4 System Structure

This section outlines the study system structure used in this thesis, which incorporates renewable energy sources such as solar panels and wind turbines, energy storage systems like batteries, and various types of loads. Accurate modelling

allows for the simulation of power flows, voltage regulation, and load-sharing dynamics while also helping to evaluate the performance of control strategies and load-shedding schemes. DC microgrid models provide insights for designing robust, scalable, and reliable energy solutions by capturing the interactions between system components.

3.4.1 Introduction

The IEEE 37 Bus Test System is a well-known benchmark network originally developed for the analysis and validation of power system models, particularly in the context of distribution networks [116]. While the traditional version of this system operates in AC (Alternating Current), growing interest in DC distribution systems—driven by the increasing penetration of renewable generation, energy storage, and DC-compatible loads has led to the development of a DC variant of the IEEE 37 Bus Test Model [117]. This modified IEEE 37 DC Bus Test System serves as a critical platform for researchers to evaluate the performance of DC distribution grids under different operating conditions, including disturbance scenarios, load variations, and control strategy implementation.

In this thesis, the IEEE 37-bus system was specifically chosen over smaller networks such as the 4- or 9-bus systems because it more accurately represents the scale, diversity, and operational complexity of a large community-level microgrid. Smaller test systems, while useful for preliminary validation, lack the topological depth and load distribution variety required to realistically test advanced energy management strategies, such as prioritised load shedding, dynamic storage control, and mixed-integer optimisation under realistic constraints. The 37-bus network includes a rich mixture of radial branches, multiple load types, and distributed generation nodes, providing a robust and scalable environment for assessing the feasibility and performance of control and optimisation techniques in real-world DC microgrid settings. This makes it a suitable testbed

for evaluating the proposed methods with the intention of future deployment in community or campus-scale microgrids.

3.4.2 Key Modifications from AC Test System

The DC version of the IEEE 37-node AC system preserves the topology of the original AC system, retaining its 37 buses and radial configuration, which is characteristic of real-world distribution networks. However, the system is reconfigured to operate in DC, requiring modifications to the components and power flow modelling. Key alterations include the replacement of transformers with DC-DC converters, adjustments to load and generation models to reflect DC voltage and current characteristics, and redefinition of protection schemes suitable for DC fault currents.

The modification from AC Test System is as follow:

- Voltage Levels: AC bus voltages are replaced with appropriate DC voltage levels suitable for distribution systems (e.g., 750 VDC, 1 kVDC, etc.).
- Converters: AC transformers are substituted with bidirectional DC-DC converters to manage voltage conversion between different sections of the network.
- Load Representation: AC loads are translated into constant power, constant current, or constant resistance DC loads, depending on the application.
- Distributed Generation: Renewable energy sources such as PV panels, which naturally generate DC power, can be directly connected to the system without the need for AC inversion.
- Protection Adjustments: Fault analysis and protection strategies are redefined to handle the fast-rising fault currents and lack of natural zero-crossing inherent to DC faults.

The implementation of the IEEE 37 DC Bus Test Model offers several significant advantages for this work, making it a highly suitable platform for analysis, simulation, and control design in DC distribution systems. These advantages include:

- **Realistic Representation of Distribution Networks**: As a standardized and widely recognized test feeder, the IEEE 37 Bus system closely reflects the structure and characteristics of a real-world radial distribution network, ensuring that analysis conducted using this model is both realistic and practically relevant [118].

- **Benchmark Comparability**: Since the AC version of the IEEE 37 Bus system is extensively documented and frequently used in academic and industrial studies, the DC version provides a valuable opportunity to directly compare the performance of AC and DC distribution networks under similar operating conditions.

- **Compatibility with Modern Energy Sources**: With the increasing penetration of renewable energy sources such as solar photovoltaics (PV), battery storage, electric vehicles (EVs), and DC-compatible loads, the importance of DC distribution grids continues to grow. The IEEE 37 DC Bus model is well-suited for studying these modern grids, enabling the development and testing of control strategies designed for renewable-dominated systems [5].

- **Simplified Power Flow Calculations**: Compared to AC load flow analysis, DC load flow equations are inherently simpler because they focus only on real power and voltage magnitudes, without requiring calculations for reactive power or phase angles. This linearization reduces computational complexity, enabling faster simulations and making the model highly efficient for large-scale studies [119].

- **Support for Advanced Control Development**: The test model serves as a flexible platform for developing and evaluating advanced control algorithms, such as voltage droop control, adaptive load shedding, and distributed energy resource (DER) coordination. Its structure can also be scaled to represent larger geographic areas, enhancing its applicability to more complex systems [120].

- **Resilience and Reliability Studies**: Due to the unique fault characteristics of DC systems—such as the absence of a natural current zero-crossing—the IEEE 37 DC Bus model is particularly useful for protection scheme development, fault detection and isolation studies, and resilience analysis under contingency scenarios [117].

- **Academic and Industry Relevance**: Finally, using a well-established benchmark system enhances the credibility of the research and aligns the work with global academic and industrial standards, making the results more transferable and comparable to existing literature and future research efforts.

3.4.3 System Structure and Configuration

The DC version of the IEEE 37 Bus system preserves the topology of the original AC system, retaining its 37 buses and radial configuration, which is characteristic of real-world distribution networks. However, the system is reconfigured to operate in DC, requiring modifications to the components and power flow modelling. Key alterations include the replacement of transformers with grid-tied converters (GTC), adjustments to load and generation models to reflect DC voltage and current characteristics, and redefinition of protection schemes suitable for DC fault currents.

The IEEE 37 Bus DC microgrid system shown in Fig 3.1, [26], [78], [115],

[84], [114] is essentially an IEEE 37-node AC test system [121] reconfigured as a DC microgrid. The operating DC voltage is 750V to comply with the guidelines of the IEC60038 standard for LVDC systems [122]. The conversion of the IEEE 37-node feeder into a DC microgrid model is a strategic choice that provides a realistic, benchmarkable, and scalable platform for testing power flow, stability, control, and protection mechanisms in DC distribution systems [123]. It supports advanced load-shedding strategies, renewable energy integration, and microgrid resilience studies, making it an ideal choice for research and practical implementation of DC microgrids [121]. The 750V DC microgrid consists of a 1MW wind turbine with a permanent magnet synchronous generator (PMSG). It is connected to node 709 using an AC/DC voltage-sourced converter (VSC). Additionally, two 0.5 MW PV generation systems are connected to nodes 712 and 722, which use DC/DC boost converters. Two 0.4 MW battery energy storage systems (BESSs) are connected to nodes 705 and 707 using bidirectional buck-boost DC/DC converters close to the area with critical loads. A bidirectional DC/AC GTC with a capacity of 1MW links the DC microgrid to the AC grid. A 0.75kV/4.8kV isolation transformer is used at node 701 to interface with the AC grid. All converters are modelled using the switching model and are represented in detail.

3.4.4 System Modelling

Power distribution in DC grids can be achieved using either a two-wire (unipolar) system or a three-wire (bipolar) system, as illustrated in Figure 3.2. In a unipolar configuration, the system consists of two conductors: one carrying a positive polarity and the other a negative polarity. This setup results in a line-to-line voltage of 2Vdc, which represents the total voltage difference between the two conductors. While the unipolar system offers simplicity and symmetry between the DC poles, it has several limitations. These include a lack of redundancy,

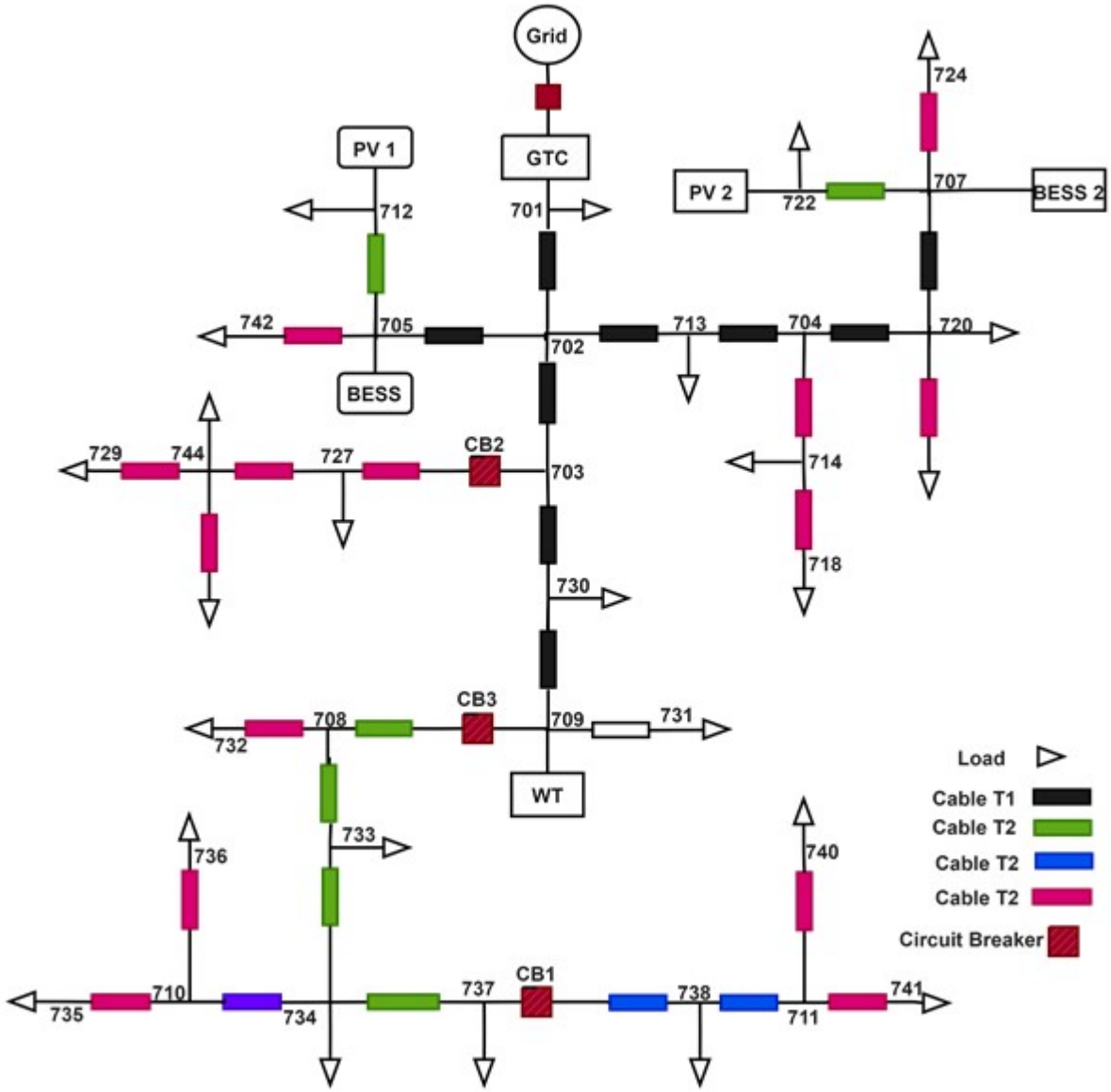

Figure 3.1: Single line diagram of IEEE 37-bus DC microgrid

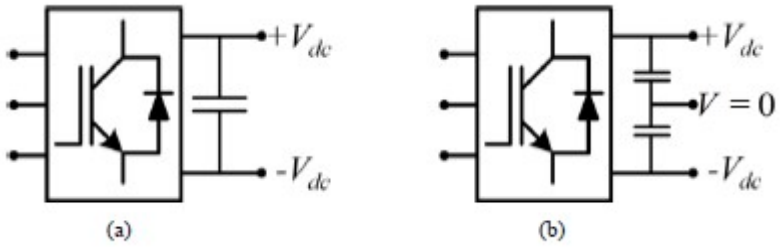

Figure 3.2: DC microgrid configuration (a) Unipolar, (b) Bipolar

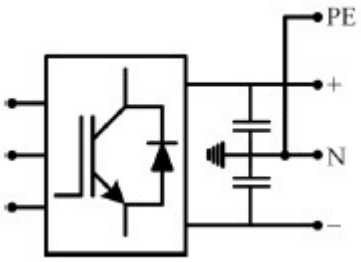

Figure 3.3: DC microgrid TN-S grounding systems

constraints in adjusting voltage levels, and a higher risk of complete system failure in the event of a single fault, making it less resilient compared to a bipolar configuration [124–126].

According to international standards, the terra neutral-separate (TN-S) grounding configuration is the most commonly recommended approach for DC microgrids [12,125]. In this setup, the middle point of the converter is connected to the ground, while the apparatus body is connected to both the neutral and protective earth, as illustrated in Figure 3.3. The TN-S configuration is widely adopted for supplying power to low-voltage DC (LVDC) residential, commercial, and industrial loads, ensuring enhanced system safety and stability in the studied DC microgrid [12, 125].

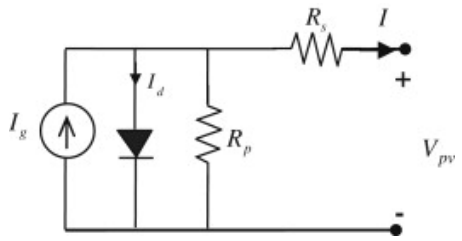

Figure 3.4: Single diode circuit model of PV

3.4.5 DER Models

This section provides a detailed model of DERs and the GTC utilized in the study system. It includes a brief description of the model.

3.4.5.1 PV Model

The DC microgrid is connected to the PV generation system via the DC/DC boost converter, as illustrated in Figure 3.5. The PV cells are represented by the single-diode circuit model of Simulink as shown in 3.4. This model is widely used as it balances simplicity and accuracy. The circuit comprises a current source, a diode parallel with the current source, a series resistance Rs, and a parallel resistance Rp are all provided based on standard datasheet parameters. [86], [127], [128], [129]. The basic equation that describes the nonlinear current-voltage characteristics of the PV cell [129] is shown below:

$$I_p v = I_g - I_d - \left(\frac{V_{pv} + R_s I_{pv}}{nkT} \right) \tag{3.1}$$

where

$$I_d = I_o \left(\exp \left(\frac{q(V_{pv} + R_s I_{pv}}{nkT} \right) - 1 \right) \tag{3.2}$$

Where Vpv is the PV cell voltage, Ipv is the PV cell current, Ig is the full-load current, Id is the diode current, Io is the reverse saturation current, q is

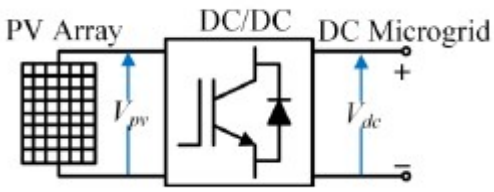

Figure 3.5: PV system connected to DC Microgrid

the charge carrier, k is the Boltzmann constant, T is the cell temperature, and n is the ideality factor. To attain the desired voltage and current levels, PV cells are connected in series (Ns) for higher voltage or parallel (Np) for higher current. These connections form a PV module. Multiple modules are then linked together to form a photovoltaic (PV) array.

3.4.5.2 Wind Turbine Model

The type of wind turbine utilised in this study is the Permanent Magnet Synchronous Generator (PMSG), a variable-speed turbine used in wind energy conversion. It offers several advantages, such as higher efficiency and power factor, no regular maintenance, and flexible active and reactive power control and dissipation, and its easy implementation are some of the reasons for using it [130]. The PMSG WT comprises rotor blades, a gearbox, and a generator. It is connected to the DC microgrid through a VSC, as shown in the figure 3.6. The mechanical power generated by the WT is extracted [131], [132]:

$$P_w = \frac{1}{2}\rho\pi R^2 V_w^3 C_p(\lambda, \beta) \tag{3.3}$$

Where P_w is the wind power(W), ρ is the air density kg/m3, R is the radius (m), and Vw is the wind speed (m/s) [131].

To extract maximum power from wind, the C_p should be kept at the maximum value (C_pmax), and the tip speed ratio should be kept around the optimal value

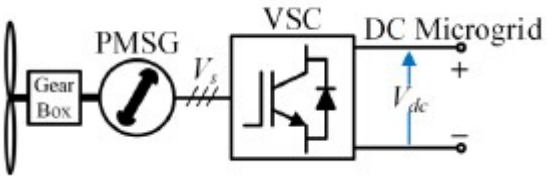

Figure 3.6: PMSG-based WT connected to the DC microgrid

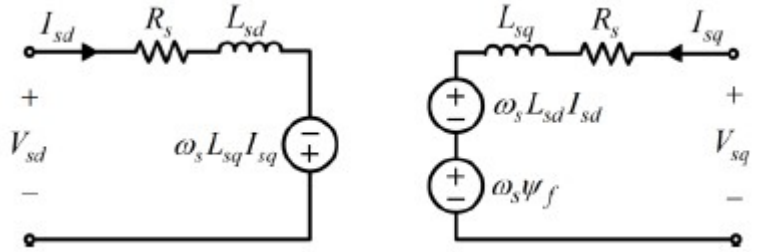

Figure 3.7: PMSG model in the d-q reference frame

($\lambda_o pt$). The WT mechanical torque is

$$T_t = \frac{P_t}{\omega_t} \tag{3.4}$$

The reference power Pref of the PMSG wind turbine is based on its rated power. The d-q reference rotating frame for the PMSG dynamics is shown in 3.7given by [41];

$$\frac{d\psi_{sd}}{dt} = -V_{sd} - R_s I_{sd} - \omega_e \psi_{sq} \tag{3.5}$$

$$\frac{d\psi_{sq}}{dt} = -V_{sq} - R_s I_{sq} + \omega_e \psi_{sd} \tag{3.6}$$

$$\psi_{sd} = (L_{sd} + L_{md}) I_{sd} + \psi_m \tag{3.7}$$

$$\psi_{sq} = (L_{sq} + L_{mq}) I_{sq} \tag{3.8}$$

where V_{sd} and V_{sq} are the stator circuit voltages, R_s is the stator resistance

winding, I_{sd} and I_{sq} are the stator d and q reference frame currents, ω_e is the rotational speed, ψ_{sd} and ψ_{sq} are the flux linkages of the stator circuit, L_{sd} and L_{sq} are the leakage inductances of the stator, L_{md} and L_{mq} are the magnetizing inductances, and ψ_m is the linkage flux [132].

Inserting equations 3.7 and 3.8 into equations 3.5 and 3.6, respectively, the stator voltage equations become:

$$V_{sd} = R_s I_{sd} + L_{sd}\frac{dI_{sd}}{dt} - \omega_s L_{sq} I_{sq} \tag{3.9}$$

$$V_{sq} = R_s I_{sq} + L_{sq}\frac{dI_{sq}}{dt} + \omega_s L_{sd} I_{sd} + \omega_s \psi_f \tag{3.10}$$

The PMSG active and reactive powers in the d-q reference frame are expressed as;

$$P_{GTC} = \frac{3}{2}\left(V_{td} I_{td} + V_{tq} I_{tq}\right) \tag{3.11}$$

$$Q_{GTC} = \frac{3}{2}\left(V_{tq} I_{td} - V_{td} I_{tq}\right) \tag{3.12}$$

while the electrical torque (T_e) is given as

$$T_e = 0.5p(\psi_m I_{sq}) + (L_d - L_q) I_{sd} Isq \tag{3.13}$$

The stator currents control the active and reactive powers of PMSG, while the corresponding voltage components control the stator current's axis components as shown in Figure 3.7 [125].

3.4.5.3 BESS Model

In this system, the battery is modelled as a controlled voltage source placed in series with a constant internal resistance. It is treated as an ideal voltage source, with its terminal voltage dynamically adjusted based on factors such as state of

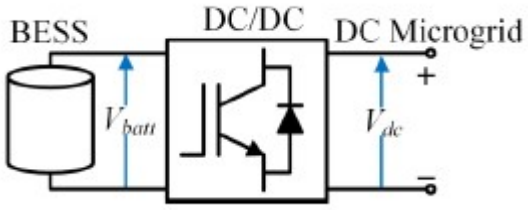

Figure 3.8: BESS model connected to the DC microgrid

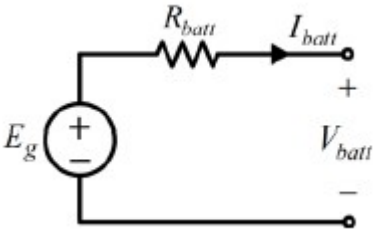

Figure 3.9: BESS circuit diagram

charge (SoC), temperature, and the charge/discharge currents.

The controlled voltage source is connected to the DC microgrid through a bidirectional buck-boost DC/DC converter, enabling both charging and discharging operations as illustrated in Figure 3.8. In this model, the charging and discharging processes are assumed to have symmetrical characteristics. The open-circuit voltage (OCV) of the battery is determined using a non-linear equation, which reflects the actual SoC of the battery at any given time. The following equations describe the behavior of the controlled voltage source. [86], [133]:

$$V_{batt} = E_g - R_{batt} I_{batt} \tag{3.14}$$

$$E_g = E_o - K\left(\frac{Q}{Q - \int_0^t I_{batt}(\tau)\, d\tau}\right) + A \cdot \exp\left(B \int_0^t I_{batt}(\tau)\, d\tau\right) \tag{3.15}$$

where E_g is the no-load voltage (V), V_{batt} is the battery voltage (V), R_batt is the battery resistance, I_{batt} is the battery current (A), E_o battery constant voltage (V), K is the polarization voltage (V), Q is the battery capacity (Ah), $\int I_{batt} dt$ is

the actual battery charge (Ah) 3.9, A is the exponential zone amplitude (V), B is the inverse of the exponential zone time constant $(Ah)^{-}1$. The state of charge of the battery is expressed as [132];

$$SOC = 100\left(1 + \frac{\int I_{batt}dt}{Q}\right) \tag{3.16}$$

To ensure the safety of its components, the BESS has specific voltage and SOC set values within which it must operate. When the SOC reaches its minimum or maximum set-values, the BESS converter stops switching to prevent the set-values from being exceeded [86], [132] [133]. The connection of BESS to the DC microgrid is shown in Figure 3.8.

3.4.5.4 Grid Tied Converter (GTC) Model

The GTC is connected to the AC grid via an output filter and an interfacing transformer, as shown in Figure 3.10. The GTC model in the direct-quadrature (d-q) reference frame is depicted in Figure 3.11 expressed as [134], [135]:

$$V_{td} = R_f I_{fd} + L_f \frac{dI_{fd}}{dt} - \omega_s L_f I_{fq} + V_{od} \tag{3.17}$$

$$V_{tq} = R_f I_{fq} + L_f \frac{dI_{fq}}{dt} + \omega_s L_f I_{fd} + V_{oq} \tag{3.18}$$

AC system and GTC terminal quantities are represented by s and t, respectively. GTC active and reactive powers in the d-q reference frame are expressed as [134], [135]

$$P_{GTC} = V_{td} I_{td} + V_{tq} I_{tq} \tag{3.19}$$

$$Q_{GTC} = V_{td} I_{tq} - V_{tq} I_{td} \tag{3.20}$$

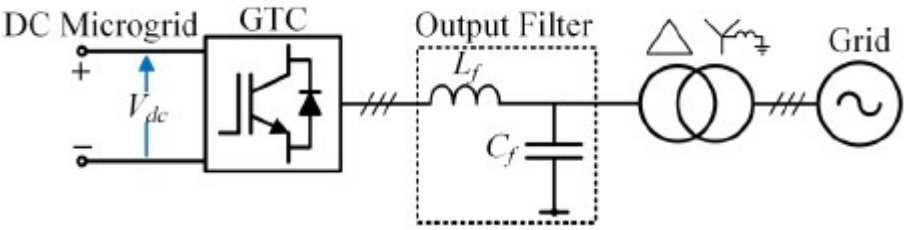

Figure 3.10: GTC connected to DC Microgrid

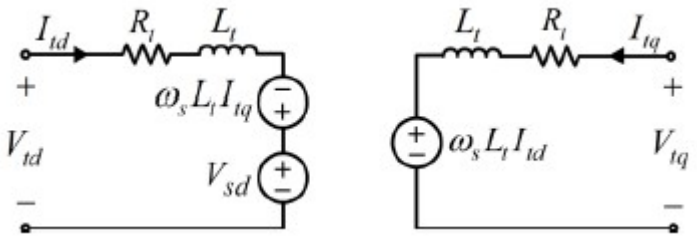

Figure 3.11: GTC in d-q reference frame

where

- R_t: Filter resistance of the Grid-Tied Converter (GTC) [Ω]
- L_t: Filter inductance of the GTC [H]
- ω_s: Angular frequency of the synchronous reference frame [rad/s]
- I_{td}, I_{tq}: d-axis and q-axis components of the output current from the GTC [A]
- V_{td}, V_{tq}: d-axis and q-axis terminal voltages at the GTC output [V]
- V_{od}, V_{oq}: output voltages at the capacitor Cf d-axis and q-axis components of the voltage at the grid side [V]

A GTC's active and reactive powers are controlled by the d- and q-axis components of its terminal currents, respectively. The d- and q-axis components of the GTC terminal current are, in turn, controlled by the corresponding GTC terminal voltage components, as seen from the equations.

3.4.5.5 Load Characterisation and Modelling

The loads in a DC microgrid can be categorized as constant resistance load (CRL), constant current load (CCL), constant power load (CPL), or a combination of these [136], [137], [138], [139]. CCL loads draw a programmed current regardless of input voltage, ensuring maximum current output under any conditions. Examples of CCL loads include LED lighting systems, BESS chargers, and EV charge piles. In CRL mode, the electronic load acts like a fixed resistor, consuming current proportional to the input voltage. It is commonly used to test battery capacity and electronic device start-up conditions. Examples of CRL loads are incandescent lamps, coffee makers, and electric stoves. CPL loads consume a set amount of power by measuring input voltage and consuming the calculated current. This ensures that the power source can provide the output power over the voltage range. Examples of CPL loads include electronic loads, power converters, and electric motor drives [140]. Load characteristic in DC systems can be represented by the polynomial load model [136], [137], [138], [139]. This model describes the relationship between the load power and voltage as follows:

$$P_{load} = A_{CRL}V^2 + A_{CCL}V + A_{CPL} \tag{3.21}$$

where A_{CRL} is the CRL coefficient, A_{CCL} coefficient and A_{CPL} is the CPL coefficient. The relationship between the current and voltage of the CRL is expressed as

$$I_{CPL} = \frac{V_{in}}{R_{CRL}} \tag{3.22}$$

where I_{CRL} and V represent the current and voltage of the CRL whle P_{CRL} and V_n represent the CRL power and nominal voltage. The current of the CRL changes when the voltage changes. The CRL can be modeled as

$$R_{CRL} = \frac{V_n^2}{P} \tag{3.23}$$

The relationship between the current and voltage of the CCL is given as

$$I_{CCL} = \frac{P_{CCL}}{V_n} \tag{3.24}$$

where I_{CCL} and P_{CCL} are the current and power of the CCL power. The current of the CCL is constant regardless of the voltage variations. The CCL is modeled using the resistance as follows

$$R = \frac{V}{I_{CCL}} \tag{3.25}$$

The relationship between the current and voltage of the CPL is expressed as follows:

$$I_{CPL} = \frac{P_{CPL}}{V} \tag{3.26}$$

where I_{CPL} and P_{CPL} represent the current and power of the CPL power. The current of the CPL changes when the voltage changes. The CPL was modeled using the resistance R_{CPL} as

$$R_{CPL} = \frac{V}{I_{CPL}} \tag{3.27}$$

3.4.5.6 Cable Models

A DC cable is essentially a distributed transmission line that can be simplified into either a lumped parameter model or a distributed parameter model, depending on the desired accuracy and simulation requirements. In this system, the PI-section model is used to represent the cables within the system. The network utilises four different sizes of 1 kV single-core XLPE cables [141]. The selection of cable size for each feeder section is based on key factors, including load current capacity, maximum allowable voltage drop, and acceptable conduction losses, ensuring optimal system performance.

The positive and negative polarity underground cables are buried at a depth

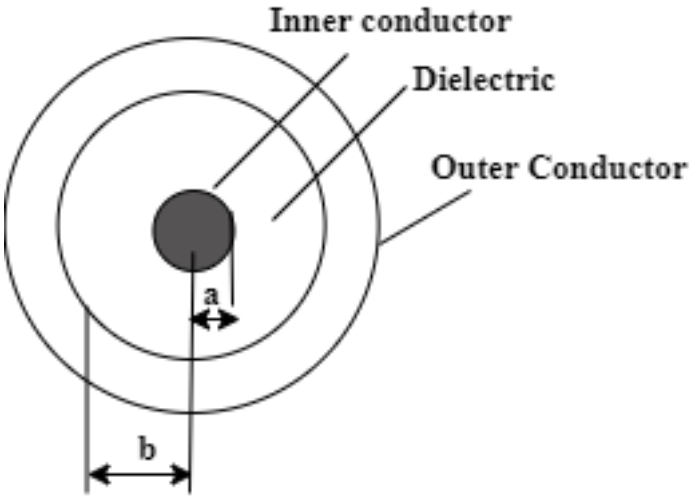

Figure 3.12: LV Cable Configuration

of 1 meter, with a horizontal separation of 0.5 meters. This standard configuration, applicable to all four cable types, is illustrated in Figure 3.12. Using this cable offers key advantages such as accurate representation of transmission line characteristics, efficient load flow and voltage drop analysis and scalability for large systems.

Further details on the cable lengths, types used for each feeder section, and the per-unit-length parameters and dimensions of each cable type can be found in the Appendix.

3.4.5.7 Circuit Breakers Model

A DC circuit breaker is essential in electrical systems and is designed to protect against overcurrent and short circuits. There are three main types of circuit breakers in the LVDC and MVDC markets: solid-state circuit breakers (SSCBs), mechanical circuit breakers (MCBs), and hybrid circuit breakers (HCBs) [142]. This model utilises an ideal circuit breaker to manage control and load-shedding processes, as they provide notable advantages over electromechanical circuit breakers. Some of these advantages include the ability to operate quickly,

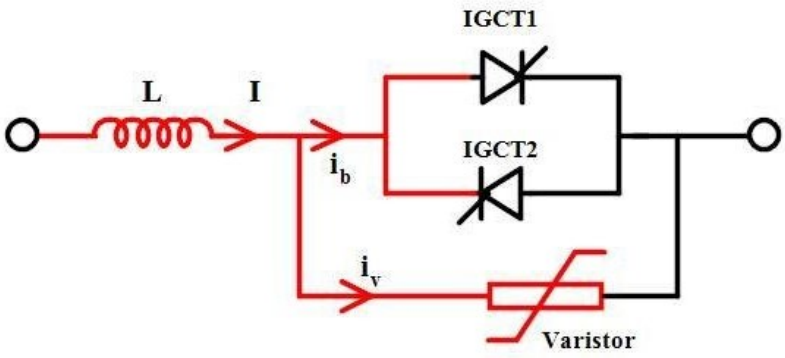

Figure 3.13: Low voltage bi-directional Solid-state circuit DC breaker [4]

which is crucial for effectively handling the rapid rise of fault currents in medium voltage DC systems, ensuring efficient protection. Also, SSCBs have short breaking times, high reliability, and high power density, making them suitable for DC applications [143].

The topologies for Solid-State Circuit Breakers (SSCBs) typically include a specific number of Integrated Gate Commutated Thyristors (IGCTs), Gate Turn-Off Thyristors (GTOs), or Insulated Gate Bipolar Transistors (IGBTs) connected in series. However, despite quick response times, SSCBs have significant on-state losses, high component costs, lack of galvanic isolation, and inadequate thermal absorption capacity [144]. The proposed SSCB topology used in this study is the IGCT, usually for DC systems with voltages less than or equal to 1 kV and low currents less than or equal to 1000 A, as shown in Figure 3.13. The model uses three SSCBs: CB1 is between nodes 727 and 707, CB2 is between nodes 708 and 709, and CB3 is between nodes 737 and 738.

3.4.6 Summary

This chapter provided a comprehensive review of control strategies in DC microgrids, along with the modelling of the IEEE 37-bus DC microgrid. The control strategies were categorized into voltage regulation and load-shedding approaches, further classified as communication-based and non-communication-based methods. The review identified key limitations in existing voltage control and load-shedding techniques, highlighting the gaps that must be addressed to improve the stability and resilience of DC microgrids. These insights form the foundation for the development of advanced DC bus voltage control methodologies and novel load-shedding schemes, which are presented in the subsequent chapters of this thesis.

In addition to the literature review, this chapter presents the detailed modelling of the IEEE 37-Bus DC test system, adapted into an LVDC equivalent. The model integrates key generation sources such as WT, PV systems, BESS, and GTC. It also includes comprehensive cable models and a variety of load types to ensure a holistic representation of the LVDC microgrid.

By systematically modelling the essential components and technologies of LVDC microgrids, this chapter establishes a robust and practical simulation framework. This ensures accurate system behaviour, appropriate component selection, and realistic dynamic performance. Consequently, the developed model provides a strong foundation for full-scale simulations, enabling the evaluation of microgrid reliability, scalability, and operational efficiency under realistic conditions.

Chapter 4

Limitations of Current DC Load Shedding Schemes and the Path to Improved Non-Communication-Based Solutions

4.1 Introduction

The previous chapter provided a comprehensive overview of existing non-communication-based DC load-shedding schemes, outlining their operational principles, advantages, and limitations. Building on this foundation, the current chapter focuses on evaluating the performance of these schemes using a standardized test system. The goal is to assess their effectiveness under consistent conditions and to identify potential improvements to address the shortcomings observed in recent implementations.

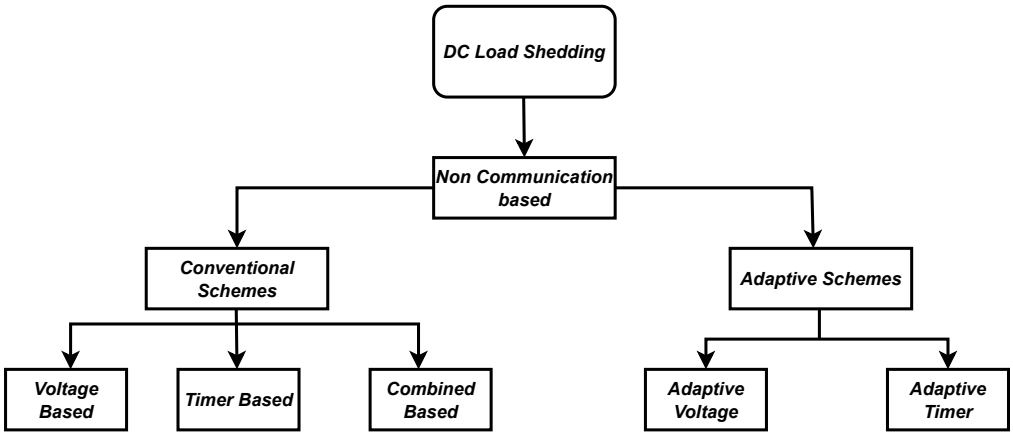

Figure 4.1: Non-communication-based DC load shedding schemes

The evaluation is guided by key performance indicators (KPIs), including circuit breaker response time, voltage stabilization (assessed by the minimum voltage during disturbances and the final steady-state voltage), and load-shedding efficiency, measured by the amount of unnecessary load disconnection. These metrics serve as benchmarks for comparing the different strategies and highlighting areas where enhancements are needed.

DC load-shedding schemes in the literature are broadly classified into two categories: conventional and adaptive. Conventional approaches include voltage-based, timer-based, and combined methods, while adaptive schemes consist of adaptive voltage-based and adaptive timer-based techniques as shown in 4.1. The performance of each of these approaches is assessed in the following subsections. The results of this evaluation will inform the development of improved load-shedding strategies by revealing existing gaps and performance limitations.

4.2 Conventional Schemes

4.2.1 Voltage-based Load-shedding Scheme

The voltage-based load-shedding scheme prioritizes non-critical loads using different voltage thresholds. It sheds i_{th} non-critical load instantly whenever the voltage observed by that load falls below the equivalent voltage threshold V_{th-i} [26, 114, 145–147].

The voltage-based method may lead to needless load shedding or over-shedding when the voltage thresholds are too close. When the difference between the voltage thresholds is considerable, it can lead to large steady-state voltage deviations, i.e., voltage sag. The loads with lower priorities are assigned higher voltage thresholds and, thus, are shed faster. The flowchart is shown in Figure 4.2. The block diagram and operation characteristics of the voltage-based load-shedding scheme are presented in Figure 4.3.

4.2.2 Timer Based Load Shedding Scheme

The timer-based load shedding strategy [20], [26], [114] uses a common voltage threshold and prioritises the non-critical loads using different time delays. This scheme sheds the ith non-critical loads whenever the voltage falls below the common voltage threshold Vth for a time period longer than the preset time delay Ti. For the scheme to operate effectively, the loads with lower priorities are usually assigned lower time delays to effect fast load shedding. The flowchart of the timer-based load-shedding scheme is presented in Fig. 4.4, while the block diagram and operation characteristics of the scheme are illustrated in Fig. 4.5.

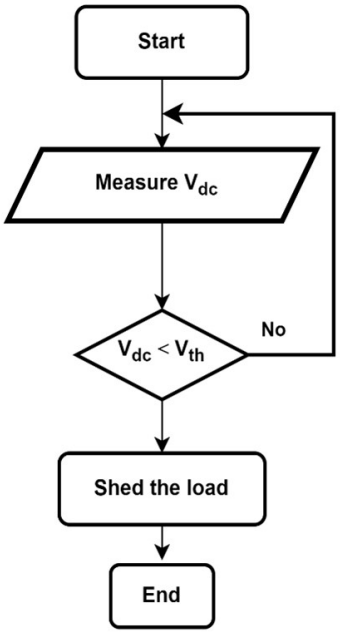

Figure 4.2: Flowchart of the voltage-based scheme.

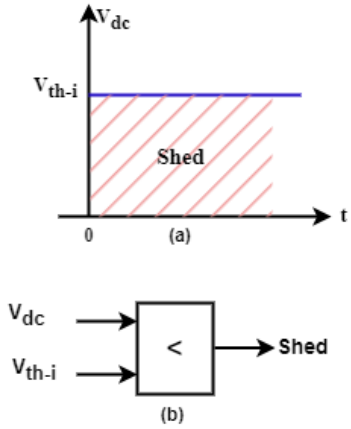

Figure 4.3: Block diagram and operating characteristics of Voltage-based scheme

4.2.3 Combined Voltage and Timer-Based Load Sheding Scheme

The combined load-shedding scheme utilizes both voltage-based and timer-based algorithms and thus operates whenever either of these two schemes operates [93] [89] [26] [114]. Two different thresholds are used on each load; the normal voltage

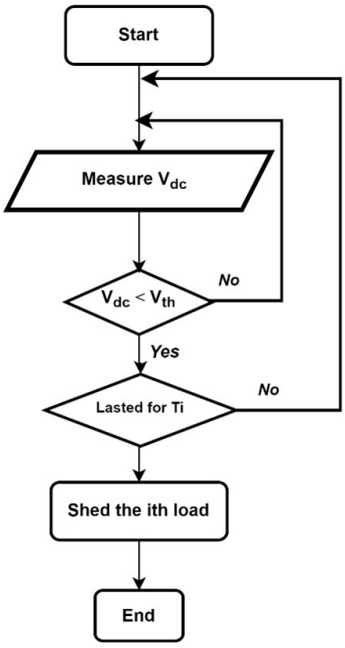

Figure 4.4: Flowchart of the timer-based scheme.

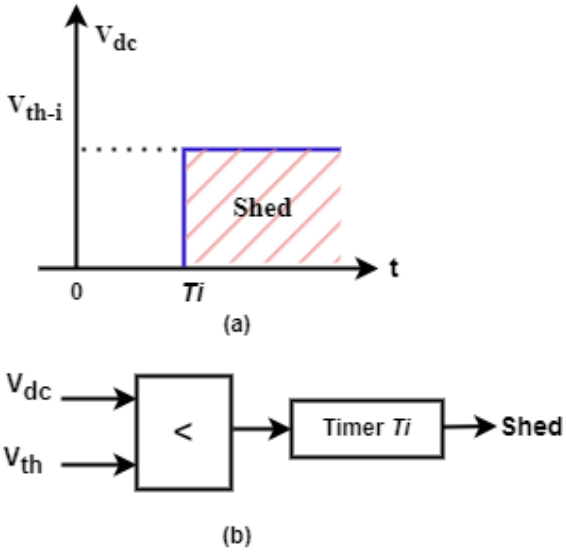

Figure 4.5: Block diagram and operating characteristics of timer based scheme.

thresholds V_{th} are used for instantly shedding the loads, similar to a voltage-based scheme; in addition, i_{th} load is shed when the voltage remains below the common threshold for a time period longer than the corresponding time delay

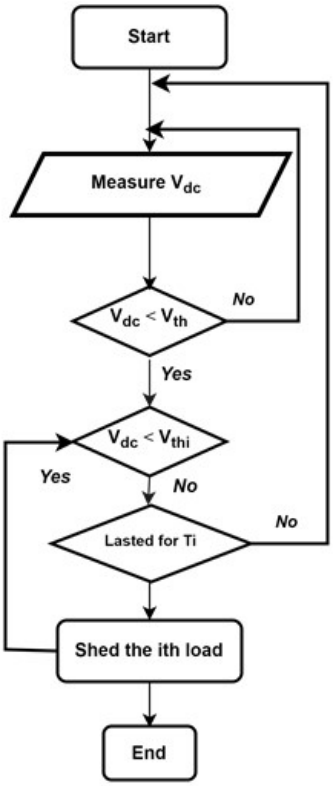

Figure 4.6: Flowchart of combined voltage and timer-based scheme.

Ti as illustrated in the Figure 4.7. A combined scheme with appropriately set voltage thresholds and time delays can alleviate the voltage sag problem caused by delayed or missed operation of the voltage-based schemes [26] [114]. The combined scheme is often used as the standard for conventional schemes. The representation of the scheme's flowchart is shown in Figure 4.5, while the Block diagram and operating characteristics of the scheme are presented in Figure 4.6.

4.3 Adaptive Schemes

4.3.1 Adaptive Voltage Load shedding Scheme

The adaptive voltage load shedding scheme utilizes an adaptive voltage threshold V_{th} that depends on the rate of change of voltage (RoCoV), as defined by:

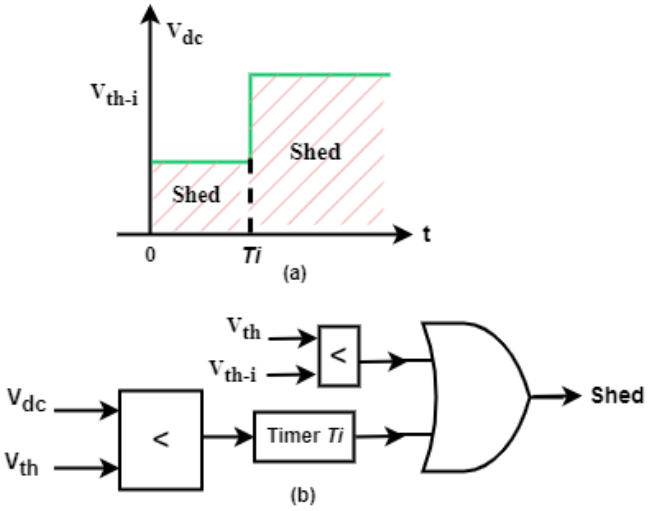

Figure 4.7: Block diagram and operating characteristics of combined based scheme

$$V_{th} = \begin{cases} V_{min}, & -k_1 < \dfrac{dV_{dc}}{dt} \leq 0 \\ V_{min} + m\left(\dfrac{dV_{dc}}{dt} + k_1\right), & -k_2 \leq \dfrac{dV_{dc}}{dt} \leq -k_1 \\ V_{max}, & -\infty < \dfrac{dV_{dc}}{dt} < -k_2 \end{cases} \tag{4.1}$$

where;

$$m = \frac{V_{max} - V_{min}}{k_1 - k_2} \tag{4.2}$$

where V_{min} and V_{max} are the minimum and maximum values of the adaptive voltage threshold. The constants k_1 and k_2 identify the values of the RoCoV at which V_{th} reaches the maximum and minimum values, respectively [97]. Load shedding occurs whenever the rate of change of voltage (RoCoV) is negative, and the locally measured voltage falls below the voltage threshold [97].

When there are large disturbances and the RoCoV is high (above -2.5 V/s), the adaptive voltage threshold V_{th} rises and causes faster load shedding to limit the voltage drop. When the RoCoV is below -0.5 V/s, there is no need for fast load shedding; the voltage threshold is automatically set to a lower value to avoid

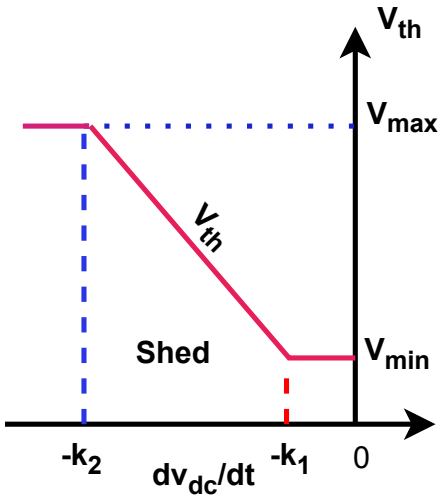

Figure 4.8: Operating characteristic of adaptive voltage load shedding scheme

over-shedding. The representative flowchart of this method is presented in Fig. 4.10.

4.3.2 Adaptive Timer based Load Shedding

The adaptive timer-based load-shedding strategy operates based on the same principle as the conventional timer-based strategy. The improvement of the adaptive approach is that it tends to shed each non-critical load using a time delay T, which adapts to the locally measured RoCoV, as defined by

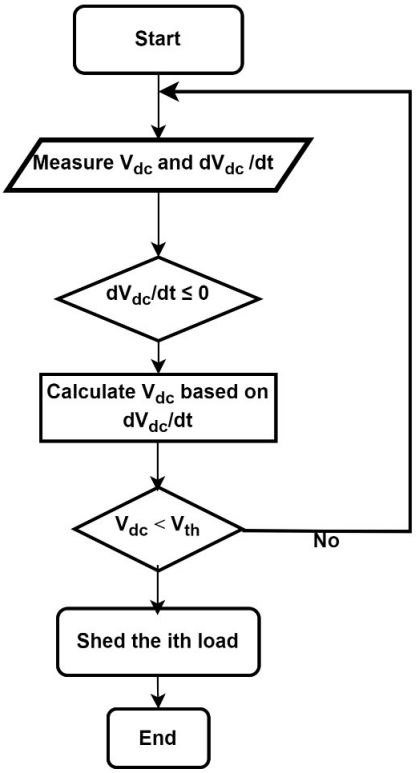

Figure 4.9: Flowchart of adaptive voltage scheme.

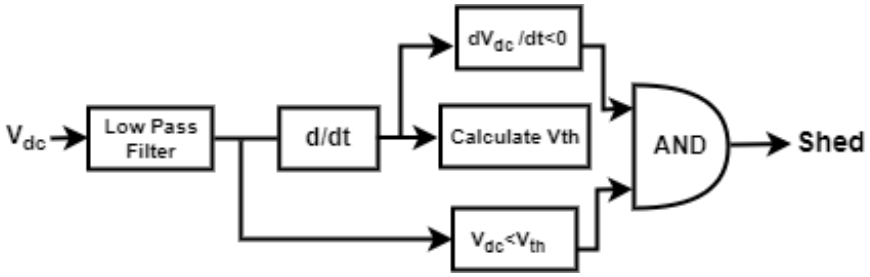

Figure 4.10: Flowchart of adaptive voltage scheme.

$$T = \begin{cases} T_{max}, & -k_1 < \frac{dV_{dc}}{dt} \leq 0 \\ \dfrac{T_{max}k_1}{|dV/dt|}, & -k_2 \leq \frac{dV_{dc}}{dt} \leq -k_1 \\ T_{min}, & -\infty < \frac{dV_{dc}}{dt} < -k_2 \end{cases} \tag{4.3}$$

where: T_{max} and T_{min} are the upper and lower limits of the adaptive time delay, respectively, and the constants k_1 and k_2 represent the RoCoV values at which the time delay T becomes equal to T_{max} and T_{min}, respectively.

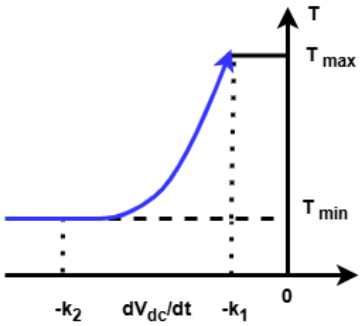

Figure 4.11: Operating characteristic of adaptive timer load shedding scheme

This technique sheds a non-critical load whenever its bus voltage remains below the common voltage threshold for some time longer than the corresponding adaptive delay, and its RoCoV is negative [115].

4.4 Performance Evaluation

4.4.1 Methodology

The methodology for implementing load shedding schemes in the test system, which has been transformed into a 750 V DC microgrid, is illustrated in Fig. 4.14 and was also described in the previous chapter as part of the test system. In this microgrid, various loads are utilized, including Constant Power Loads (CPL), Constant Resistance Loads (CRL), and Constant Current Loads (CCL).

The system is designed for a three-step load shedding process that employs three fast-acting solid-state circuit breakers (SSCB). When load shedding is required, the circuit breakers are tripped in a specific sequence: CB1 is triggered first, followed by CB2, and finally, CB3 if the load remains greater than the generation capacity. Non-critical loads are connected to these circuit breakers, as

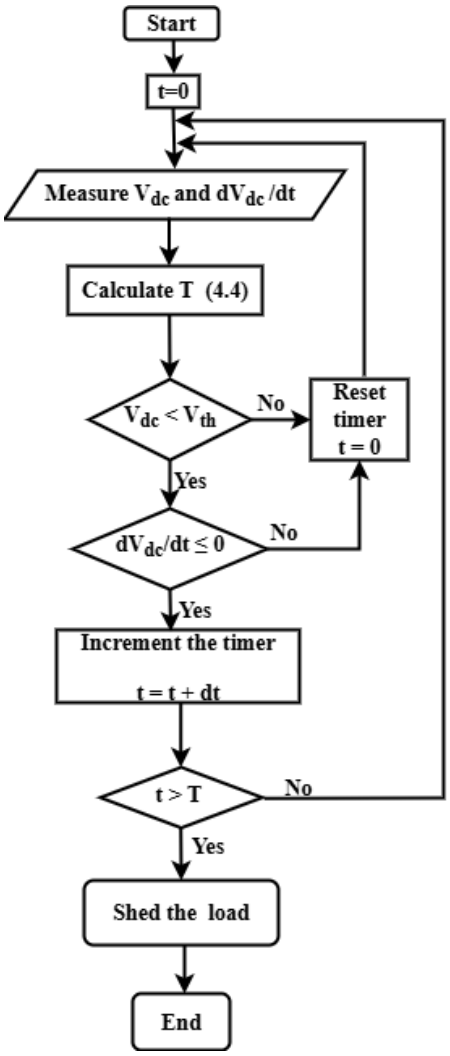

Figure 4.12: Flowchart of adaptive timer scheme.

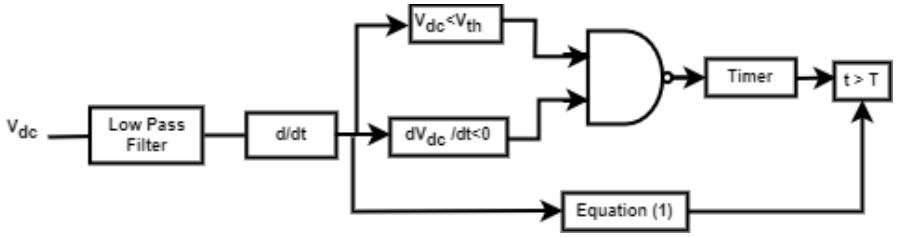

Figure 4.13: Block diagram of adaptive timer scheme.

shown in Fig. 4.14. The sheddable load capacity for each circuit breaker is as follows: 148 kW for CB1, 148 kW for CB2, and 234 kW for CB3.

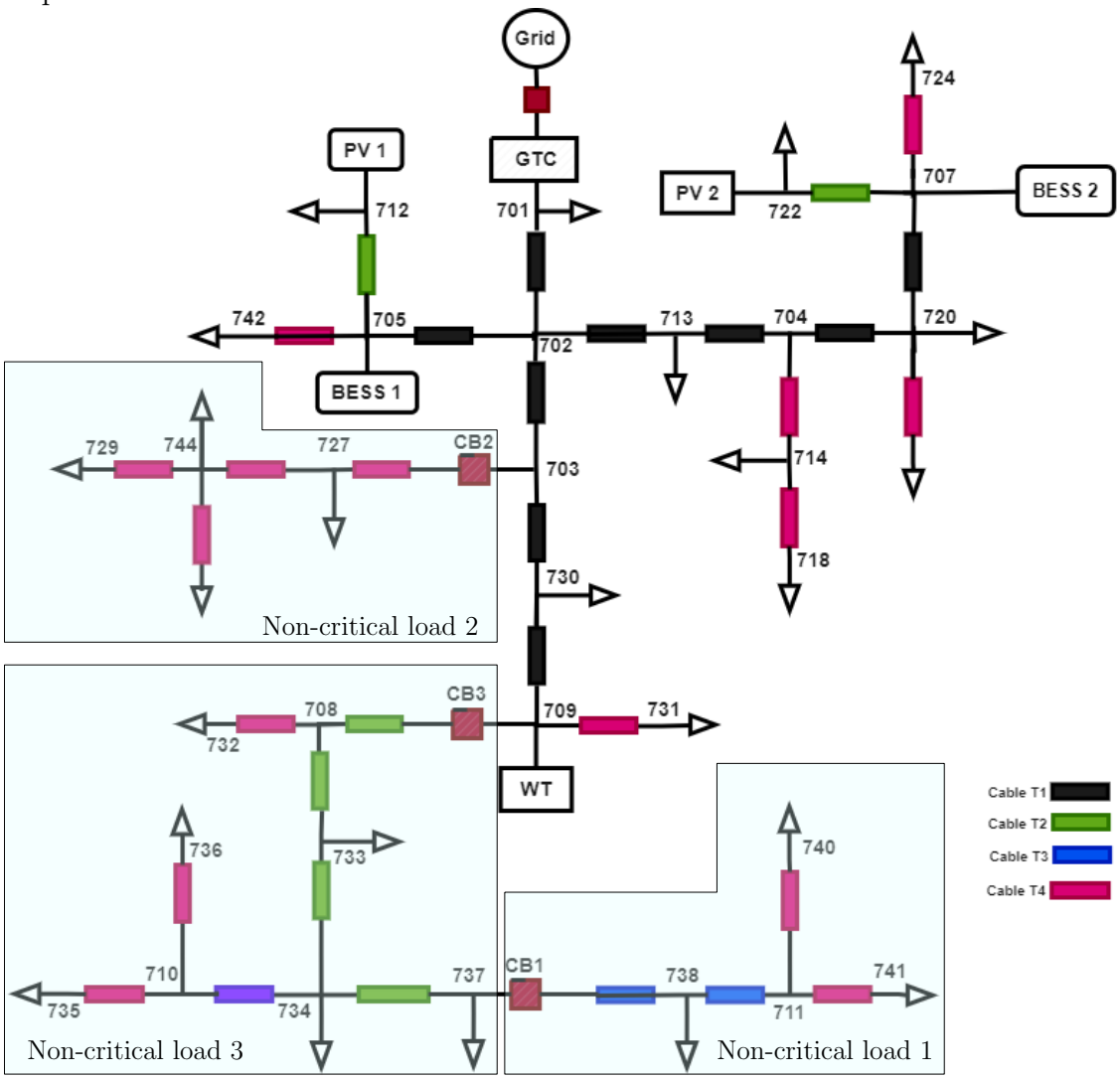

Figure 4.14: Single Line Diagram of the System

In this study, significant voltage drops across the lines have been observed. Therefore, the highest load-shedding voltage threshold for all non-critical loads is set at 675 V, which corresponds to a -10% variation to prevent load shedding during normal operating conditions. When the bus voltages exceed 700 V, the microgrid is considered to be in normal operating conditions.

The total load of the microgrid is 1260 kW, and the characteristics of the distribution line cables, including their descriptions and types, are detailed in [135].

4.4.2 Performance Metrics

The performance metrics of the study are to prevent the system from operating at low voltage, avoid over-shedding by maintaining power balance by disconnecting the smallest loads, and fast shedding to minimize the magnitude and duration of the voltage sag. The voltage variations of the critical loads are similar to each other. Therefore, node 702 is used to investigate the performance of the load-shedding strategies [26]. Two case studies are described in the following subsections. These case studies evaluate the performance of the voltage-based, timer-based scheme, combined scheme, adaptive voltage scheme and the adaptive timer-based schemes. The following metrics are employed to evaluate and compare the performance of the schemes:

- Response Time: The time taken for circuit breakers to trip following a disturbance.
- Voltage Stabilisation: The scheme's ability to maintain the voltage within a specified range is measured by the minimum voltage of critical loads during a disturbance and the final voltage after the disturbance is resolved.
- Load-Shedding Efficiency: Assessed by the extent to which unnecessary load shedding is prevented and the precision in shedding non-critical loads proportional to the magnitude of the disturbance.

4.4.3 Case Study 1: Small Disturbance

This case study evaluates the performance of the proposed schemes under a small disturbance of 200 kW. Initially, the wind turbine operated in MPPT mode, generating 700 kW, while the PV units were inactive. The total load demand was 1.21 MW, and the microgrid bus voltages ranged between 740 V and 780 V.

A gradual reduction in wind speed caused the wind turbine's power output to

decrease from 700 kW to 500 kW within 0.5 s, leading to a drop in microgrid bus voltages. The analysis is conducted using three voltage thresholds: $V_{th_1} = 720\,\text{V}$, $V_{th_2} = 690\,\text{V}$, and $V_{th_3} = 675\,\text{V}$.

4.4.3.1 Voltage Based Scheme

In the voltage-based scheme, one group of non-critical loads was disconnected by tripping circuit breaker CB1 at $t = 0.525\,\text{s}$. This action was triggered when the corresponding bus voltages fell below the threshold $V_{th_1} = 720\,\text{V}$, as shown in Fig. 4.15a.

As a result, 0.148 MW of non-critical loads was shed, reducing the total microgrid load to 1.05 MW, as illustrated in Fig. 4.15b.

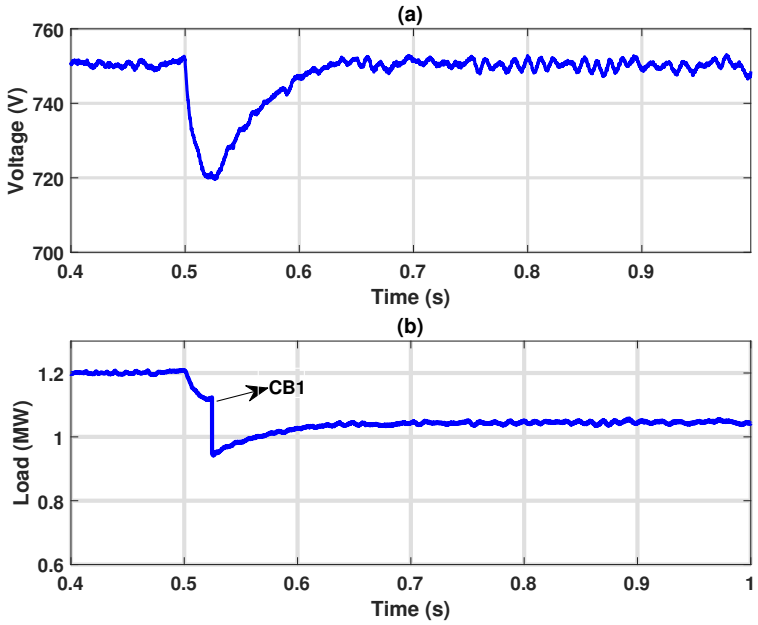

Figure 4.15: Performance of Voltage based Scheme; **a)** DC Voltage **b)** Load power

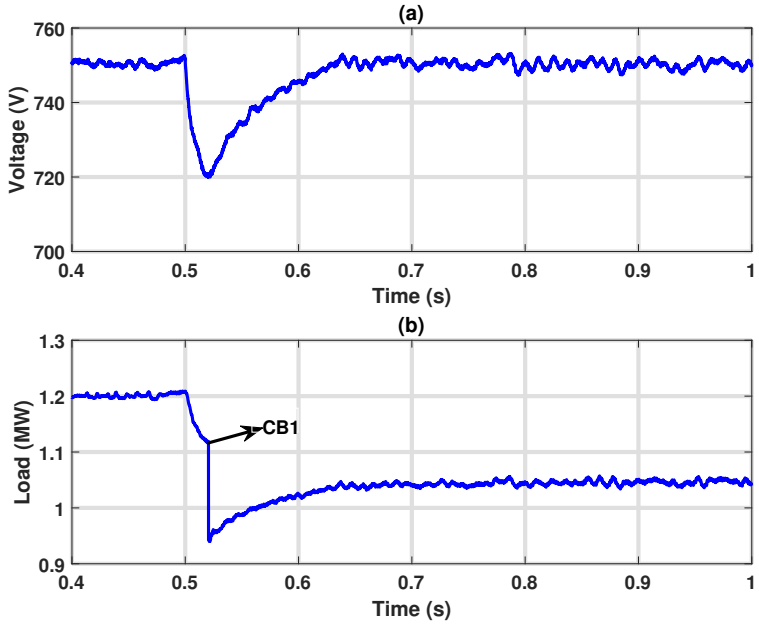

Figure 4.16: Performance of Timer based Scheme; **a)** DC Voltage **b)** Load power

4.4.3.2 Timer Based Scheme

In this scheme, CB1 was tripped as soon as the bus voltages dropped below 720 V, as shown in Fig. 4.16a. The trip occurred at $t = 1.521$ s. With the timer preset to an interval of 10 ms, the voltage recovered quickly, stabilizing at 750 V within 0.04 s after the disturbance.

Similar to the voltage-based scheme, 0.148 MW of non-critical loads was shed, maintaining the microgrid load at 1.05 MW, as shown in Fig. 4.16b.

4.4.3.3 Combined Based Scheme

The combined scheme, which integrates both voltage and timer criteria, tripped CB1 at $t = 0.520$ s, slightly faster than either individual method. This quicker response was due to the synergy between voltage monitoring and timer control.

Given the small magnitude of the disturbance, only CB1 was disconnected, shedding 0.148 MW of load. The resulting 1.05 MW demand was adequately

met by the available 1.1 MW generation capacity, as shown in Fig. 4.17b. The corresponding voltage profile is presented in Fig. 4.17a.

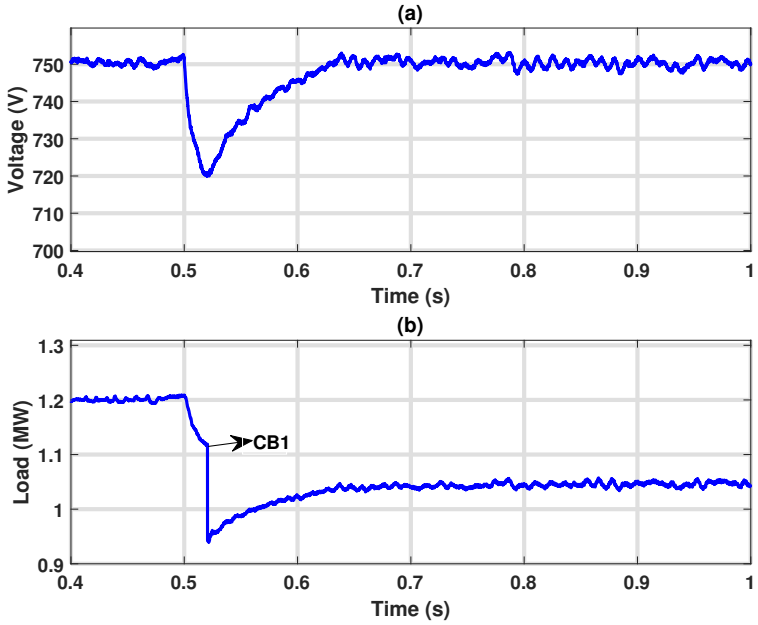

Figure 4.17: Performance of Combined based Scheme; **a)** DC Voltage **b)** Load power

4.4.3.4 Adaptive Scheme

The adaptive scheme employs both voltage and timer mechanisms enhanced with a Rate of Change of Voltage (RoCoV) criterion, which adjusts the shedding response based on disturbance severity. For this small disturbance, both the adaptive voltage-based and adaptive timer-based methods produced identical results.

CB1 was tripped at $t = 0.519$ s, the fastest response among all schemes, shedding 0.148 MW of load. The voltage was restored to 750 V shortly after disconnection, as shown in Fig. 4.18a, while the final load profile is given in Fig. 4.18b.

The voltage-based scheme responded at 0.525 s, the timer-based at 1.521 s, and the combined scheme slightly faster at 0.520 s. The adaptive scheme, using

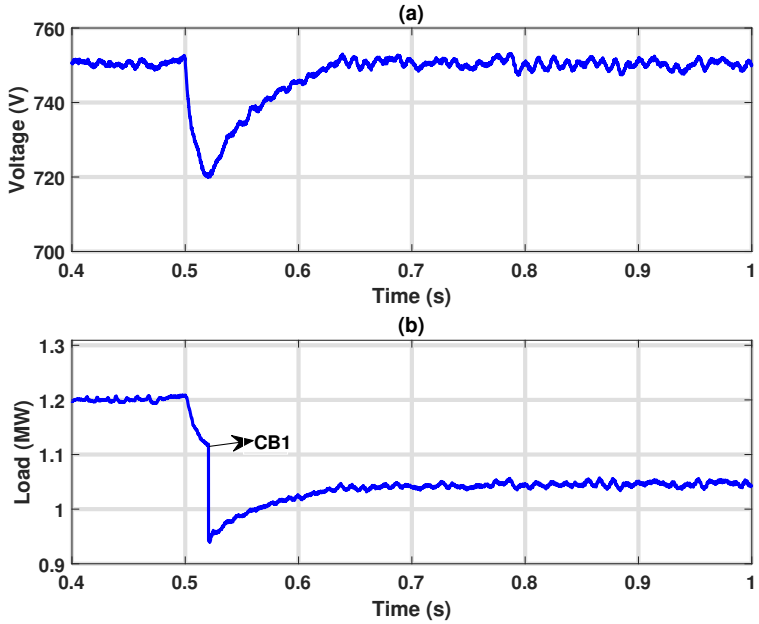

Figure 4.18: Performance of Adaptive based Scheme; **a)** DC Voltage **b)** Load power

Table 4.1: Summary of all Schemes in Case 1

Scheme	Trip Time CB1 (s)	V_{min} V	V_{Final} V
Voltage Based	0.523	719	750
Timer Based	0.521	719	750
Combined Based	0.520	720	750
Adaptive Based	0.519	720	750

a Rate of Change of Voltage (RoCoV) criterion, achieved the fastest response at 0.519 s. While all schemes restored voltage effectively, the adaptive method demonstrated the quickest reaction time to the disturbance, as shown in Table 4.1.

4.4.4 Case Study 2: Large Disturbance

At $t = 1.5$ s, an internal fault occurred, resulting in the disconnection of the wind turbine from the microgrid. In response, each BESS increased its output to a maximum of 0.41 MW. However, this was insufficient to meet the total demand

and sustain system stability. Consequently, the bus voltages experienced a sharp decline, leading to further instability in the microgrid.

4.4.4.1 Voltage Based Scheme

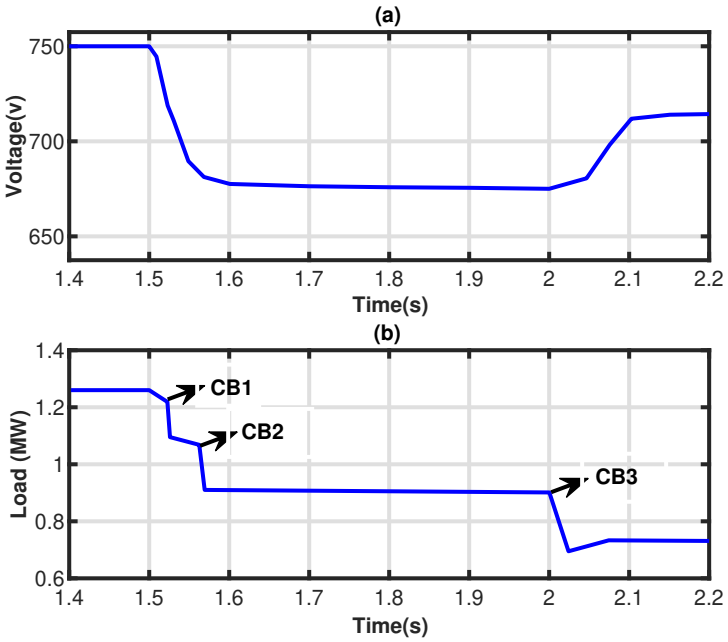

Figure 4.19: Performance of Voltage based Scheme; **a)** DC Voltage **b)** Load power

The voltage-based scheme trips the three CBs whenever the corresponding bus voltages fall below the preset thresholds V_{th_1}, V_{th_2}, and V_{th_3}, respectively. The performance of the voltage-based scheme is investigated using the voltage thresholds $V_{th_1} = 715$ V, $V_{th_2} = 690$ V, and $V_{th_3} = 675$ V. Based on the configuration of the circuit breakers, a total of 0.53 MW non-critical loads were shed (148 kW, 148 kW, and 234 kW at CB1, CB2, and CB3, respectively). The corresponding time for tripping the CBs were at: t = 1.54 s, 1.58 s, and 2.0 s as shown in Fig. 4.19 The last load-shedding step is delayed for 0.43s because the imbalance between the load and generation in the microgrid becomes small after the second group of loads is shed. Because of the delayed last load shedding step, the critical

loads experience a voltage sag for a relatively long time (about 0.43 s) before the last shedding step. The voltage was finally restored to 715 V. The load stands at 0.73 MW, which the generation of 0.815 MW can accommodate.

4.4.4.2 Timer Based Scheme

The timer-based scheme trips the three CBs whenever the corresponding bus voltages remain below the common voltage threshold V_{th} for periods longer than the T1, T2, and T3 delays, respectively. The performance of the timer-based scheme is investigated using preset voltage threshold, $V_{th_1} = 715\,\text{V}$, $V_{th_2} = 690\,\text{V}$, and $V_{th_3} = 675\,\text{V}$ respectively.

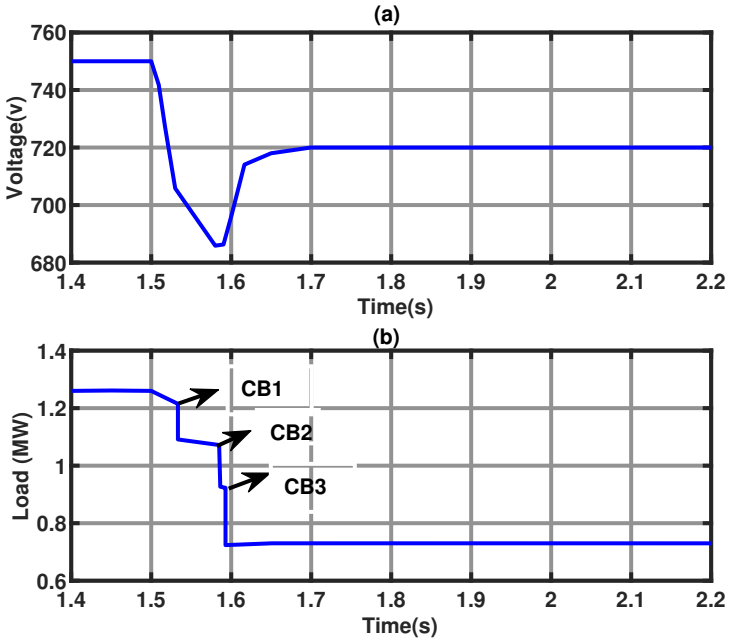

Figure 4.20: Performance of Timer based scheme: **a)** DC Voltage **b)** Load power

Time delays were set at 0.01 s, 0.02 s and 0.03 s. A total of 0.53 MW of non-critical loads were shed (148 kW, 148 kW, and 234 kW at CB1, CB2, and CB3, respectively). The time for tripping CB1, CB2, and CB3 were set at $t = 1.531$ s, 1.582 s, and 1.593 s as shown in Fig. 4.20. The voltage seen by the critical loads is

regulated at an acceptable voltage of 720 V within a relatively short time (about 0.17 s) after the disturbance. The loads were shed from 1.26 MW to 0.73 MW. The total generation of 0.815 MW can now accommodate the load. Due to the short time delays, the timer-based scheme effectively limited the magnitude and duration of voltage sags, as shown in Fig. 4.19. However, excessively short delays can lead to premature and unnecessary load shedding, as the timer may trigger disconnection before the voltage reaches its preset threshold [26]. Conversely, longer timer settings delay the shedding response, potentially resulting in deeper voltage sags or undervoltages. This trade-off highlights a key limitation of timer-based schemes in balancing fast response with selectivity.

4.4.4.3 Combined Based Scheme

The combined load shedding scheme uses the features of both voltage-based and timer-based schemes; hence, it trips the three CBs whenever the corresponding bus voltages fall below the thresholds $V_{th_1} = 715\,\text{V}$, $V_{th_2} = 690\,\text{V}$, and $V_{th_3} = 675\,\text{V}$ respectively, or remains below the common voltage threshold Vth = 675 V for periods longer than $\text{T}_1 = 0.01\,\text{s}$, $\text{T}_2 = 0.02\,\text{s}$, and $\text{T}_3 = 0.03\,\text{s}$ respectively. Fig. 4.21 shows that the combined scheme sheds 0.53 MW non-critical loads by

tripping the CB1, CB2, and CB3 at t = 1.517 s, 1.562 s, and 1.582 s, respectively. As a result, the lowest voltage seen by the critical loads is 685 V, and the voltage is regulated at 718 V within a relatively short time (0.16 s) after the disturbance. The results show that the combined load shedding scheme does not suffer from the voltage sag issues as in Fig. 4.19 and improves the voltage regulation time seen in Fig. 4.20.

4.4.4.4 Adaptive Voltage Based Scheme

The adaptive voltage thresholds used for all three steps of load shedding are automatically set between the range of 715 V to 675 V; this adaptive scheme

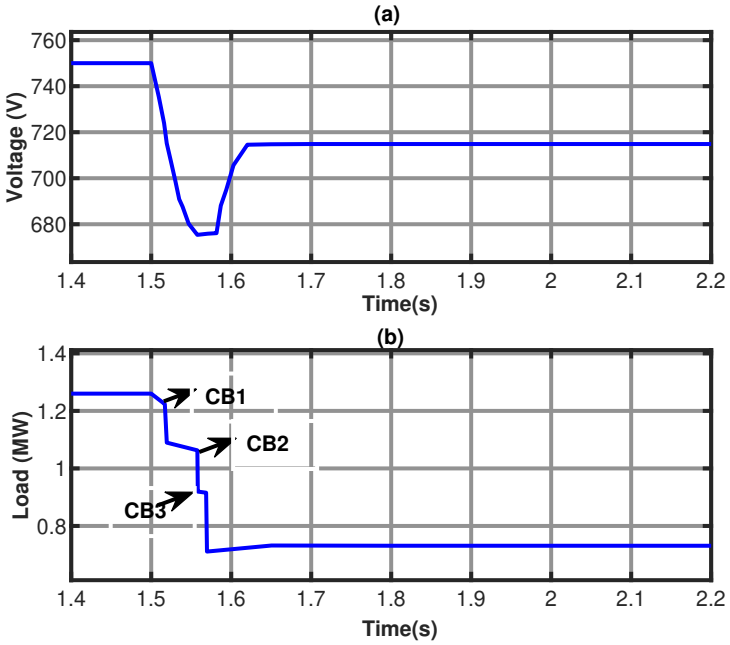

Figure 4.21: Performance of Combined based scheme: **a)** DC Voltage **b)** Load power

sheds all three groups of the non-critical loads as soon as the corresponding bus voltages fall below 690 V as shown in Fig. 4.22. This load shedding scheme trips the CB1 to CB3 at t = 1.516 s, 1.533 s, and 1.533 s, respectively. Due to the faster reaction of the scheme, the voltage does not fall below 690 V and is regulated at 720 V within a short span of 1.2 s after the occurrence of disturbance.

4.4.4.5 Adaptive Timer-based Scheme

The adaptive timer-based scheme sheds two groups of the non-critical loads by tripping the CB1 and CB2 at t = 1.519 s, and 1.665 s, respectively. The CB1 is tripped fast because the magnitude of the corresponding RoCoV is large. Consequently, the voltage seen by the critical loads does not fall below 685 V, and is regulated at 701 V within 0.17 s after the disturbance as shown in Fig. 4.23. This scheme prevents unnecessary tripping of the CB3 when the RoCoV becomes positive after the second step of load shedding.

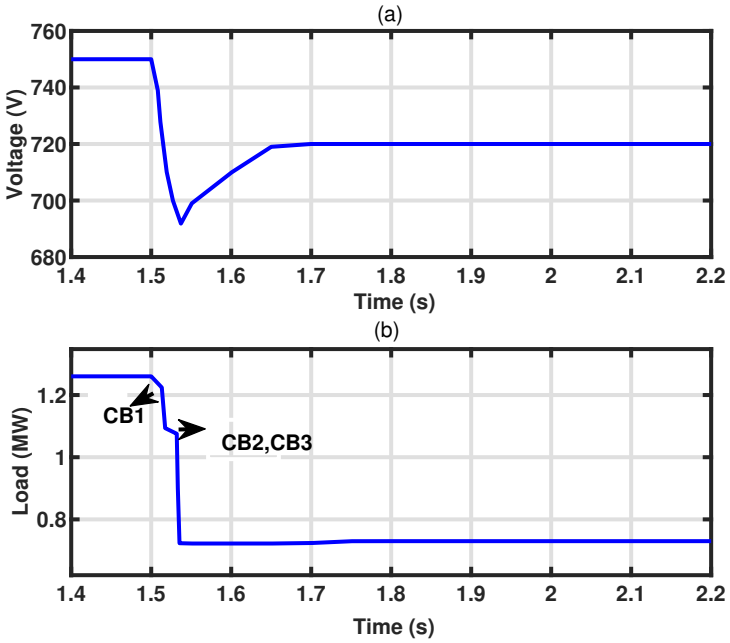

Figure 4.22: Performance of Adaptive Voltage based scheme: **a)** DC Voltage **b)** Load power

Fig. 4.24 summarises the voltage profile of all the load-shedding schemes presented. It shows the voltage drops and the voltage at which all the schemes are regulated.

Table 6.1 summarises the performance of five different load-shedding schemes, comparing them in terms of the trip times of circuit breakers (CB1, CB2, and CB3) and the minimum voltage (V_{min}) observed during the shedding process. Each scheme employs a different approach to triggering load shedding, with the adaptive schemes designed to adjust dynamically. In contrast, the conventional schemes rely on static parameters (like voltage or time). The performance comparison can be summarised as

- Fastest Trip times: The Adaptive Voltage scheme consistently shows the fastest trip times across all circuit breakers. This highlights its ability to respond quickly to real-time grid conditions, especially voltage variations,

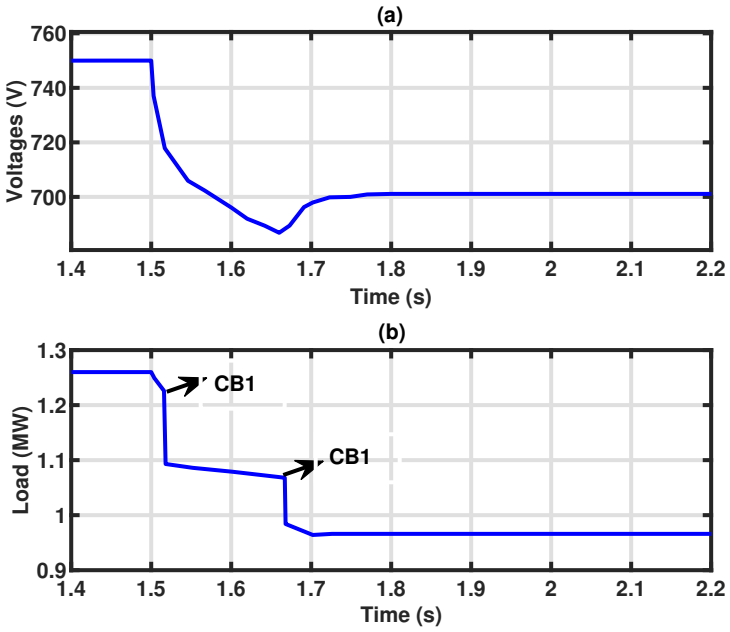

Figure 4.23: Performance of Adaptive Timer based scheme: **a)** DC Voltage **b)** Load power

ensuring faster protection actions.

- Slowest Trip Times: The Voltage Based scheme has the slowest trip time for CB3 (2.012 seconds), which is significantly longer than the other methods, indicating that it may be less efficient in responding to severe disturbances that require fast disconnection of loads.

- Voltage Stability: In terms of maintaining voltage levels, the Adaptive Voltage scheme performs best, achieving a minimum voltage of 690 V. This implies that this scheme is more effective in preventing voltage sags during load-shedding operations. The Voltage and Combined schemes have the same V_{min} of 675 V, indicating that these methods may result in slightly deeper voltage sags, which could negatively impact critical loads in the microgrid.

The Adaptive Voltage scheme demonstrates superior performance in terms of

Table 4.2: Summary of all Load Shedding Schemes in Case 2

Scheme	**Trip Time CB1 (s)**	**Trip Time CB2 (s)**	**Trip Time CB3 (s)**	$\mathbf{V}_{min}$ **(V)**
Voltage Based	1.542	1.583	2.012	675
Timer Based	1.531	1.582	1.593	685
Combined Based	1.517	1.562	1.582	675
Adaptive Voltage Based	1.515	1.533	1.533	690
Adaptive Time Based	1.519	1.665	-	685

trip times and voltage stability compared to other schemes, indicating that real-time adaptive mechanisms offer a significant advantage in microgrid protection. The Adaptive Time-Based scheme shows slightly longer trip times for CB2, and no data is available for CB3, which is likely due to the time delay and may indicate how it prioritises load shedding.

This limited performance impacts both operational efficiency and reliability. Over-shedding leads to underutilization of available resources and economic losses, while delayed shedding can result in voltage sags, equipment degradation, and system instability. The ultimate burden falls on critical consumers, such as hospitals, data centres, or remote communities, who may face interruptions due to the failure to safeguard essential loads. These shortcomings translate into tangible losses: increased power wastage, financial costs from downtime or equipment stress, degraded reliability indices, and weakened energy security, especially in isolated or weakly supported microgrids.

The analysis emphasises the necessity of an advanced load-shedding scheme that can optimally shed loads in the DC microgrid while maintaining system reliability and regulating voltage to an acceptable level, thereby improving the system's resilience.

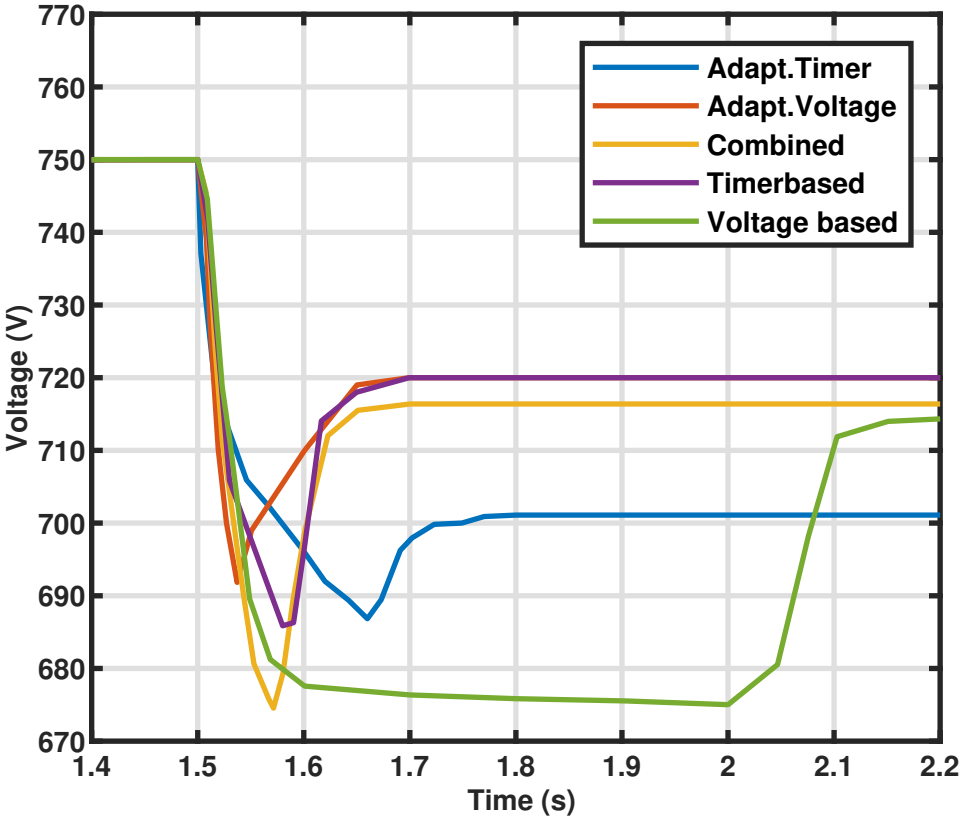

Figure 4.24: Voltage Comparison of the existing DC load shedding schemes

4.5 Summary

In this chapter, the performance of existing non-communication-based load-shedding schemes was investigated and compared using the IEEE 37-bus DC microgrid test system. The results demonstrated that conventional load-shedding strategies, which rely solely on fixed voltage or time thresholds, are prone to significant voltage sags and unnecessary disconnection of non-critical loads. In contrast, adaptive schemes incorporating RoCoV detect power imbalances rapidly, thereby reducing voltage deviations and improving response time. However, these schemes still have notable limitations, particularly their tendency to expose critical loads to lower voltage levels when shedding lower priority loads.

Simulation results showed that the voltage-based disconnects non-critical loads when bus voltages fall below predefined thresholds. While conceptually straightforward, its performance is highly sensitive to the choice of threshold margins. Narrow margins can cause over-shedding and underutilization of available generation, whereas wide margins allow excessive voltage deviations before corrective action, potentially endangering sensitive equipment.

The timer-based scheme sheds loads after a fixed delay if voltages remain below a set threshold. Short delays improve reaction speed but can result in premature disconnections, while longer delays reduce the risk of over-shedding but allow larger and potentially damaging voltage sags to occur before action is taken.

The combined scheme integrates both voltage and timer triggers, enabling load shedding when either condition is met. This improves operational flexibility and responsiveness but still inherits the fundamental weaknesses of both fixed-threshold and fixed-delay approaches, limiting its adaptability under varying disturbance scenarios.

The adaptive voltage-based scheme improves responsiveness by using RoCoV to adjust load shedding based on the rate of voltage change. However, it employs a lower voltage threshold for shedding lower-priority loads, which can expose critical loads to unacceptably low voltages in systems with many shedding steps. The adaptive timer-based scheme similarly uses RoCoV but attempts to reduce the number of shedding steps by employing longer delays; this, too, risks allowing critical loads to experience deeper voltage dips before corrective action occurs.

Across all schemes, these limitations affect both operational efficiency and reliability. Over-shedding wastes available resources and causes unnecessary economic losses, while delayed shedding risks voltage instability, equipment stress, and potential blackouts. In critical infrastructure settings such as hospitals, data centers, or remote communities, these shortcomings translate into tangible im-

pacts: power interruptions, degraded reliability indices, and reduced energy security, particularly in isolated or weakly supported microgrids.

Addressing these issues calls for more advanced, optimisation-driven load-shedding strategies that balance the need for fast response with the protection of critical loads. Such strategies should minimise unnecessary disconnections, preserve system stability, and maintain resilience during both minor and severe disturbances. The development of these improved load-shedding approaches for future DC microgrids will be presented in the following chapters.

Chapter 5

Disturbance Detection and Voltage Control in DC Microgrids Using Voltage Derivative Techniques

5.1 Introduction

One of the key challenges in DC distribution systems is ensuring effective disturbance detection and voltage control. The presence of voltage source converters (VSCs) within a DC microgrid necessitates rapid responsiveness, protection, and efficient isolation of faulted sections from the network. Due to the large DC capacitors and the low impedance of DC cables, system disturbances can lead to high transient currents and voltage spikes, posing significant risks to system stability and overall reliability.

This chapter explores two critical aspects related to disturbance detection and decentralised control in a DC microgrid. First, it introduces a novel method for detecting disturbances using voltage derivative (dv/dt) parameters, eliminating

the need for high-bandwidth communication systems. The proposed approach allows for the rapid detection of disturbances and precise estimation of their magnitude, ensuring swift response and system protection.

Additionally, the chapter presents an enhanced DC bus signalling control strategy, which utilises voltage threshold-based signalling to coordinate decentralised control of distributed energy resources (DERs) and loads. This strategy regulates bus voltages, maintains power balance, and minimises the adverse effects of unequal voltage levels on the coordinated participation of DERS. By reducing reliance on costly high-bandwidth communication systems, the approach enhances both system scalability and resilience.

To validate the effectiveness of these strategies, their performance is evaluated under various operating conditions and disturbance scenarios, considering both grid-connected and islanded operation modes of the DC microgrid. The proposed methods are verified through time-domain simulations conducted in MATLAB/Simulink using a detailed DC microgrid model, demonstrating their robustness in real-world applications.

5.2 System Configuration

The LVDC microgrid system described in this study is a modified version of the IEEE 37-node AC system, restructured into a four-area configuration, as illustrated in Figure 5.1. By dividing the LVDC microgrid into four distinct areas, the disturbance detection process is enhanced through improved fault localisation, better isolation capabilities, optimised protection coordination, and reduced computational complexity. This approach minimises disruptions within the system and ensures the efficient deployment of sensors, ultimately enhancing the overall reliability and stability of the microgrid.

The system operates as a microgrid with a DC voltage of 750 V, in compliance

with the IEC 60038 standard for LVDC systems. The DC microgrid features a 1 MW PMSG-based WT classified as DG4, connected in Area 4. Additionally, a combination of a 0.5 MW PV generation system and a 0.4 MW BESS are connected through node C and node A, representing DG2 and DG3 in Area 2 and Area 3, respectively. Furthermore, a 1 MW bidirectional DC/AC GTC interfaces the DC microgrid with the AC grid through a 0.75 kV/4.8 kV isolation transformer at node B, which constitutes DG1 in Area 1 of the microgrid. All converters are represented in detail using switching models, and the ratings and parameters of the distributed energy resources (DERs) are provided in the Appendix.

Each area of the system has a different load capacity: Area 1 can accommodate 1.5 MW, Area 2 has a capacity of 1.2 MW, Area 3 can handle 1.4 MW, and Area 4 also has a load capacity of 1.5 MW. Additionally, DC circuit breakers are installed at each bus to facilitate load-shedding in a specified area without disconnecting the entire system.

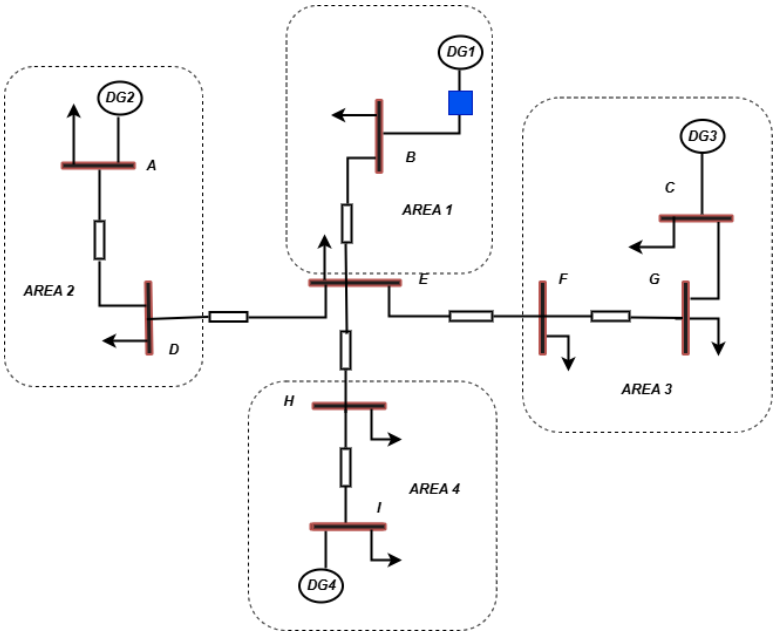

Figure 5.1: Restructured IEEE 37 DC bus System Model into 4 Areas.

5.3 Disturbance Identification

A key challenge in DC microgrid systems is the effective detection and localisation of disturbances. DC microgrids typically contain power electronics components such as converters, which require fast disturbance detection and the rapid isolation of faulted sections to maintain system stability. Large DC capacitors and low cable impedance in such systems can also result in high transient currents and sharp voltage spikes during disturbance events [148]. Additionally, any sudden imbalance between DG and load can cause significant voltage fluctuations within the microgrid, potentially compromising system stability and operational reliability.

To accurately identify the location of a disturbance within the microgrid, the Rate of Change of Voltage (RoCoV) is employed as a key indicator. By monitoring the local RoCoV at different bus voltages, the affected area can be effectively pinpointed. The RoCoV provides a clear and measurable response to disturbance events, making it a practical and reliable tool for disturbance detection and localisation in DC microgrids. The local Rate of Change of Voltage (RoCoV) at the bus voltages is mathematically expressed as follows:

$$\text{RoCoV} = \frac{V(t) - V(t - \delta t)}{\delta t} \tag{5.1}$$

where V is the system's voltage, t is the initial time, and dt is the time difference between two voltage samples [135]. The result of applying RoCoV in each area is presented in the subsequent subsection.

5.3.1 Application of the Voltage Derivative Algorithm in Detecting Disturbances

The disturbance identification process employs the voltage derivative (dv/dt) method, as depicted in the block diagram in Figure 5.2. It begins with measuring the DC bus voltage (V_{dc}), which is then passed through a low-pass filter to reduce the impacts of switching ripples and noise. The filters are of the fourth-order Butterworth type, and the cutoff frequency is 0.5kHz. The sampling time of the voltage signal is 10 ms. This step ensures that only significant voltage variations are used in the disturbance detection.

After filtering, the process calculates the voltage derivative (dv/dt or RoCoV) of the filtered V_{DC} signal as shown in equation (5.1). The voltage derivative is a key indicator for identifying disturbances in the DC microgrid, as disturbance events or sudden load changes often show up as sharp voltage drops with large negative derivatives.

The obtained dv/dt is subsequently fed into an adaptive threshold calculation block, where an adaptive threshold voltage (V_{th}) is determined based on the rate of voltage change [115], as explained in equations (5.2) and (5.3).

$$V_{th} = \begin{cases} V_{min}, & -k_1 < \dfrac{dV_{dc}}{dt} \leq 0 \\ V_{min} + m\left(\dfrac{dV_{dc}}{dt} + k_1\right), & -k_2 \leq \dfrac{dV_{dc}}{dt} \leq -k_1 \\ V_{max}, & -\infty < \dfrac{dV_{dc}}{dt} < -k_2 \end{cases} \tag{5.2}$$

where V_{min} and V_{max} are the minimum and maximum voltage limits. The constants k_1 and k_2 identify the values of the RoCoV at which V_{th} reaches the maximum and minimum limit of voltages.

The system checks if the condition RoCoV $< -k_1$ is met, where k_1 is a preset threshold based on system characteristics. If the derivative exceeds this threshold

negatively, it signifies a disturbance within the microgrid. Once a disturbance is identified, the process moves to the final output K, which acts as a trigger or control signal. This activates protection mechanisms such as load shedding, voltage control, or system reconfiguration to contain the disturbance and sustain system stability. This systematic approach, from monitoring V_{DC} to generating output K, ensures fast and accurate disturbance detection and localisation within the DC microgrid.

Beyond disturbance detection, this method provides valuable information about the magnitude and geographic impact of disruptions at each bus within the system, enabling the assessment of the propagation and severity of disturbances. The sensitivity of the algorithm is validated by sequentially applying identical disturbances at different locations and analysing their effects on system performance. The disturbance magnitude at each location is also compared against a predefined acceptable range determined by the voltage derivative algorithm, ensuring consistent and accurate disturbance characterisation across the microgrid.

5.3.1.1 Cases Explained

The magnitude of disturbances in this case study is classified into three categories: small, moderate, and severe. It is essential to define the RoCoV thresholds $(k1, k2)$ alongside the voltage limits (V_{min}, V_{max}). For this case study, the DC bus voltage (Vdc) is designed to operate around 750 V, with the microgrid's design limits set as $V_{min} = 690V$ and $V_{max} = 850V$. The RoCoV thresholds are carefully chosen to match the sensitivity required for disturbance detection, with $k_1 = 500V/s$ representing the boundary for small disturbances and $k_2 = 2000V/s$ for severe disturbances. Using these defined values, the slope m required for the adaptive threshold calculation can be computed using:

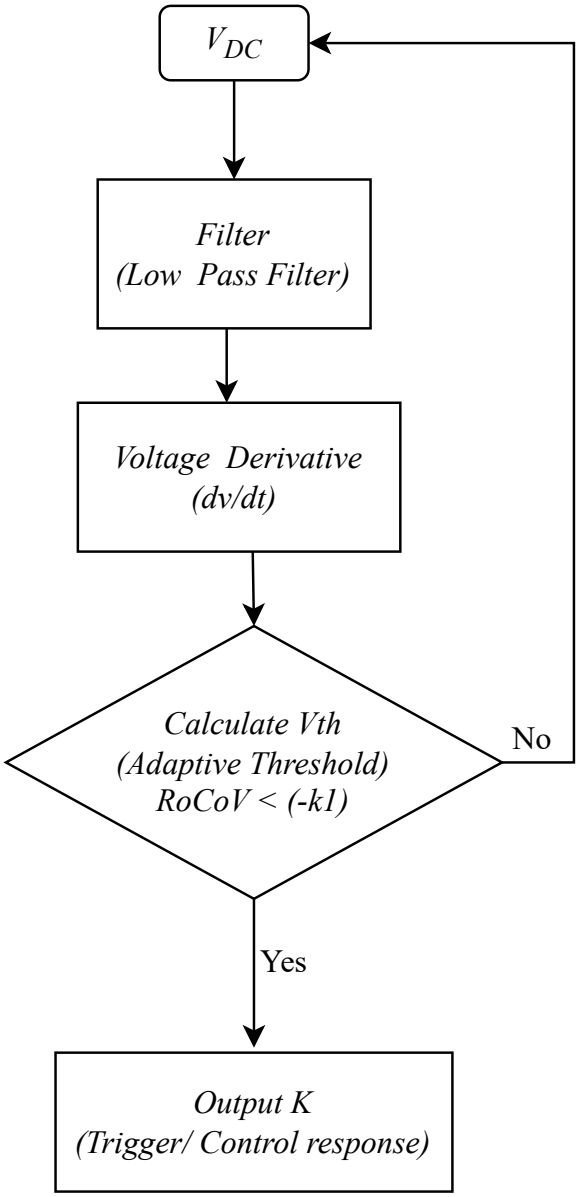

Figure 5.2: Flowchart of Disturbance Identification

where;

$$m = \frac{V_{max} - V_{min}}{k_1 - k_2} \tag{5.3}$$

where:

- V_{max} is the maximum DC bus voltage,
- V_{min} is the minimum DC bus voltage,
- k_1 and k_2 are the RoCoV thresholds defining the boundaries for moderate and severe disturbances, respectively.

Using the design values:

$$V_{max} = 850 \text{ V}, \quad V_{min} = 690 \text{ V}, \quad k_1 = 500 \text{ V/s}, \quad k_2 = 2000 \text{ V/s},$$

the slope can be computed as:

$$m = \frac{850 - 690}{500 - 2000} = \frac{160}{-1500} = -0.1067$$

- **Small or No Disturbance:**

$$-k_1 < \frac{dV_{dc}}{dt} \leq 0 \tag{5.4}$$

In this range, the rate of voltage drop is small, indicating a slow decrease or stable voltage. The threshold is set to the minimum value:

$$V_{th} = V_{min} \tag{5.5}$$

This reflects a normal or lightly disturbed operating state, and no control action is taken.

- **Moderate Disturbance:**

$$-k_2 \leq \frac{dV_{dc}}{dt} \leq -k_1 \tag{5.6}$$

Here, the voltage drop is more pronounced. The threshold increases linearly with the magnitude of the negative RoCoV:

$$V_{th} = V_{min} + m\left(\frac{dV_{dc}}{dt} + k_1\right) \tag{5.7}$$

This adjustment helps the system become more sensitive and reactive to growing disturbances.

- **Severe Disturbance:**

$$\frac{dV_{dc}}{dt} < -k_2 \tag{5.8}$$

This condition reflects a sharp voltage drop, typically caused by a large disturbance or sudden generation loss. The threshold is set to its maximum as shown in (5.8), this places the system on high alert, enabling immediate control actions such as voltage regulation and load shedding.

$$V_{th} = V_{max} \tag{5.9}$$

This case ensures a smooth and proportional transition in the threshold value between mild and severe disturbance conditions.

To manage disturbances effectively, the system employs a dynamic voltage threshold V_{th} that adjusts based on RoCoV, a widely recognized indicator of power imbalance in DC microgrids.A negative RoCoV a loss of generation or sudden increased in loads, while a positive RoCoV reflects excess generation. In this study, thresholds for categorizing disturbance severity were determined em-

pirically through simulation-based sensitivity analysis using the IEEE 37-bus DC microgrid. These thresholds reflect the system's observed response characteristics under various fault and imbalance scenarios.

Under normal conditions in this case study, when RoCoV is above $-500V/s$, no corrective action is required, and the V_{th} is maintained at a nominal value of approximately 750 V. During moderate disturbances, where RoCoV falls between -500 V/s and -2000 V/s, V_{th} increases linearly according to the computed slope m. This adaptive adjustments primes the system for potential voltage control interventions while avoiding premature load shedding.

In the event of severe disturbances, identified by RoCoV dropping below -2000 V/s, the system responds by setting V_{th} to its minimum value of 690 V, thereby triggering immediate voltage regulation mechanism and possible load shedding to maintain system stability. This adaptive strategy enables the microgrid to distinguish between minor fluctuations and critical events, allowing for graded responses that balance resilience with minimal disruption to load continuity.

5.3.2 Simulation Result

The impact of RoCoV on disturbance is illustrated in the simulation results provided below. The analysis presented in Figure 5.3 below, demonstrates that when a 500 kW disturbance occurs in Area 1, the voltage derivative (-k1) is highest in Area 1, while the responses in Area 4 are comparatively smaller. This indicates that Area 1 is relatively closer to the disturbance. As the effects of the disturbance spread further from the source, they diminish, resulting in even smaller responses observed in Areas 2 and 3, as illustrated in Figure 5.3b. This pattern shows that the impact of the disturbance is strongest near its origin and decreases with distance.

To validate this observation, similar analyses were conducted for disturbances in Areas 2, 3, and 4. In Figure 5.4a, a 250 kW disturbance was introduced in

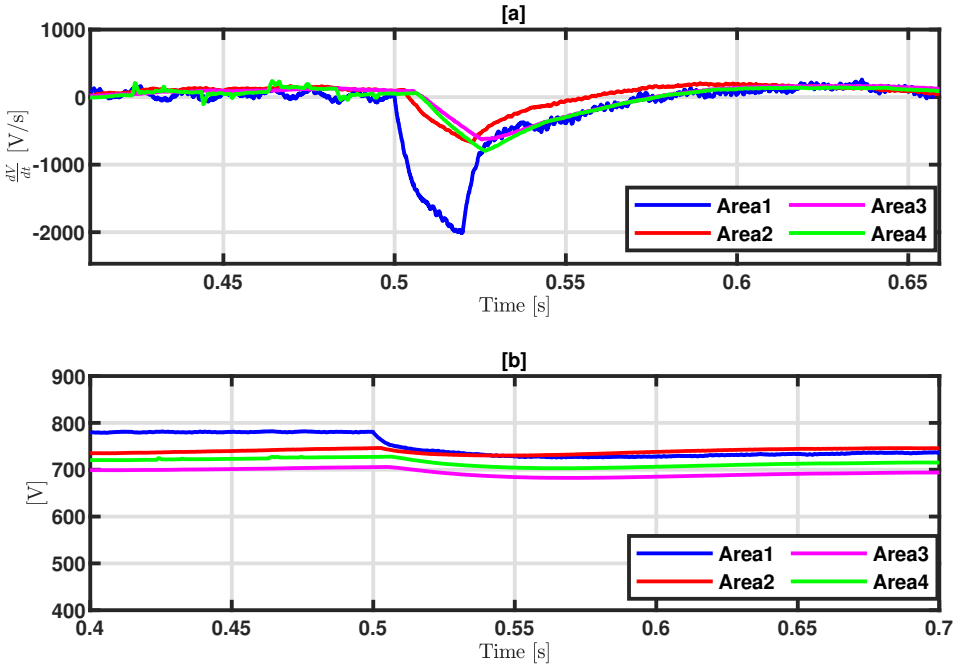

Figure 5.3: Disturbance at Area 1

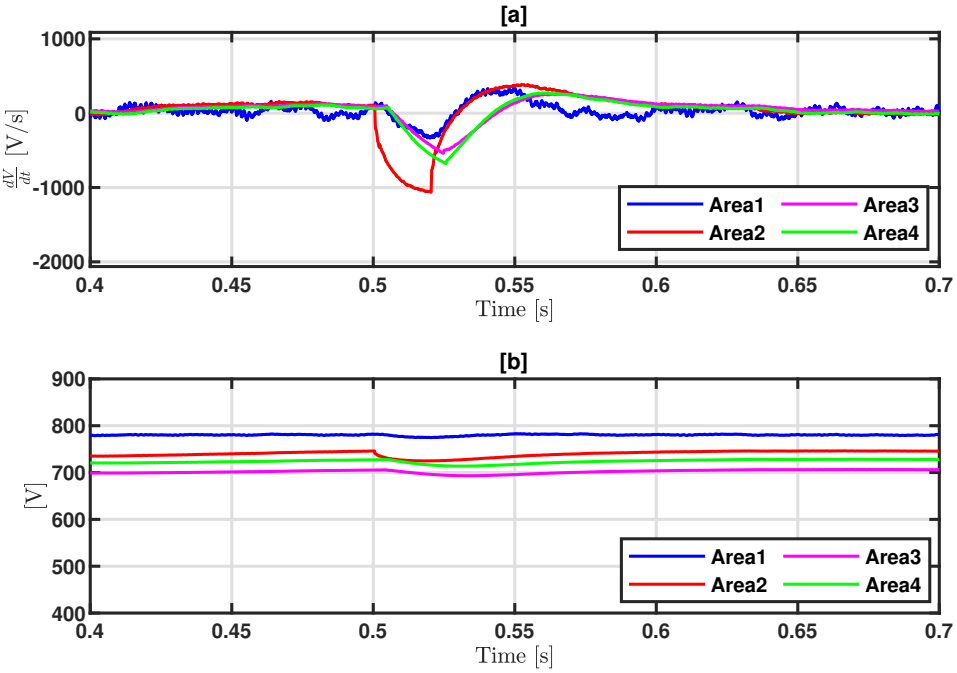

Figure 5.4: Disturbance at Area 2

Area 2, leading to the highest differential voltage response of -1000 V/s. This was followed by Area 4 with -600 V/s, Area 3 with -560 V/s, and the lowest response in Area 1 at -250 V/s. The effects on the bus voltages are presented in Figure 5.4b.

In another scenario, when a 500 kW disturbance was introduced at the far end of Area 3, the highest voltage differential response occurred in Area 3, measuring -2000 V/s. This was followed by Area 4 at -200 V/s, Area 2 at -180 V/s, and the lowest impact in Area 1 at -90 V/s, as shown in Figure 5.5a, with the voltage effects illustrated in Figure 5.5b.

In the final scenario, an 800 kW disturbance was applied in Area 4. Figure 5.6 shows that the highest voltage response occurred in Area 4 at -2850 V/s, followed by Areas 3 and 2, which had responses of -251 V/s and -249 V/s, respectively. Area 1 exhibited the lowest voltage response. to its greater distance from the disturbance source.

In all cases, the results consistently show that the highest voltage derivative responses occur at the location of the disturbance, with decreasing responses in areas farther away. This consistent pattern emphasises the localised impact of disturbances within the microgrid system, as highlighted in [149].

In conclusion, the analysis conducted across various areas of the microgrid system reveals a consistent pattern in how disturbance impacts are distributed. Regardless of the disturbance's magnitude or location, the highest voltage differential responses were consistently nearest to the disturbance source. As the disturbance propagated outward, the voltage response diminished, demonstrating the localised nature of these impacts.

This pattern was evident in different scenarios, including a 500 kW disturbance in Area 1, a 250 kW disturbance in Area 2, a 500 kW disturbance in Area 3, and an 800 kW disturbance in Area 4. In each case, the most significant voltage

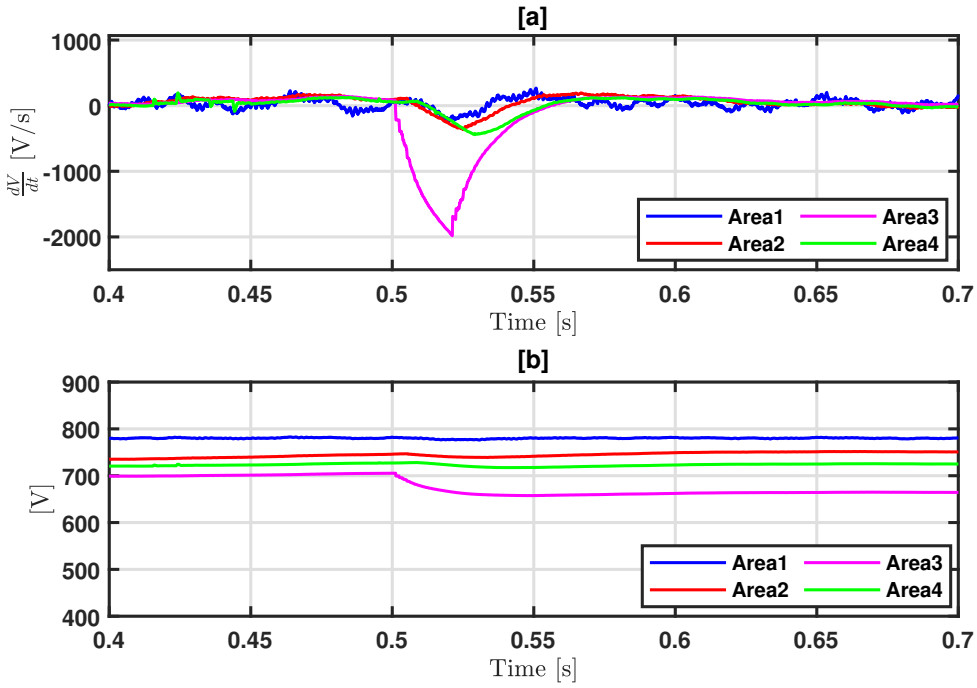

Figure 5.5: Disturbance at Area 3

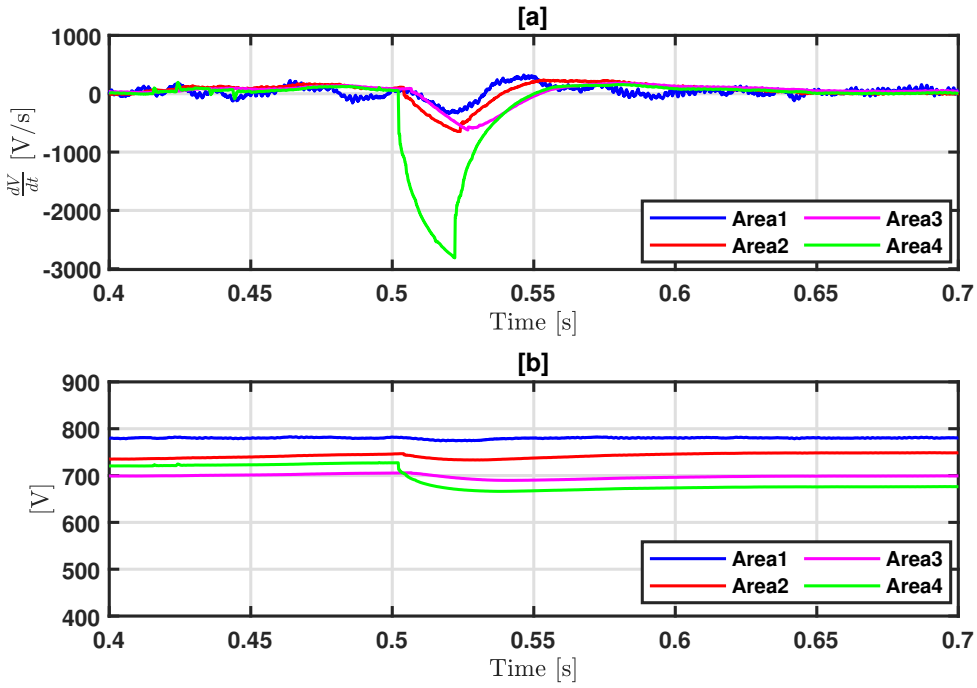

Figure 5.6: Disturbance at Area 4

fluctuations occurred at the disturbance origin, with progressively smaller effects as distance increased.

These findings emphasise the importance of localised monitoring and managing disturbances within DC microgrids. The limited spatial extent of voltage disturbances suggests that targeted control actions and protection strategies can be effectively implemented to reduce their impacts. It also underscores the necessity for accurate and responsive voltage monitoring systems, which are essential for maintaining the operational stability, reliability, and overall resilience of DC microgrids, particularly in decentralised, remote, or communication-limited environments.

5.4 DC Microgrid Control

Once a disturbance is detected, as discussed in the previous section, precise localisation and control become essential for minimising system disturbances and ensuring the coordinated management of DERs and loads. Effective disturbance management helps protect the healthy sections of the system, reducing the likelihood of further disruptions. Additionally, robust disturbance control is crucial for preventing voltage imbalances across buses, which could otherwise disrupt the coordinated efforts of DERs to stabilise bus voltages. This section implements an adaptive DC Bus signalling control to maintain stable performance despite disturbances. This strategy ensures effective voltage regulation, power sharing, and a load-shedding mechanism. The following sections will evaluate the effectiveness of the proposed control strategy under various operating conditions and disturbance scenarios.

5.4.1 Conventional Droop Control

The study of droop control is fundamental to effective voltage and frequency regulation in microgrid systems, particularly in managing the coordinated operation of synchronous generators and inverter-based resources within the microgrid [150]. Droop control plays a critical role in enabling the parallel connection of multiple generation units while proportionally sharing load based on their power capacities. Each generation unit is assigned specific voltage droop characteristics, which define allowable deviations from nominal values in response to variations in load demand [151]. This decentralized control approach ensures stability, enhances scalability, and eliminates the need for high-bandwidth communication between DERs, making it especially suitable for islanded or remote microgrid configurations.

In a grid-connected DC microgrid, the GTC is responsible for maintaining stable DC bus voltages by operating in constant voltage control mode. However, during the transition to islanded mode, this responsibility shifts to the BESS, which switches to droop control mode to stabilise the DC terminal voltages [48].

In conventional droop control, the converter generates an output current that is directly proportional to the deviation of the DC bus voltage from a predefined reference value in Figure 5.7. This method allows multiple DERs to operate in parallel without requiring communication infrastructure, thereby facilitating decentralised control and enhancing the robustness and scalability of DC microgrid operations [78].

The relationship between voltage and current in a droop-controlled DER system is described in equation (5.11). The reference voltage, V_{dc}^{*}, represents the voltage level when no load is applied. The output voltage, output current, and virtual resistance of the i_{th} DER's is represented by V_{dci}, I_{dci}, and R_{di}, respectively. Figure 5.7 depicts the droop characteristic of equation (5.12), where the slope of

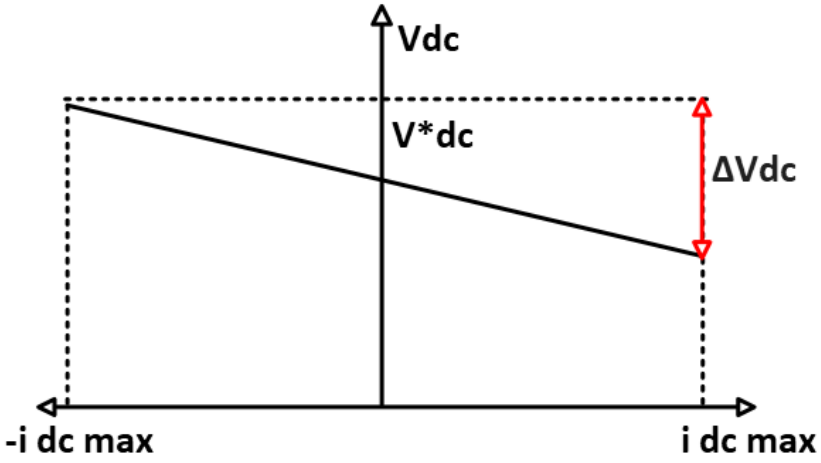

Figure 5.7: Voltage-current characteristic of a droop-controlled DER

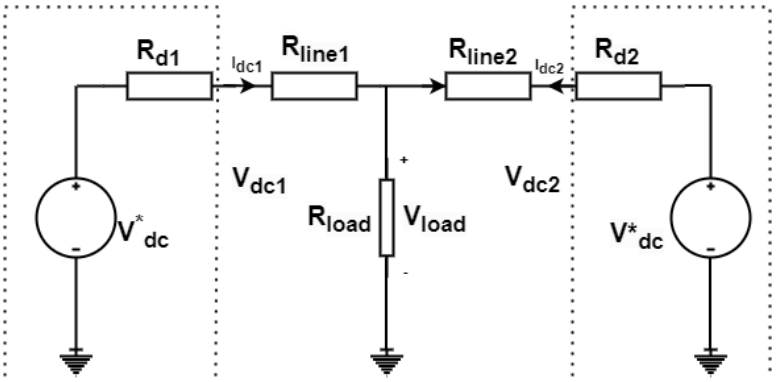

Figure 5.8: Simplified model of a DC microgrid with two droop-controlled converters

the voltage-current (V-I) curve corresponds to the value of R_{di} [151], [152].

$$V_{dci} = V_{dc}^{*} - R_{di} I_{dci} \tag{5.11}$$

Figure 5.8 shows a simplified model of a DC microgrid with two DERs supplying power to a load. Considering the line resistances R_{line1} and R_{line2}, the V-I characteristics of the DERs can be calculated as in [93];

$$V_{load} = V_{dc}^{*} - R_{d1} I_{dc1} - R_{line1} I_{dc1} \tag{5.12}$$

$$V_{load} = V_{dc}^{*} - R_{d2}I_{dc2} - R_{line2}I_{dc2} \tag{5.13}$$

Equation (5.5) describes the relationship between the DERs' output currents. In practice, the line resistances are neither necessarily equal nor negligible. Hence, to achieve acceptable power sharing between the droop-controlled DERs in the simple DC microgrid of Figure 5.9, the virtual resistance should be determined to satisfy equation (5.6). However, (5.3) and (5.4) do not apply to realistic DC microgrids with multiple loads and more than one DER may be connected to each line.

$$\frac{I_{dc1}}{I_{dc2}} = \frac{R_{d2} + R_{line2}}{R_{d1} + R_{line1}} \tag{5.14}$$

$$\frac{R_{d1}}{R_{d2}} = \frac{R_{line1}}{R_{line2}} \tag{5.15}$$

The conventional droop control strategy is a simple operating characteristic used for all DER operating conditions in the islanded microgrid. The values of virtual resistances significantly affect system stability, voltage regulation, and power-sharing accuracy. Smaller virtual resistances result in more precise voltage regulation but less accurate power-sharing, and vice versa. The DC Bus Signalling (DBS) control strategy proposed in the next section improves DC microgrid voltage regulation and power sharing by using more advanced operating characteristics.

5.5 Adaptive DC Bus Signalling Control

The DBS control strategy [20, 86, 87] uses predefined DC voltage ranges to determine the operational modes of DERs and GTC. Each component's mode changes instantly when the corresponding bus voltage falls within these ranges. Current DBS control strategies differ in how they define these modes. Still, they often

require high-rated GTCs or BESSs to manage power imbalances or excessively curtail renewable generation instead of storing excess energy [88,89]. This section proposes an enhanced DBS control strategy for DC microgrids that includes an adaptive algorithm for DERs. This algorithm dynamically adjusts voltage thresholds in response to varying load demands and generation levels, improving system responsiveness and efficiency. By selectively activating power generation, this approach reduces the need for large GTC and BESS installations, thereby enhancing cost efficiency and optimizing DER utilization. The proposed strategy's performance is evaluated under grid-connected and islanded conditions, testing various scenarios of generation fluctuations and load disturbances. Results indicate that the enhanced DBS control effectively improves the reliability and resilience of DC microgrids, especially in areas with limited infrastructure.

5.5.1 Voltage Thresholds

The voltage threshold utilisation is designed to determine the operational states of the proposed control, which requires careful selection [153]. Bus voltage deviations may exceed acceptable levels if the voltage thresholds are too far apart. Conversely, setting the thresholds too close together can lead to unnecessary curtailment of the output power of DERs [154]. Additionally, inaccuracies in sensors and voltage ripples can result in oscillatory behaviour. Therefore, for effective coordination of the operating characteristics of all DERs, voltage thresholds must be selected judiciously [148].

In this study, the chosen voltage thresholds are V_{th1}= 770 V, V_{th2}= 750 V, V_{th3}= 720 V, V_{th4} = 675V and V_{th5} = *loadshedding* which limit the range of voltage deviations to $\pm$10% as indicated in [121]. This setting ensures no gaps or overlaps between operational states, enabling smooth transitions even under large disturbances. Recognising that inappropriate voltage thresholds can negatively impact power-sharing and voltage regulation within the DC microgrid is

important.

5.5.2 Operation states of proposed DBS control

The proposed strategy for controlling RESs, BESSs, and GTCs involves dividing their operation into four states. These states are illustrated in Figure 5.9. The operation state of each DER and GTC is determined by comparing its DC bus voltage with five voltage thresholds, namely V_{th1}–V_{th5}. Under steady state, the power balance equation for the DC microgrid can be expressed using the power balance equation [86], [89], [93].

$$P_{RES} + P_{BESS} + P_{GTC} - P_{LOAD} = 0 \tag{5.16}$$

where P_{RES},P_{BESS},P_{GTC}, and P_{LOAD} represent the total active powers of the individual RES and load, respectively. It is recommended that only one of the power sources be adjusted at a time using the proposed DBS control strategy in each state. This helps to maintain power balance and regulate the DC bus voltages. However, in non-compact microgrids where bus voltages are unequal, it may be necessary for more than one converter to adjust their power simultaneously to regulate the bus voltages.

5.5.2.1 Operation State 1

This state represents the scenario where the excess power in the DC microgrid is beyond the level that can be exported by the GTC or absorbed by BESS(s), and thus renewable power generation has to be curtailed. The GTC exports its maximum power to the AC grid when the DC microgrid is grid-connected. The BESS(s) operate in full-power charging adjust its input power to maintain a balance and regulate the DC voltage.

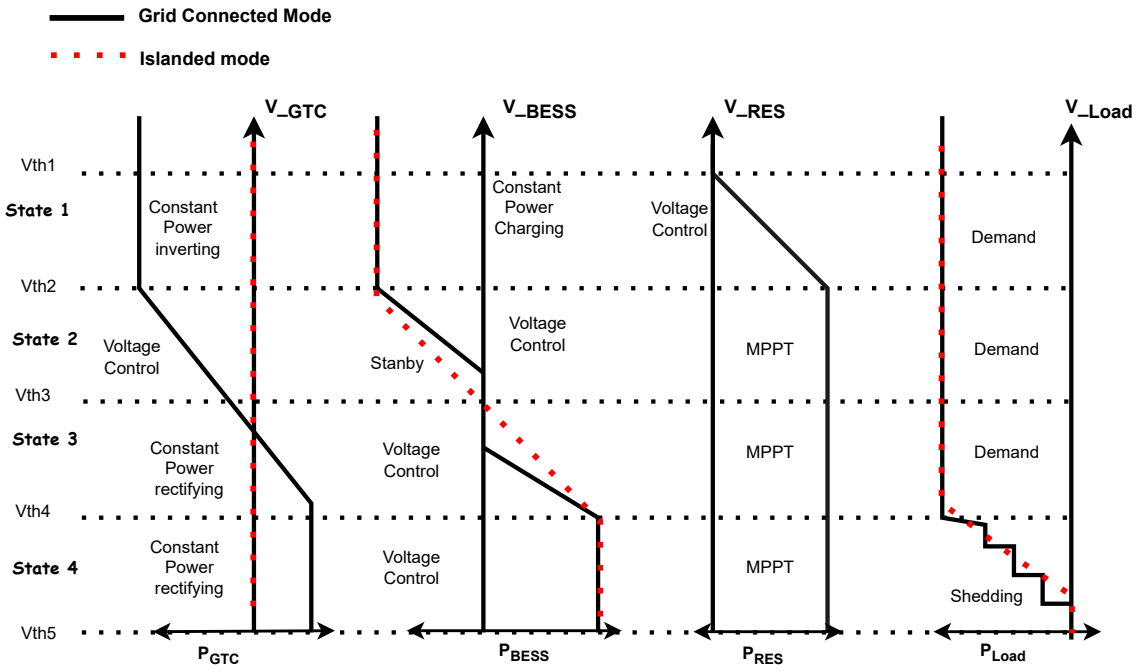

Figure 5.9: Proposed DBS operation states of GTC, BESS, RES and Load

5.5.2.2 Operation state 2

In operation state 2, the GTC and BESS work together to maintain power balance in the DC microgrid during abnormal conditions. When the microgrid is connected to the primary grid, the GTC is responsible for regulating voltage. However, when operating in islanded mode, the BESS takes over voltage regulation while RESs function in MPPT mode.

5.5.2.3 Operation state 3

In this operational state, BESSs can effectively compensate for power deficits within the DC microgrid without requiring load shedding based on specific thresholds. When connected to the grid, the GTC optimally imports power from the AC grid. The RESs operate in MPPT mode. Additionally, the BESSs are dynamically configured to regulate their output power, ensuring balance and facilitating

DC voltage regulation.

5.5.2.4 Operation state 4

In this final state, when the microgrid's power shortage surpasses the capacity of the GTC or BESS, it is necessary to disconnect non-critical loads to prevent voltage collapse. The GTC receives the maximum power available from the AC grid. Renewable energy sources function in Maximum Power Point Tracking (MPPT) mode, while BESSs operate in full power discharging mode.

5.5.3 Structure of Controllers

5.5.3.1 BESS Control

The BESS plays a critical role in maintaining power balance in both grid-connected and islanded modes by regulating the DC bus voltage. Figure 5.10 illustrates the control block diagram of the BESS. To ensure the safe and reliable operation of the system, the BESS must operate within predefined voltage and state of charge (SOC) ranges. Exceeding these ranges may lead to battery degradation or unsafe operation; hence, when the SOC approaches its maximum or minimum limits, the BESS controller disables switching actions to prevent overcharging or deep discharging, in line with practices recommended in [86]. In the grid-connected mode, the BESS voltage references limits $V_{dc-H}*$ and $V_{dc-L}*$ are set to 1.150 and 0.980, respectively, while the droop gain K_1 governs the proportional power response to voltage deviation. In islanded mode, tighter control is necessary due to the absence of grid support. Therefore, the voltage reference is fixed at 0.99 p.u., and the droop gain K_2 at 0.075 is applied to regulate power exchange. However, the choice of these parameters is not arbitrary—they must be tuned carefully to ensure stable voltage regulation, appropriate power sharing, and SOC sustainability. For instance, a larger droop gain improves responsiveness but may lead

to instability or aggressive SOC swings, while a smaller gain offers smoother operation at the cost of slower disturbance mitigation. Similarly, the voltage limits (V^*_{dc-H}) and (V^*_{dc-L}), should be set based on system voltage tolerance, converter dynamics, and battery chemistry. Improper tuning may cause either unnecessary BESS activation (leading to faster wear) or delayed response, resulting in system undervoltage or overvoltage. Tuning is often performed through iterative simulation and sensitivity analysis under different loading and fault conditions.

The control operates as follows: if the DC voltage (V^*_{dc}) drops below the lower threshold (V^*_{dc-L}), BESS injects power. Conversely, if V^*_{dc} rises above the upper threshold (V^*_{dc-H}), the BESS absorbs excess power to destabilize the voltage. When V^*_{dc} is within the acceptable limits, the BESS either operates in a standby mode with minimal intervention or remains idle. The transition between operating modes is autonomously detected using the RoCoV), as detailed in [86, 133, 155]. While the control framework is effective, proper parameter tuning is essential to balance voltage stability, battery life, and system resilience, especially in high-renewable or fluctuating load environments.

5.5.3.2 PV Control

The PV system is designed to extract maximum available power through MPPT and regulate the DC bus voltage via a boost converter interfaced with a DC grid. DBS determines the mode of operation for each PV (voltage control or MPPT mode) based on the DC voltage value of the connected bus. In voltage control mode, the control block within the boost converter receives a reference voltage (typically denoted V_{dc}) and outputs the reference inductor current needed to regulate the output. This reference current is then used in a current-controlled inner loop, where the duty cycle of the boost converter's PWM signal is calculated in the Duty Control block. This nested control structure enables fast current regulation and stable voltage tracking under varying generation and load

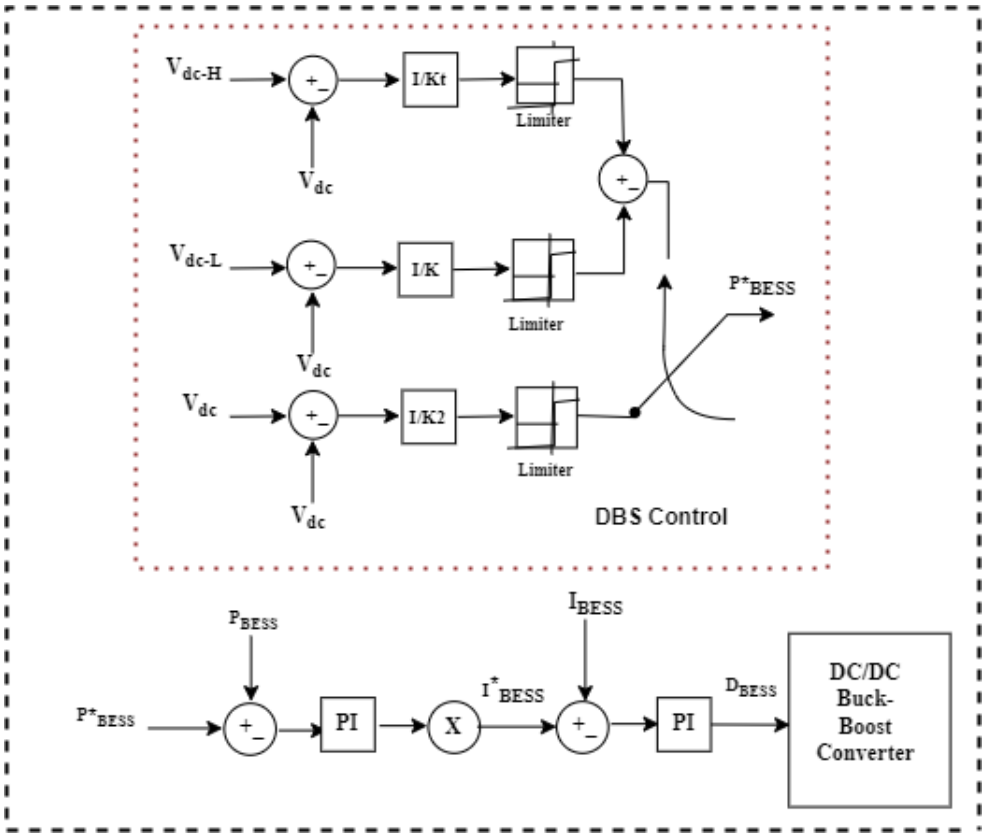

Figure 5.10: Control block diagram of BESS

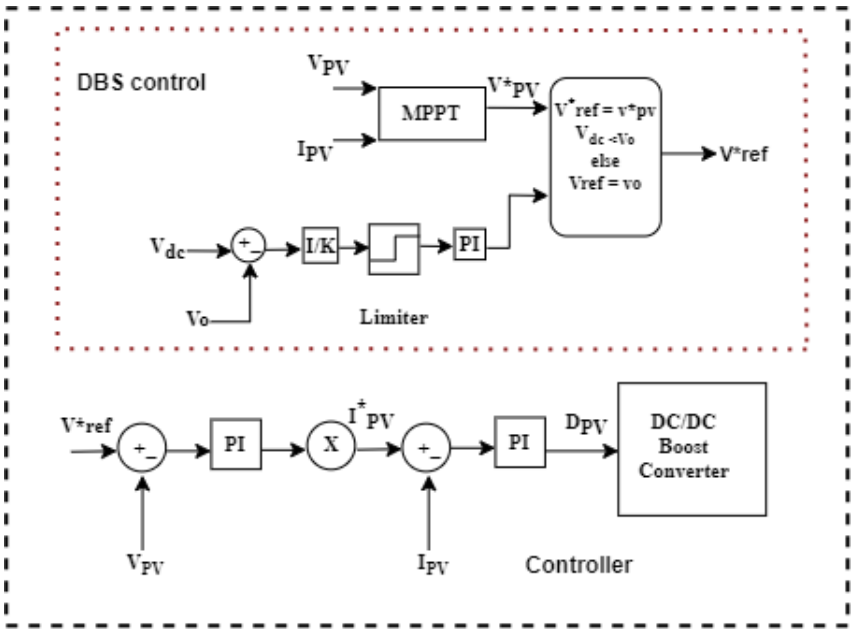

Figure 5.11: Control block diagram of PV

conditions [86], [156], [157].

The control parameters, specifically the voltage reference V_{dc} is 1.09p.u. and the droop garin K is 0.024, play a critical role in defining the converter's response characteristics. The voltage reference sets the steady-state target for the bus voltage, while the droop gain determines how aggressively the PV unit responds to voltage deviations affecting both voltage stability and power sharing among multiple units. Figure 5.11 presents the complete control block diagram of the PV system, illustrating the integration of MPPT, voltage regulation, and current control functionalities under a unified framework. Proper tuning of these parameters is essential to ensure seamless mode transitions and prevent power oscillations or overcompensation, especially in multi-source DC microgrids with distributed control schemes.

5.5.3.3 WT Control

The PMSG-type wind turbine (WT) control system consists of two controllers: the pitch angle controller and the VSC controller. The pitch angle controller is responsible for regulating the aerodynamic torque by adjusting the blade angle to maintain the turbine speed within its optimal operational range, especially under high wind conditions. This prevents mechanical overspeed and protects the turbine from structural stress. The VSC controller, on the other hand, operates in the d–q reference frame, implements vector control to manage both active and reactive power flows [158]. The control mode of the VSC is determined by the DBS operation state, which assesses system conditions. In MPPT mode, the VSC regulates the generator-side converter to maximise the energy extracted from wind by controlling the active power. In voltage control mode, typically activated during disturbances or grid disconnection, the VSC adjusts its output to regulate the DC bus voltage, thereby contributing to system stability. Simultaneously, the VSC manages reactive power to maintain the stator terminal voltage within

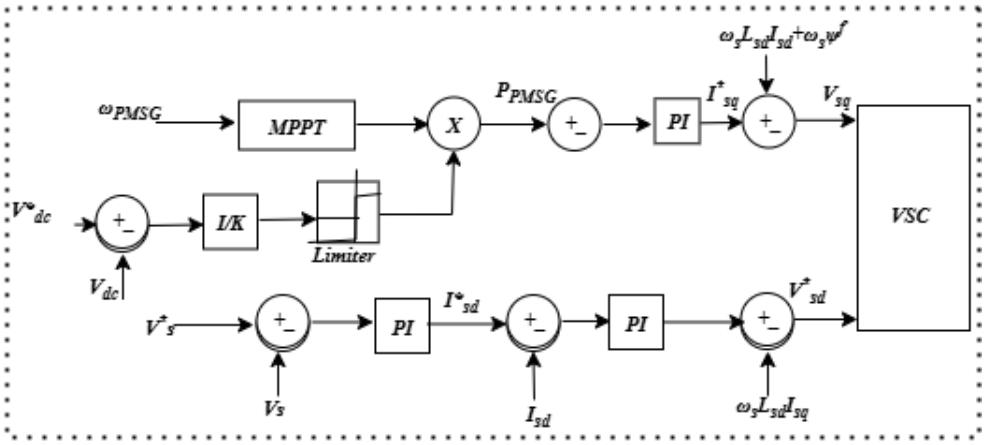

Figure 5.12: Control block diagram of WT

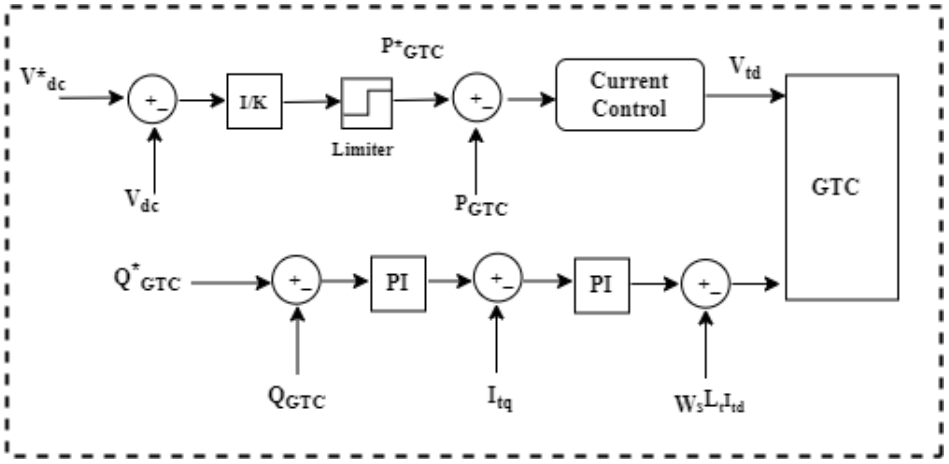

Figure 5.13: Control block diagram of GTC

acceptable limits [133].

The complete control block diagram of the PMSG-type WT is shown in Figure 5.12, where the WT voltage reference Vdc* and the droop gain K are 1.1 and 0.025 p.u., respectively, which define how the WT contributes to DC voltage regulation. The droop gain determines the sensitivity of power output to voltage deviations and must be carefully tuned to ensure smooth power sharing and stability. Together, these controllers enable the WT to operate flexibly across a range of conditions, balancing maximum power extraction with grid-supportive behaviour under fault or transition scenarios.

5.5.3.4 GTC Control

In grid-connected mode, the GTC plays a crucial role in regulating both active and reactive power exchange to meet the AC grid requirements and regulate the DC bus voltage. This dual functionality ensures that the DC microgrid remains stable and synchronised with the main grid during normal operation. To achieve this, the GTC employs the vector control method in the d–q reference frame, a widely adopted approach due to its ability to decouple the control of active and reactive power components [134]. As shown in the control block diagram in Figure 5.13, the GTC uses a DC voltage reference V_{dc} = 1.0 p.u. to maintain voltage stability on the DC side. The droop gain K = 0.0025 p.u. is used to implement voltage-droop control, which modulates the converter's power output in response to deviations in DC voltage. This facilitates coordinated power sharing between the GTC and other DERs, such as PV systems or BESS units, especially in scenarios involving fluctuating loads or renewable generation. Proper tuning of the droop gain is essential to ensure system stability, avoid control conflicts, and maintain reliable power flow in the hybrid AC/DC interface. The control strategy ensures that the GTC provides dynamic support to the DC bus while adhering to grid codes and maintaining power quality on the AC side.

5.5.4 Simulation Analysis of DBS Control

This section evaluates the performance of the proposed DC Bus Signalling (DBS) control strategy under various generation and load disturbances in both grid-connected and islanded DC microgrids. Time-domain simulation studies are conducted using the DC microgrid study system illustrated in Figure 5.1.

Before the disturbance at t= 2 s, the DC microgrid operates in a stable state, with DER terminal voltages ranging from 740 V to 780 V. At this point, the WT and PV systems are both running in MPPT mode, generating 1 MW and 0.5

MW, respectively. At the same time, the total power demand is 1.15 MW. The BESS draws 0.14 MW to maintain the power balance, and the GTC exports 0.47 MW to the AC grid.

5.5.4.1 Case study 1: Response Power Demand Decrease

At t = 2 s, as shown in Figure 5.14b, the total power demand decreases from 1.15 MW to 0.76 MW, leading to a significant increase in the bus voltage to approximately 800 V. This disturbance is characterised by an excess of power generation relative to reduced demand which was explain in operation state 1. In response, the GTC and BESS absorb additional power from the DC microgrid to prevent further voltage escalation, as depicted in Figure 5.14c.

Furthermore, as shown in the same figure, the WT also curtails its output following the load drop, reducing its power contribution by approximately -0.25 MW. This behaviour highlights the coordinated response among DERs under the proposed DBS control strategy. While the GTC and BESS actively absorb surplus power, the WT reduces its generation to help mitigate overvoltage. Including wind curtailment in the DER coordination logic ensures a more balanced and stable system response to sudden power surpluses as illustrated in operation state 1.

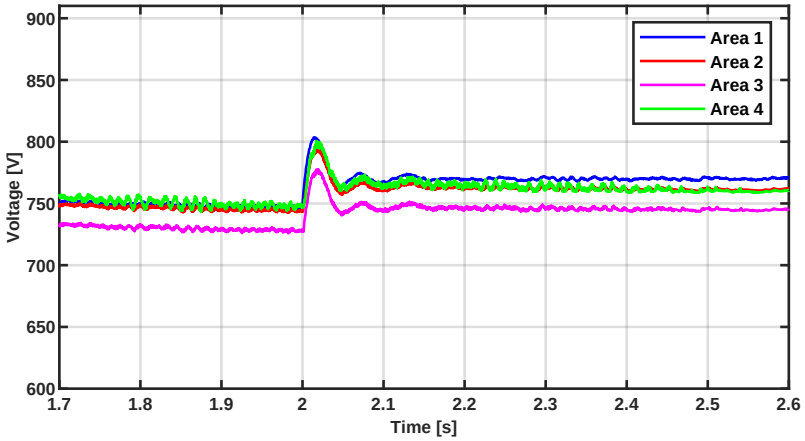

(a)

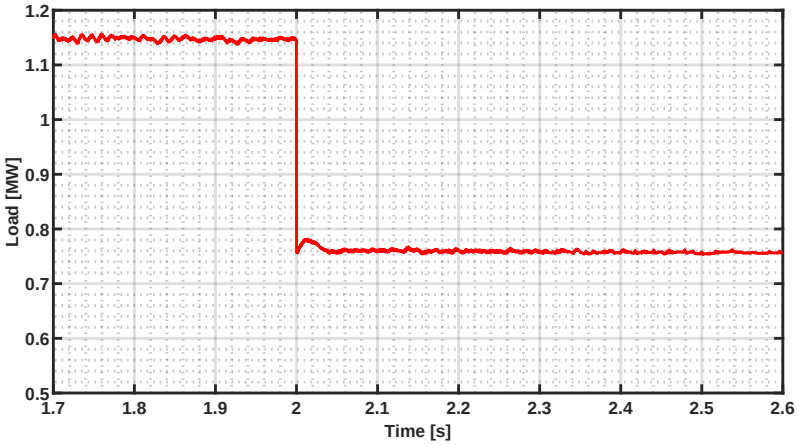

(b)

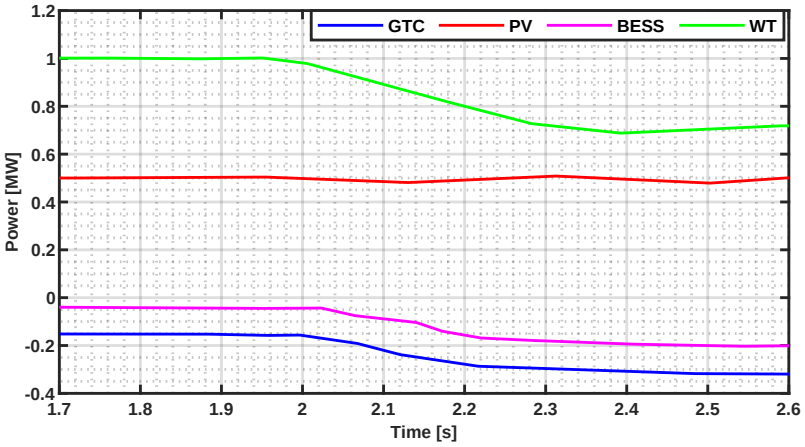

(c)

Figure 5.14: Case Study 1: (a) DER Terminal voltages. (b) Total load of the System (c) DER Power responses

This case study explains operation state one and highlights the variability in terminal voltages of DERs under practical operating conditions. Not all DERs will respond uniformly to a disturbance, which can lead to imbalances across the system [96]. However, the proposed DBS control strategy mitigates these imbalances by effectively managing voltage fluctuations. The results confirm that the DBS control strategy successfully regulates the DC bus voltage levels, with the highest recorded voltage being 770 V and the lowest being 750 V, as depicted in Figure 5.14a. Additionally, the strategy delivers a stable and acceptable dynamic response, even in the face of large disturbances, such as a significant power surplus in a grid-connected microgrid.

5.5.4.2 Case study 2: Transition from Grid Connected to Islanded Mode

This scenario represents operation state 2, focusing on the behaviour of the DC microgrid during the transition from grid-connected to islanded mode. Before t = 2s, the DC microgrid operates steadily, with DER terminal voltages ranging from 740 V to 780 V, while connected to the GTC. At t = 2 s, the system experiences a disturbance caused by the disconnection of GTC, initiating a switch to islanded Mode 2. In this mode, the stability of the DC bus voltages relies solely on the BESS and RESs. The transition results in a slight voltage drop, followed by a coordinated response across DERs as shown in Figure 5.15.

To counter this disturbance, the DERs dynamically adjust their power outputs. The BESS increases its power injection, drawing 0.37 MW; the WT increases their generation from 0.5 MW to 1 MW, and the PV systems increase their output from 0.25 MW to 0.55 MW to support the load. These adaptive responses ensure voltage stability during the transition. The case study confirms that the DBS control strategy ensures proper voltage regulation and dynamic response during critical transitions, providing stability and resilience in islanded

microgrids.

It should be noted that after t = 2s, the GTC power should be zero, but does not settle at zero, continuing to export a small amount of power. This is caused by constant power loads (CPLs), which attempt to maintain fixed power during transients. Their nonlinear behaviour can momentarily force the GTC to compensate, even if logically disconnected. Numerical stiffness or controller lag also contributes to this unintended export.

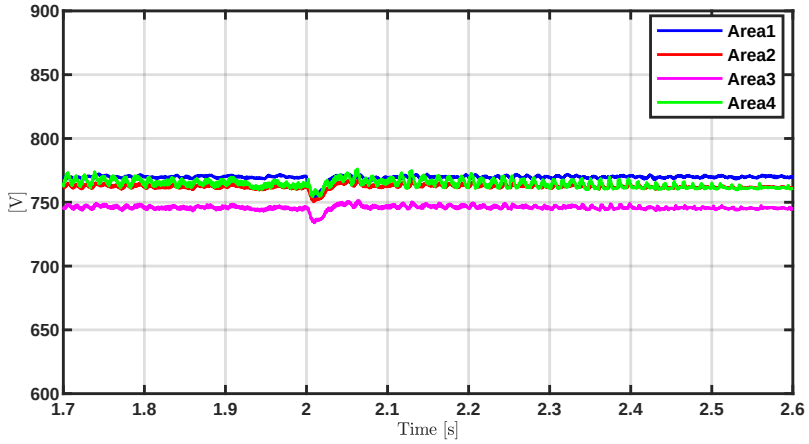

(a)

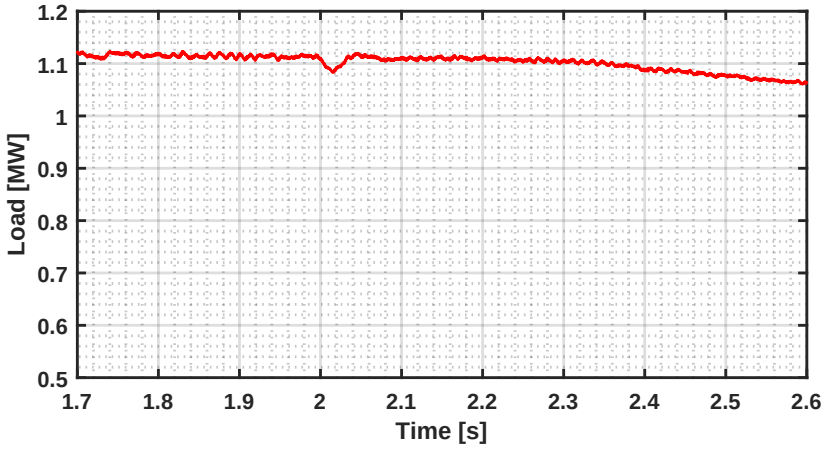

(b)

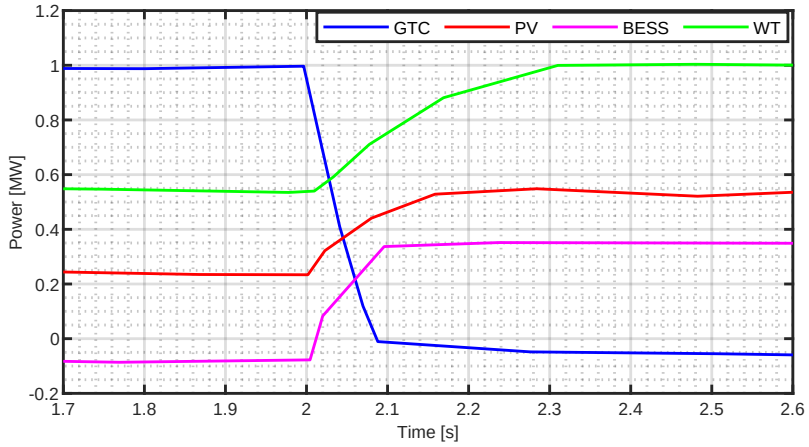

(c)

Figure 5.15: Case Study 2: (a) DER Terminal voltages. (b) Total load of the System (c) DER Power responses

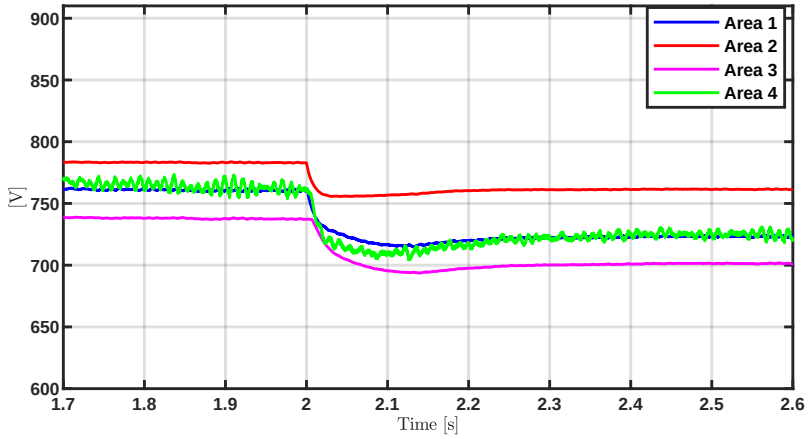

(a)

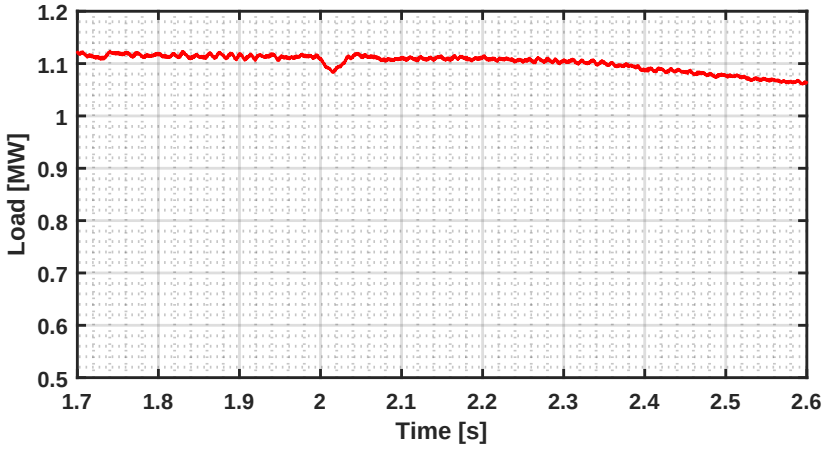

(b)

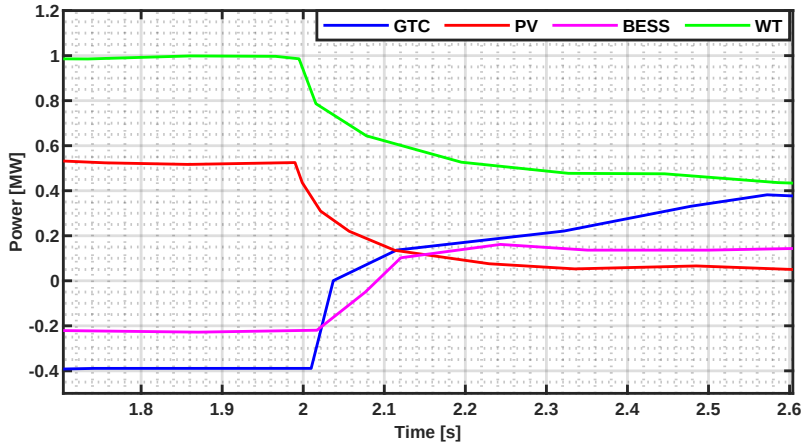

(c)

Figure 5.16: Case Study 3: (a) DER Terminal voltages. (b) Total load of the System (c) DER Power response

5.5.4.3 Case study 3: Power Deficit and Voltage Source Control

This case study illustrates operation state 3, where the microgrid experiences a generation deficit due to a reduction in the output of RES. At t = 2 s, both the the WT and PV systems exhibit significant power drops due to simulated technical disturbance. WT output falls from 1 MW to 0.5 MW, while the PV output drops from 0.5 MW to 0.18 MW, as shown in Figure 5.16c. This combined reduction in RES generation introduces a power shortfall of approximately 0.82 MW, threatening the voltage stability of the DC microgrid.

To maintain the system's power balance, the GTC and BESS respond promptly by increasing their power outputs by 0.4 MW and 0.2 MW, respectively.This collaborative compensation between dispatchable units ensures that the DC bus voltage remains stable, recovering to around 700 V, as shown in Figure 5.16a—well within the acceptable voltage range defined for Mode 3.

This case study illustrates how effective the DBS control strategy is in maintaining voltage stability and ensuring proper power distribution, even during significant power deficits. By utilising voltage-sourced control, the microgrid can operate efficiently without the need for oversized BESSs or RESs.

5.5.4.4 Case study 4: Load shedding for Power Deficit Management

In this final case study illustrating operation state 4, the islanded DC microgrid experiences a severe power deficit caused by a drastic drop in renewable energy generation. The response of the system is evaluated in two phases: (i) without any corrective control, and (ii) with the implementation of a two-step load-shedding scheme.

Initially, the islanded DC microgrid operates steadily, as described in case study 4. At t = 2 s, WT output is 0.5 MW, while the PV systems are offline due to technical issues. This leads to a severe voltage drop across the entire microgrid, as shown in Figure 5.17. In response, the BESS injects its maximum output of

0.4 MW into the system. However, with the power demand exceeding available generation, the bus voltages fall below the acceptable range of 695 V, leading to voltage instability and potential collapse.

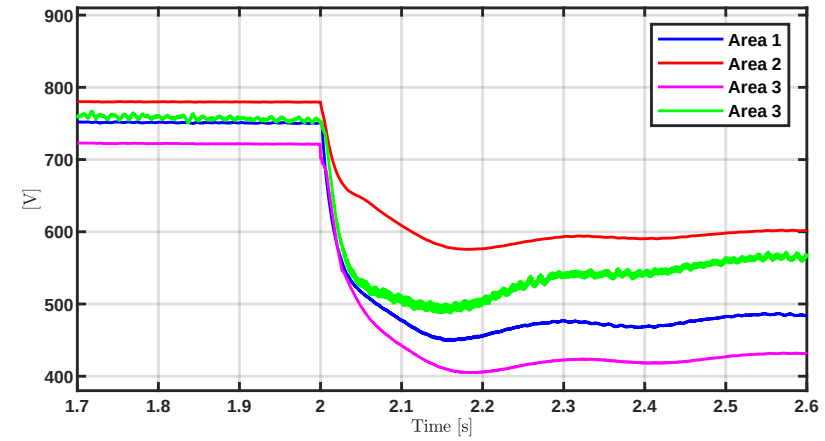

(a)

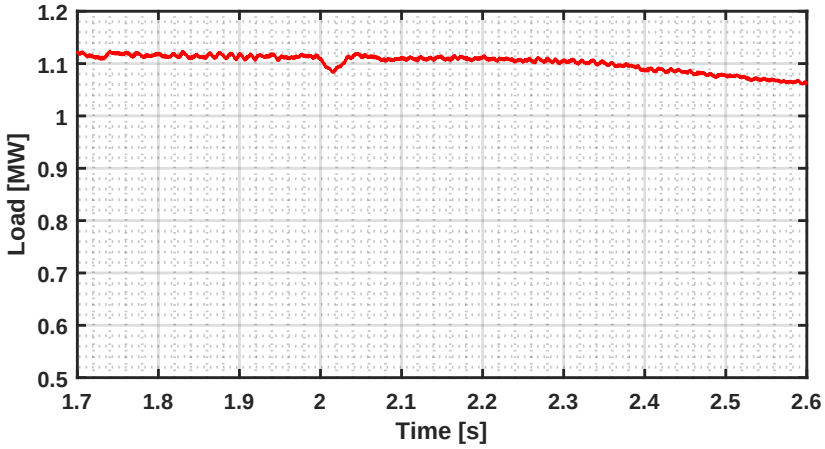

(b)

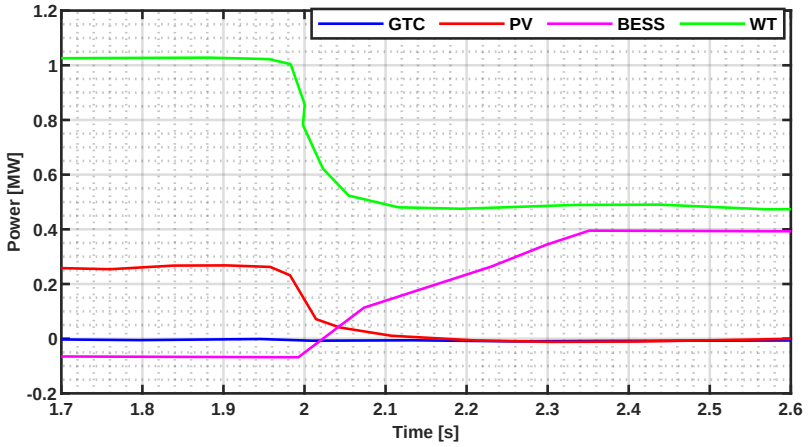

(c)

Figure 5.17: Case Study 4: (a) DER Terminal voltages. (b) Total load of the System (c) DER Power response

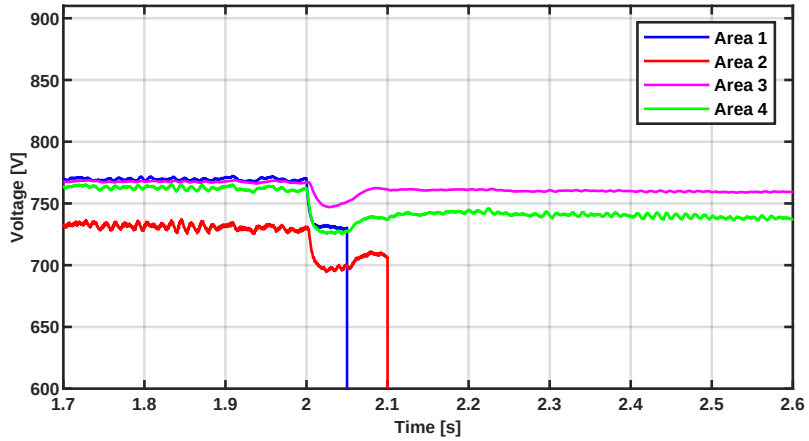

(a)

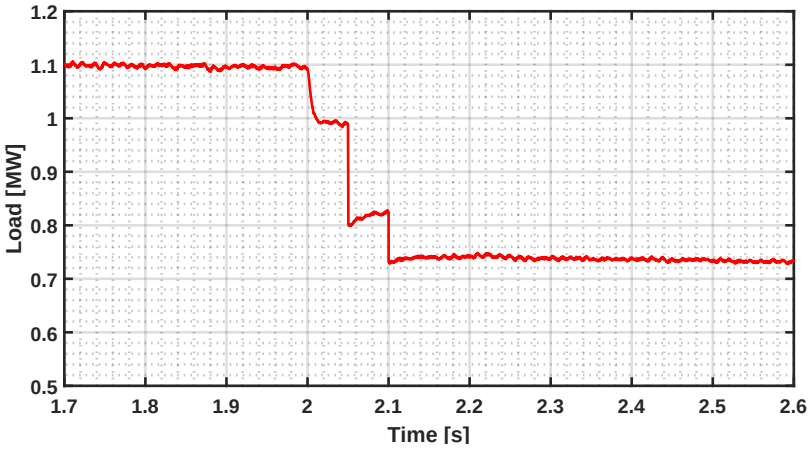

(b)

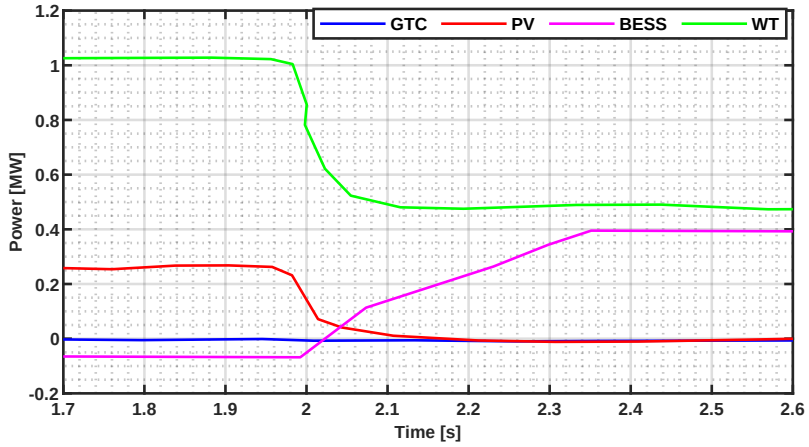

(c)

Figure 5.18: Case Study 4 (ii): (a) DER Terminal voltages. (b) Total load of the System (c) DER Power response

A two-step load-shedding strategy is applied to avoid system collapse, as depicted in Figure 5.18. At t = 2 s, non-critical loads amounting to 0.2 MW are shed in the first step, reducing the power deficit. A further disturbance of 0.4 MW triggers a second load-shedding step, balancing generation with demand. Following these measures, the microgrid stabilizes with bus voltages regulated at 750 V, and the total power demand is reduced to 0.71 MW. This case study highlights the critical role of load-shedding in managing severe power deficits in islanded microgrids. By dynamically shedding non-critical loads, the DBS control strategy ensures system stability, prevents voltage collapse, and maintains reliable operation during disturbances.

5.6 Summary

This chapter presented the implementation of an adaptive voltage-based strategy for disturbance detection and localization in DC microgrids without the need for high-bandwidth communication systems. By utilizing voltage derivative (dv/dt) parameters, the proposed method enables fast and accurate detection of disturbances and assessment of their magnitude across different areas of the microgrid. This capability not only allows for the rapid identification of the disturbance location but also facilitates the determination of appropriate control actions required to mitigate the disturbance, based on the magnitude of the RoCoV. This adaptive approach enhances the responsiveness and effectiveness of the control system in maintaining voltage stability and system integrity under dynamic and fault-prone operating conditions.

In the second part of this chapter, an adaptive DBS control strategy was developed to mitigate the adverse effects of DC bus voltage fluctuations. This control strategy employs dynamically adjusted voltage thresholds to regulate bus voltage levels and maintain voltage regulation. To assess the effectiveness of the

proposed strategy, a series of case studies were carried out under different operating conditions and disturbance scenarios, including grid-connected and islanded modes.

Simulation results demonstrated that the adaptive DBS control strategy successfully maintains power balance, limits DC bus voltage deviations within the acceptable limit of +/-10% specified by IEC 60038, facilitates smooth transitions between operational states, and provides a satisfactory dynamic response to system disturbances.

The proposed DBS control strategy provides a practical and resilient approach for enhancing voltage regulation and stability in DC microgrids, especially in remote areas or situations with limited communication. This strategy significantly boosts the reliability and operational efficiency of DC microgrids; however, it prompts load shedding whenever the load demand exceeds the microgrid's capacity due to a major disruption. This serves as the foundation for the following chapter on the implementation of optimized load shedding strategy.

Chapter 6

Novel Optimal Timer-based Load shedding Scheme using Mixed Integer Linear Programming

6.1 Introduction

In the previous chapter, the dynamics of disturbances in microgrids and the importance of controlling them based on their magnitude were explored. A critical insight was that load shedding becomes essential when power demand exceeds generation capacity to safeguard the microgrid's integrity. This chapter introduces a novel load-shedding scheme designed specifically for DC microgrids, addressing some of the limitations in conventional methods. The proposed load-shedding scheme is a non-communication-based approach that relies on time delays and a mixed-integer linear programming (MILP) algorithm to determine the optimal combination of non-critical loads to be shed. This strategy comes into play when a disturbance persists beyond a predetermined time delay at any DC bus, triggering a load-shedding event to restore balance. The distributed nature of this control strategy enhances the system's resilience and adaptability, solv-

ing challenges like over-shedding, which is common in conventional timer-based strategies with shorter delays. Unlike existing step-by-step techniques, where loads are sequentially shed, the proposed scheme can shed multiple non-critical loads simultaneously. This improves efficiency, especially in larger networks with many loads, by optimising the shedding process and selecting the best combination of loads for disconnection. The key features and advantages of this novel load-shedding scheme include:

- Protection of DC Microgrid Voltage Stability: The scheme ensures voltage stability across the microgrid by maintaining power balance under significant disturbances, preventing voltage collapse and protecting system integrity.

- Optimized Shedding in Large Networks: The MILP-based approach allows shedding non-critical loads without a predefined sequence, ensuring the most practical combination of loads is disconnected to restore balance.

- Prevention of Critical Load Exposure: The scheme minimizes the risk of under-shedding, ensuring that critical loads are not subjected to prolonged under-voltage conditions, which could jeopardize their operation.

- Effective Operation with Short-Time Delays: Conventional methods often struggle with over-shedding when short-time delays are used. This scheme avoids that by providing a more precise load-shedding response, even with minimal delays.

In the subsequent sections, we will compare the proposed load-shedding scheme with the adaptive timer strategy. Performance evaluation results, derived from various case studies, will demonstrate the effectiveness of this approach in different disturbance scenarios and illustrate its potential to improve the reliability and efficiency of DC microgrids.

6.2 Overview of Optimisation Techniques

Optimisation in power systems aims to reduce errors and improve efficiency in generating, transmitting, and distributing electrical power [159], [50]. This involves finding the best operating parameters and control settings to achieve specific goals [160], [161]. Various optimisation techniques are employed to improve system performance, including classical optimisation methods, metaheuristic algorithms, analytic approaches, and hybrid methods [162].

Traditional or classical techniques rely on mathematical models and benefit from sparsity techniques in large-scale power systems. These methods use both constrained and unconstrained optimisation approaches, such as linear programming, quadratic programming, and mixed-integer programming [161] [163] form the foundation for stability-constrained power system operation [162].

Artificial intelligence (AI) or heuristic techniques have also effectively addressed many power system problems. Combined with conventional mathematical approaches, they further enhance the power system optimisation system [164] [165]. Examples of AI techniques include Artificial Neural Network (ANN) [164], Fuzzy Logic [166], Genetic Algorithm [167], [168], [169], and Particle Swarm optimisation (PSO) [170], [171], [172] [163].

To effectively address complex real-world problems, hybrid AI techniques that combine two or more methods are recommended. This integration allows for leveraging the strengths of each other while compensating for their weaknesses [159], [161]. Optimisation is extensively used in DC microgrids for Energy Management Systems (EMS), which aims to ensure optimal performance, efficient resource utilisation, and effective control of energy flow within the system. Load balancing, grid stability, and integration of renewable energy sources are the key objectives of an EMS in a DC microgrid [173], [174], [175], [147], [176]. Load shedding optimisation is equally crucial in non-communication-based sce-

narios as it is in communication-based AC systems [177]. Therefore, DC-based load-shedding strategies should be optimised and implemented using appropriate optimisation techniques.

6.3 Mixed Integer Linear Programming Formulation

In this work, the MILP timer-based load-shedding scheme is implemented as a non-communication-based optimisation-enhanced scheme. The MILP optimisation is performed offline to determine the optimal shedding sequence, the specific non-critical loads to disconnect, and the corresponding timer settings for each circuit breaker (CB). These parameters are then pre-programmed into the local controllers associated with each CB.

The operational logic is entirely local. Each CB controller continuously monitors its own locally measured DC bus voltage. When the voltage remains below the common threshold for a specified duration T_d, the controller triggers load shedding. Each CB has an assigned delay T_d, with the first CB operating after an initial delay of 20 ms and subsequent CBs after successive 10 ms intervals.

The integrated design combines the responsiveness of a timer-based threshold mechanism with the decision-making capability of MILP. The timer ensures that disconnections only occur if the voltage deviation persists, thereby avoiding unnecessary load shedding during short-lived transients. Meanwhile, the MILP algorithm ensures that only the optimal amount of non-critical load is shed to restore stability without over-shedding.

Because all decisions are made locally based on pre-embedded optimisation results and real-time voltage measurements, no communication network is required between CBs or with a central controller. This preserves the inherent robustness, simplicity, and scalability of non-communication-based schemes while enhancing

their decision quality through offline MILP optimisation.

6.3.1 Role of MILP in the Load Shedding Scheme

The MILP approach is employed here to solve the optimisation problem, determining the optimal amount of non-critical load to shed. Unlike traditional linear programming techniques [178], [179], MILP handles both continuous and discrete variables. In this scheme, variables, such as the status of circuit breakers, are constrained to binary values (0 or 1), representing their ON or OFF states [180]. This binary decision process makes MILP highly suitable for load shedding applications, where circuit breakers (CBs) either disconnect or remain connected depending on the system's condition [181]. The primary objective of this scheme is to minimise the disruption to system reliability while ensuring the DC bus voltage stays within acceptable limits. The MILP algorithm allows the system to determine the amount and order of load shedding in response to varying conditions, balancing system stability and optimal load management.

6.3.2 Problem Formulation

The optimisation problem is defined by considering a microgrid connected to a total number of n loads, consisting of both critical and non-critical loads, connected to the microgrid through CBs. Non-critical loads CBs can be switched off when power demand exceeds the available supply, while critical loads remain always connected. The loads are represented by $L_1, L_2, \ldots, L_n$.

The total load connected to the microgrid at any moment is the sum of all individual loads is given as:

$$L_T = L_1 + L_2 + \ldots + L_n. \tag{6.1}$$

The system's total load must not exceed the microgrid capacity for stable oper-

ation. This is expressed by the power constraint, given as:

$$P_{\min} \leq L_T \leq P_{\max} \tag{6.2}$$

where $P_{\min}$ (700 kW) represent the minimum power requirement for critical loads and $P_{\max}$ (1180 kW) represents the microgrid's maximum power supply. The constraint (6.2) ensures critical loads are always powered, and the total load never exceeds the available power. Furthermore, the total loads cannot exceed the maximum capacity of the supplied power $P_{\max}$ from the DERs. The upper limit $P_{\max}$ corresponds to the total capacity of the microgrid before any event. while $P_{\min}$ is determined by the size of the critical loads, which cannot be shed at any given time. Therefore, if m denotes the number of non-critical loads that can be shed, then the non-shedable critical loads are denoted L_{CL}.

Let $x_1,\ x_2,\ \ldots\ x_m$ represent the state of the CBs attached to the non-critical loads in various areas in the microgrid, and each variable can take either 0 to indicate an OFF-state or 1 to indicate an ON-state, implying, the states can only take integer values 0 and 1. Therefore, at any given time, the total number of loads connected to the network can be expressed in terms of the CBs state variables as

$$\begin{aligned} L_T = x_1 L_1 + x_2 L_2 + \ldots \\ + x_m L_m + \ x_{CL} L_{CL} \end{aligned} \tag{6.3}$$

where X_{CL} and L_{CL} are the circuit breaker and the load of the critical loads. It is important to highlight the difference between Equation (6.1) and Equation (6.3). While Equation (6.1) represents a straightforward summation of all connected loads, Equation (6.3) incorporates control variables x_i (where $i = 1, 2, \ldots, m$) to enable the selective disconnection of non-critical loads. This approach facilitates optimised load shedding while ensuring that critical loads remain unaffected.

6.3.2.1 Objective Function and Optimisation

The objective function of the load-shedding problem is to maximise the connected load while maintaining system stability. Let the objective function be denoted as J, then the optimisation problem can be defined as $J = L_T$.

It's important to note that the critical load circuit breaker always stays switched on. This means it's a constant value that doesn't impact the outcome of the optimisation problem [182], [183]. As a result, we can simplify the problem significantly by rewriting the objective function based only on non-critical loads and circuit breakers (CBs).

$$J = x_1 L_1 + x_2 L_2 + \ldots + x_m L_m. \tag{6.4}$$

This objective function represents the total non-critical load that should remain connected, while critical loads are always connected and do not impact the optimisation. The decision-making process is constrained by the system's power limits. The power constraint for determining CB states of non-critical loads is expressed as:

$$\mathbf{L}^T \mathbf{x} \leq \mathbf{P}_{\text{con,max}} \tag{6.5}$$

$$-\mathbf{L}^T \mathbf{x} \leq -\mathbf{P}_{\text{con,min}} \tag{6.6}$$

in which

$$\mathbf{x} = \begin{bmatrix} x_1 \\ x_2 \\ \vdots \\ x_m \end{bmatrix}, \ \mathbf{L} = \begin{bmatrix} L_1 \\ L_2 \\ \vdots \\ L_m \end{bmatrix},$$

$$\mathbf{P}_{\text{con,max}} = P_{\text{max}} - L_{n-m}$$

$$\mathbf{P}_{\text{con,min}} = P_{\text{min}}$$

Also, $(\cdot)^T$ represent the transpose of vector $(\cdot)$. Considering the objective function in (6.4) and the power constraints in (6.5) and (6.6), The overall MILP formulation for solving the load-shedding problem is:

$$\begin{aligned} &\max_{x_1,x_2,\ldots,x_m} \quad J \\ &\text{subject to :} \\ &\qquad \mathbf{x} \in \{0,1\}^m, \\ &\begin{bmatrix} \mathbf{L}^T \\ -\mathbf{L}^T \end{bmatrix} \mathbf{x} \leq \begin{bmatrix} \mathbf{P}_{\max} \\ -\mathbf{P}_{\min} \end{bmatrix} \end{aligned} \tag{6.7}$$

In the simulation, this maximisation problem can be converted to a minimisation problem by negating the objective function for ease of solving.

The load-shedding scheme is primarily governed by voltage regulation. In grid-connected mode, voltage is regulated through the main grid, while in islanded mode, the regulation behaviour differs. Due to this, the acceptable operating voltage range of 720 V to 780 V is considered for this study as in [114]. A threshold voltage of 720V is used to initiate load shedding due to potential voltage drops in long transmission lines within the microgrid. This threshold can be adjusted for smaller systems with shorter lines. This results in voltage drops across the lines, which may cause considerable bus deviation. Therefore, for all three groups of non-critical loads, the V_{th} is set at 720 V. This value can be increased in microgrids with shorter lines. When the measured DC bus voltage V_{dc} drops below the threshold and persists for T_d, the MILP algorithm solves the optimisation problem to determine the optimal combination of loads to shed based on the power imbalance as shown in (6.7). In islanded mode, the battery energy system maintains power balance and regulates the DC bus voltage. Figure 6.1 provides a flowchart of the MILP load-shedding scheme.

The key steps of the MILP load shedding process are as follows:

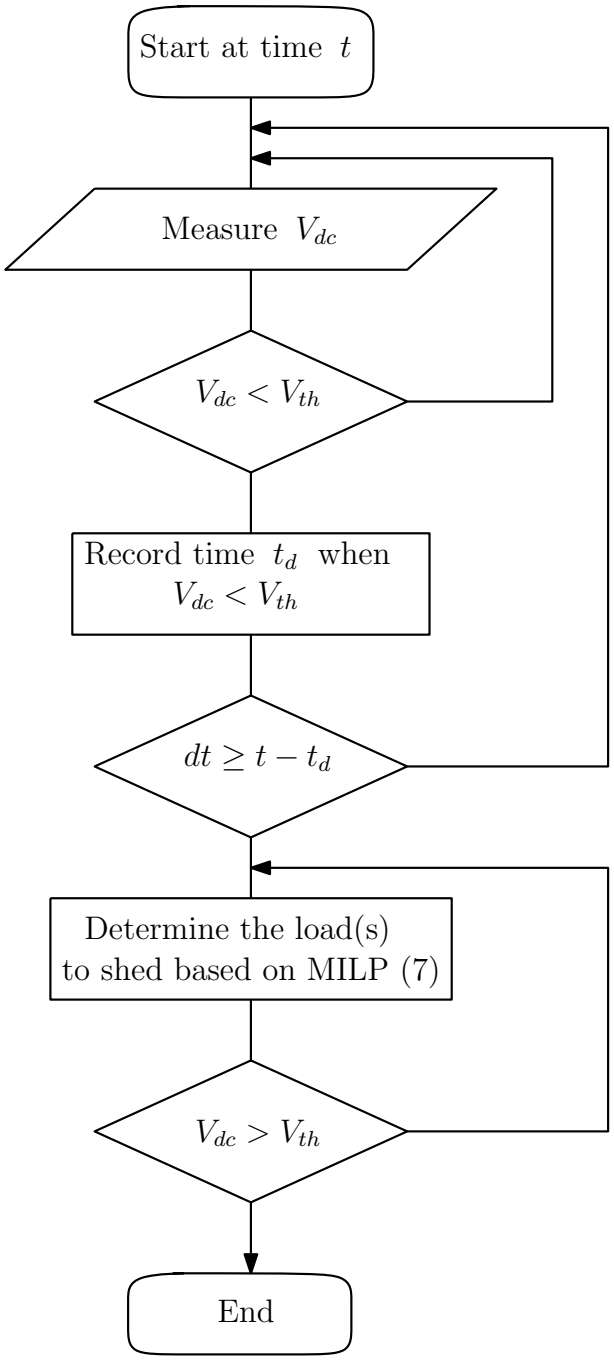

Figure 6.1: Flowchart of MILP load shedding scheme

- V_{dc} is measured and compared with the voltage threshold V_{th}
- The timer mechanism ensures the system does not shed loads prematurely. T_d represents the time delay, t is the current time, and Tr is the time of disturbance.
- The timer continuously monitors V_{dc}; when the voltage drops below V_{th} and the time difference between the current time and the time of disturbance exceeds the delay timer, the load-shedding process is initiated.
- The MILP problem is formulated and solved as soon as the shedding process is initiated to determine the non-critical loads to shed.
- This continues until V_{dc} becomes greater than V_{th}

The MILP solver continues to find loads that can be shed every 10 ms based on the power imbalance between the available power and the loads until the network's V_{dc} reaches a value above the threshold voltage, V_{th}. Therefore, non-critical loads will be shed based on the magnitude of the imbalance. Three case studies will be examined: small disturbances, large disturbances, and the transition from grid-connected to islanded mode to evaluate the effectiveness of the load shedding scheme.

6.4 Simulation Model of The System

The system considered for implementing the proposed load shedding scheme is a low-voltage direct current (LVDC) microgrid shown in Fig. 6.2. The system is essentially an IEEE 37-bus AC microgrid [121] converted to a 750 V DC microgrid [93]. The microgrid comprises two photovoltaic (PV) systems, two battery energy storage systems (BESS), a wind turbine (WT), and different loads. The loads considered are constant power loads (C_{PL}), constant resistance loads (C_{RL}), and

Table 6.1: DC microgrid electrical parameters

GTC	$S_Transformer$ = 1 MVA	Transformer: 0.75 kV/4.8 kV
	SGTC = 1 MVA	C_{dc} = 20 mF
	V_{rated} =750 VDC	F_{sw} = 2.7 kHz
WT	P_{WT} = 1 MW	V_{rated} = 690 V
	S_{PMSG} = 1.1 MVA	C_{dc} = 20 mF
PV	P_{PV} = 5 x 0.1 MW	Max Irradiation= 1000 w/ˆm2
	V_{OC} = 950.5 V	I_{SC} = 714 A
	C_{dc} = 10 mF	F_{sw}= 2.7 kHz
BESS	P_{BESS} = 2×0.5 MW	V_{rated} = 700 V
	Capacity = 580Ah	C_{dc}= 10 mf
Load	Total Load	P_{load} = 1308 kW
	Non-Critical	P_{NCLoad} = 553 kW
	Critical	P_{cLoad} = 750 kW

constant current loads (C_{CL}). The microgrid is interfaced with the utility using a grid-tie converter (GTC). The microgrid system has three fast-acting solid-state circuit breakers (CB) for three-step load shedding. When non-critical loads need to be shed, each CB is tripped. The MILP algorithm is utilised to decide which circuit breaker or combination of circuit breakers to activate when load shedding is necessary to prevent the microgrid's total load from exceeding its generation capacity. CB1, CB2, and CB3 are connected to the non-critical loads, as depicted in Fig. 6.2. The microgrid has a total sheddable load of 200 kW, 148.5 kW, and 182.5 kW for each CB's non-critical loads. The voltage drops across the lines are significant in this study; hence, a high load-shedding voltage threshold of 675 V is set for all non-critical loads to prevent shedding under normal operating conditions. The microgrid is operating normally when bus voltages are over 690 V. The microgrid has a total load of 1170 kW, and the distribution line's length varies based on the cable type used. The system's description, distance, and line types are available in [114] and the appendix. This DC microgrid network is implemented in the MATLAB/Simulink environment.

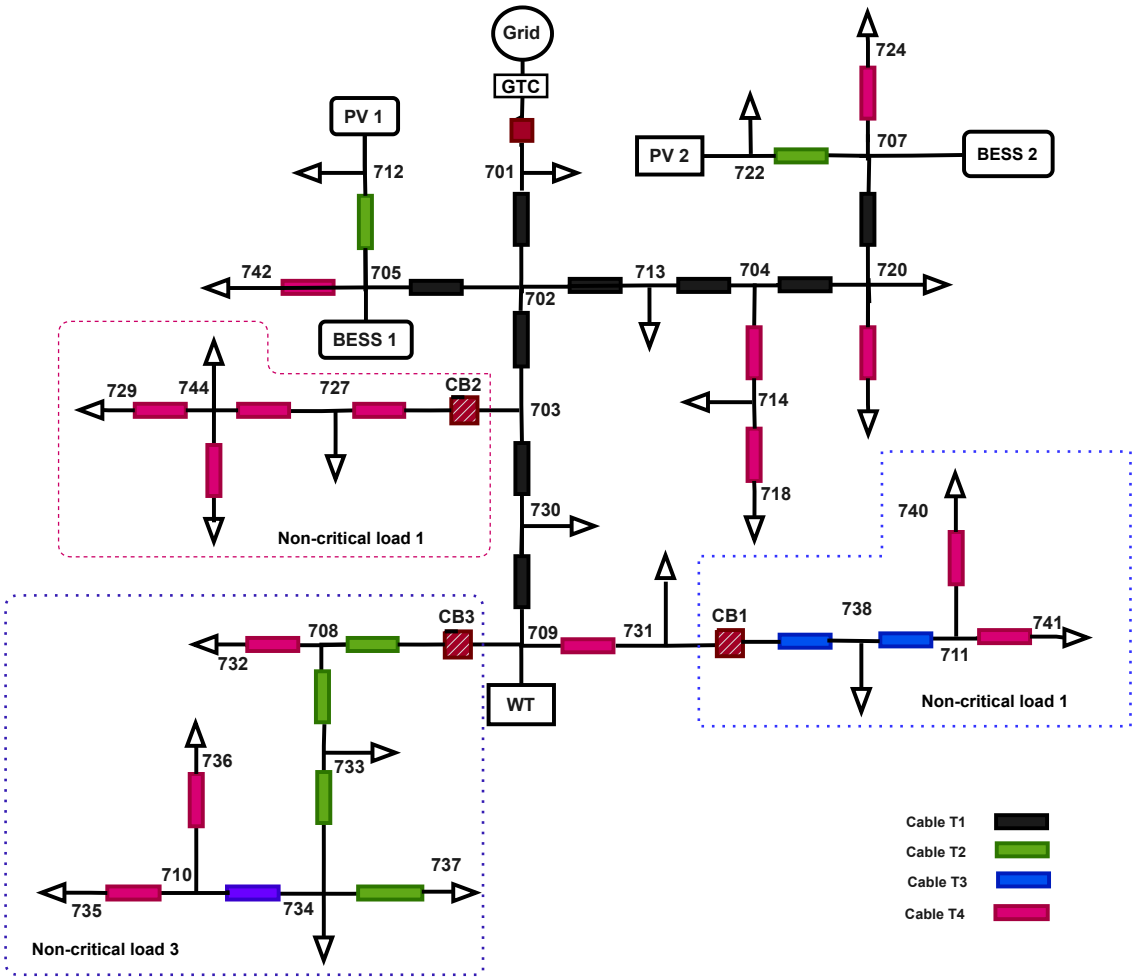

Figure 6.2: Electric model of the DC microgrid

6.5 Results and Discussions

The islanded DC microgrid is in a steady state, where the power generated by the PV system is zero, and the WT generates 1 MW of power in the maximum power point tracking mode. At time 0.5 s, disturbances will be introduced into the system. These disturbances are caused by the gradual power reduction of the WT, leading to reduced power generation. In such cases, load shedding is necessary. The loads are tripped based on the magnitude of the power imbalance observed by the system. Three case studies are described in the following subsections. These case studies evaluate the performance of the adaptive strategy and the proposed MILP timer-based scheme. The following metrics are employed to evaluate and compare the performance of the scheme:

- Response Time: The time taken for circuit breakers to trip following a disturbance.
- Voltage Stabilisation: The scheme's ability to maintain the voltage within a specified range is measured by the minimum voltage of critical loads during a disturbance and the final voltage after the disturbance is resolved.
- Load-Shedding Efficiency: Assessed by the extent to which unnecessary load shedding is prevented and the precision in shedding non-critical loads proportional to the magnitude of the disturbance.

The DC microgrid network was simulated with a sampling time of $5, \mu$s. The MILP-based load-shedding problem was solved using MATLAB's `intlinprog` function, with computation times consistently under 2–$3, \mu$s, demonstrating the feasibility of real-time or online implementation. While this confirms efficiency for the studied network size, it is acknowledged that the computational burden may increase significantly with a larger number of nodes, variables, or constraints. Therefore, future work should investigate the scalability of the algorithm

and identify optimal deployment points within the microgrid, such as local controllers or centralized EMS units, where online optimization can be reliably executed. Additionally, although MILP typically guarantees convergence, practical deployment must include safeguards against rare convergence delays or failures, especially under fast-changing operating conditions.

6.5.1 Case Study 1: Small Disturbance

This case study examines the performance of a proposed scheme under small disturbances (200 kW). Initially, the wind turbine generated 700 kW of power in MPPT mode, but the PV units were not operational. The loads consumed 1.18 MW, and the voltages ranged from 720 V to 780 V. Due to changes in wind speed, the wind turbine's power generation declined gradually from 700 kW to 500 kW in 0.5 seconds, causing a decrease in microgrid bus voltages. A comparison was made between the performance of the adaptive timer scheme [114] and the proposed MILP timer-based scheme. In the MILP timer-based scheme, a time delay of $T_d = 20$ ms was utilised to enable the system to process any disturbances. In contrast, the adaptive scheme maintained a time delay of 15 ms, as reported in [114].

6.5.1.1 Adaptive Scheme

Figure 6.3 illustrates the voltage and power during a small disturbance. At the time $t = 0.528$ seconds, the system responded by tripping CB1 with a load of 200 kW as shown in Fig. 6.4, because the voltage had fallen below the threshold of 720 V to 719 V. CB1 has shed loads, and the voltage of the critical loads was regulated at 750 V, as shown in fig 6.3a. After shedding, the microgrid's load was maintained at 980 kW, as shown in fig 6.3b.

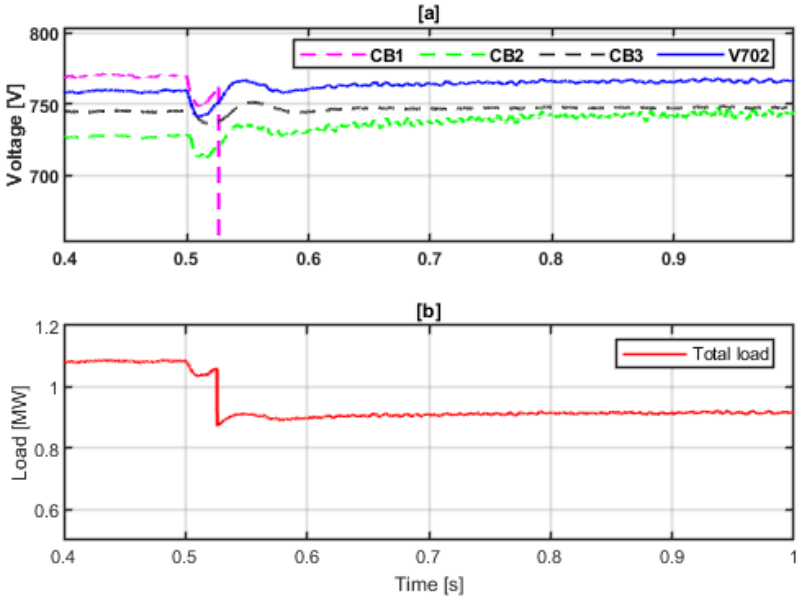

Figure 6.3: Case study 1: Performance of Adaptive scheme on small disturbance; **a)** DC Voltage measured at CB1, CB2, CB3 **b)** Load power

6.5.1.2 Proposed MILP Timer-based scheme

Fig. 6.5 illustrates the performance of the proposed MILP timer-based scheme during a small disturbance. As shown in Fig. 6.6, non-critical loads were shed by tripping CB2 with a load of 178 kW at $t = 0.524$ seconds. CB2 tripped when the voltage dropped from 720 V to 719 V. The voltage was then regulated at 750 V after shedding. Fig. 6.5b illustrates the responses of the total load power, 1180 kW, before the disturbance and after the circuit breakers were tripped at 1.002 kW.

According to the results, the MILP timer-based scheme shed non-critical loads slightly faster than the adaptive scheme. The proposed scheme has tripped CB2, which has a total non-critical load of 178 kW. On the other hand, the adaptive scheme tripped CB1, which has a non-critical load of 200 kW. This shows that

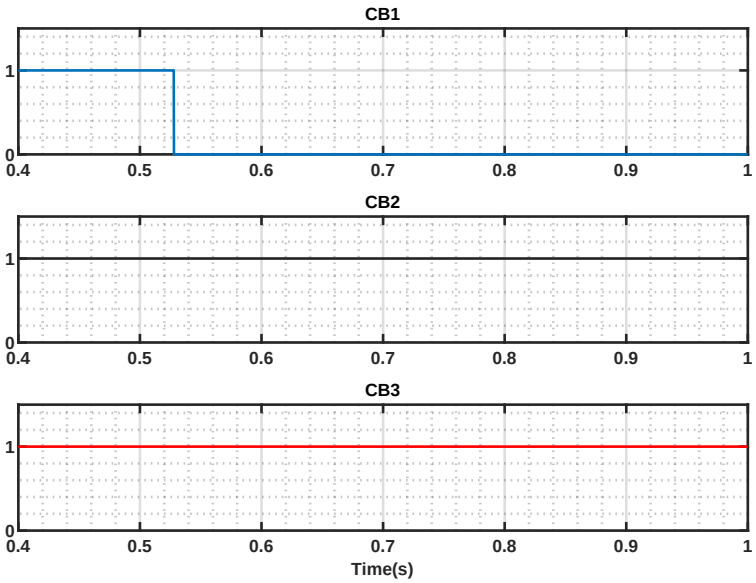

Figure 6.4: Case study 1: Circuit breakers states of the non-critical loads under adaptive timer scheme

the MILP timer-based scheme is capable of shedding loads of the same magnitude as the disturbance observed.

6.5.2 Case study 2: Large Disturbance

This case study focuses on the performance analysis of the adaptive timer-based scheme and the MILP timer-based scheme when exposed to a large disturbance. Before the disturbance, the DC microgrid operated in a stable state with faulty PV generation. The wind turbine generated 1 MW of power while operating in MPPT mode. The total power demand was 1.18 MW, and two BESSs regulated the DC bus voltages, each providing 0.27 MW of power and maintaining the voltage levels between 720 V and 770 V.

At time t=0.5s, an internal fault caused the wind turbine to disconnect from

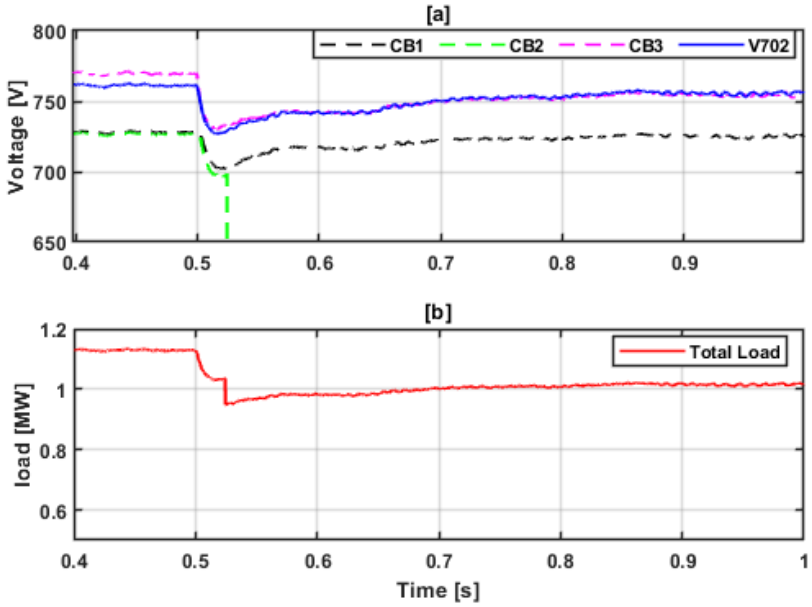

Figure 6.5: Case study 1b: Performance of MILP Scheme on small disturbance; **a)** DC Voltage measured at CB1, CB2, CB3 **b)** Load power.

the microgrid. As a result, each BESS outputted a maximum of 0.41 MW, which was not enough to sustain the system's stability. Consequently, the voltage on the bus decreased significantly, leading to further instability in the system.

6.5.2.1 Adaptive Timer-Based Scheme

Fig. 6.7 illustrates how the voltage and power behaved when an adaptive timer-based scheme was employed. The CB1 and CB2 were tripped at $t = 0.519$ s and $t = 0.56$ s, respectively, as shown in Fig. 6.8. Due to the magnitude of the ROCOV, CB1 reacted quickly. CB3 was not tripped since ROCOV became positive after shedding CB1 and CB2 as explained in [115]. As a result, the voltage for the critical loads went down to 690 V, close to the lowest threshold of 680 V. The voltage of the critical loads was regulated and maintained at 720

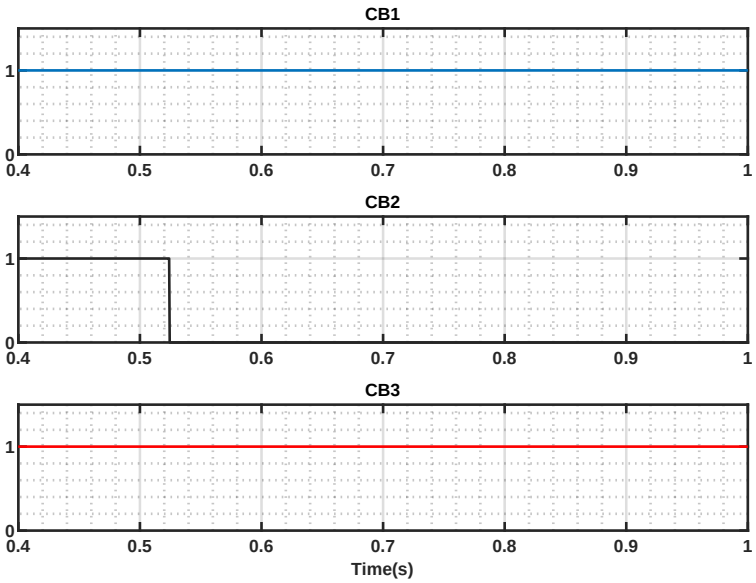

Figure 6.6: Case study 1b: Circuit breakers states of the non-critical loads under MILP scheme

V after 0.25 s of the disturbance, as shown in Fig. 6.7a. The total load in the system after CB1 and CB2 were tripped was 0.91 MW, as illustrated in Fig. 6.7b

6.5.2.2 Proposed MILP Timer-based Scheme

Fig. 6.9 illustrates how the proposed MILP timer-based scheme responds to a significant disturbance. At $t = 0.52$ s, CB2 trips to shed non-critical loads in area 2. CB1 and CB3 tripped simultaneously at $t = 0.5234$ s. As a result, the voltage of the critical loads did not drop below 690 V and returned to 740 V within 0.20 s after the disturbance hit the system, as shown in Fig. 6.9a. This proves the proposed MILP timer-based scheme responds quicker than the adaptive schemes. All non-critical loads were shed within a period of 3.4 ms at the occurrence of the disturbance, as shown in Fig. 6.10. After CB1, CB2, and

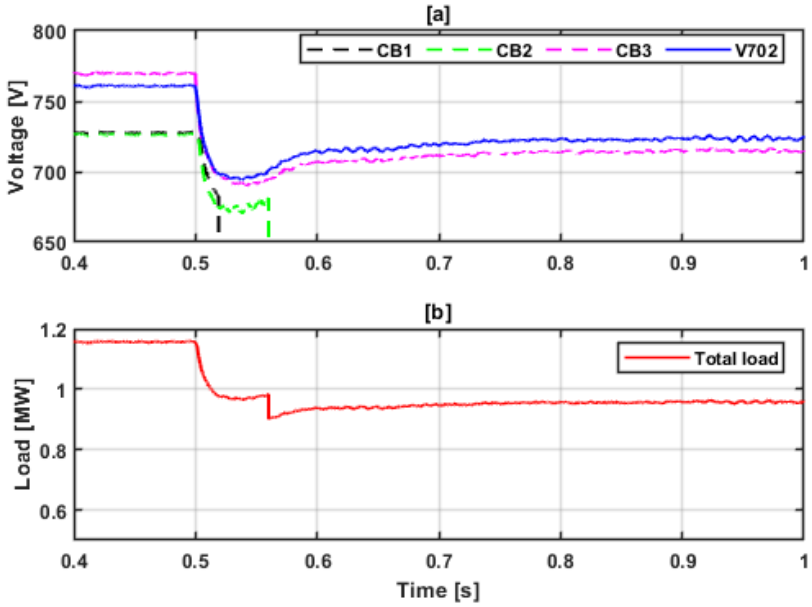

Figure 6.7: Case 2a: Performance of adaptive Scheme; **a)** DC Voltage measured at CB1, CB2, CB3 **b)** Load power

CB3 tripped, the total load in the system became 0.72 MW, as shown in Fig. 6.9b. Disconnecting all non-critical loads in this case study, where the disturbance is severe, ensures that critical loads can be fully supported, especially when the supply is limited to BESS. This strategy helps prevent voltage collapse, maintains system stability, and avoids overloading the BESS. It also allows for a faster and more reliable response during disturbances. The total load is reduced to a manageable level (0.72 MW), ensuring that available power is allocated efficiently to essential services for a good period of time.

6.5.3 Case Study 3: Islanded Event

This case study examines the performances of adaptive and MILP timer-based strategies after an islanding event, at $t < 0.5s$, the microgrid is grid-connected.

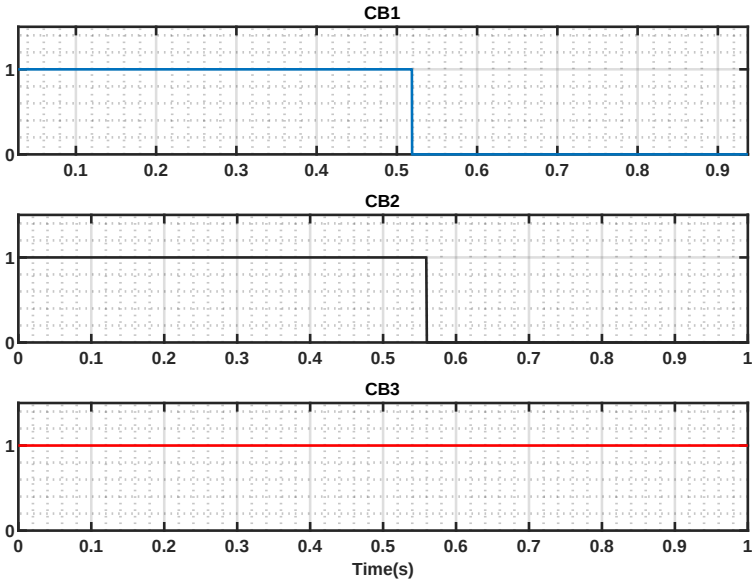

Figure 6.8: Case 2a: Circuit breakers states of the non-critical loads under adaptive scheme

The wind turbine generates 0.20 MW of power. However, the PV units do not produce any power at night. The BESSs provide 0.16 MW of power, while the power demand in the microgrid is 1.18 MW. The GTC imports 0.88 MW from the utility grid to maintain power balance. The GTC also ensures that the DC bus voltages remain between 720 V and 770 V.

Due to an unintentional islanding event at $t = 0.5$ s, the GTC stops importing power from the host utility grid. To react to this disturbance, each BESS provides its rated power of 0.410 MW to the islanded microgrid. However, more than this power is needed to meet the power demand in the islanded system; they will immediately fall. The performance of the subsequent adaptive timer strategy and the proposed MILP timer-based strategy is presented below.

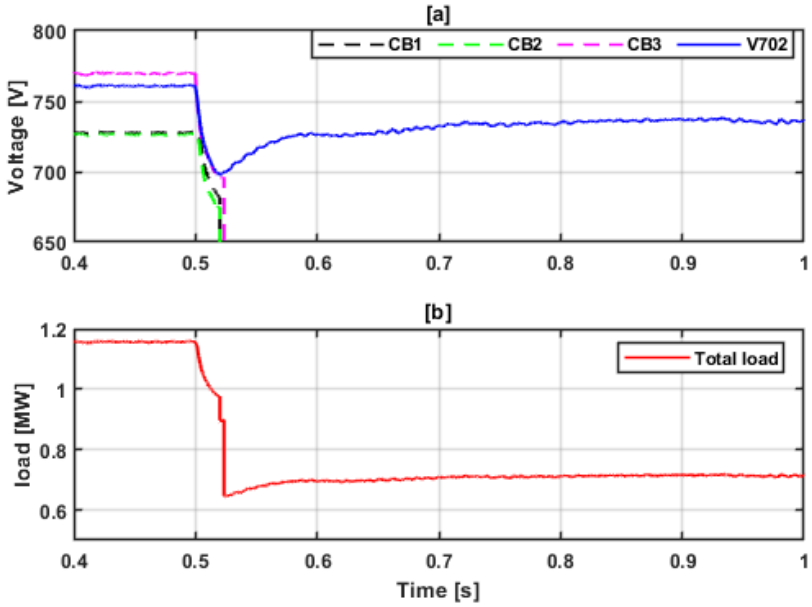

Figure 6.9: Case 2: Performance of MILP Scheme; **a)** DC Voltage measured at CB1, CB2, CB3 **b)** Load power

6.5.3.1 Adaptive Timer-based Scheme

The adaptive timer strategy sheds non-critical loads on CB1 and CB2 at 0.52 s and 0.667 s, respectively. The CB1 tripped fast due to the high magnitude of ROCOV, while CB2 took longer to shed due to the time delay used. This resulted in a voltage sag, but the critical load voltage remained above 690 V. CB3 did not trip due to the ROCOV being positive, and the voltage of the critical loads was restored to 705 volts within 0.15 seconds, as shown in Fig. 6.11 and 6.12.

6.5.3.2 Proposed MILP Timer-based Scheme

The proposed MILP load-shedding scheme sheds non-critical loads on CB2 and CB3 at time 0.52 s, as shown in Fig. 6.14. This reduces the total load power demand to 925 kW, and the critical load voltage is regulated to an acceptable

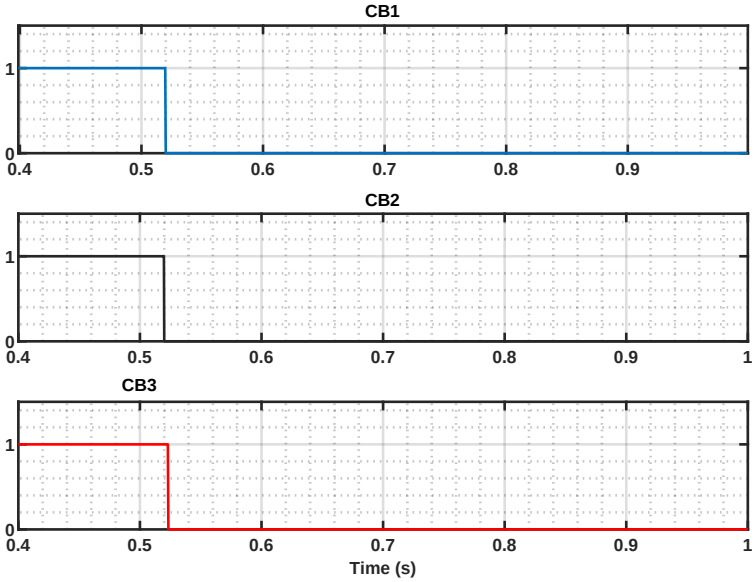

Figure 6.10: Case 2: Circuit breakers states of the non-critical loads under MILP scheme

level of 717 V within approximately 0.25 s after the disturbance shown in Fig. 6.13.

Based on the results of three case studies, the proposed MILP timer-based schemes have been shown to perform better regarding the speed (time) of shedding and the number of loads to shed in different disturbances, as shown in 6.2. Some of the advantages of the proposed MILP timer-based scheme over adaptive schemes can be summarised as follows:

- The adaptive scheme requires a predetermined CB1, CB2, and CB3 sequence to activate the breakers when disturbances occur. On the other hand, the proposed MILP timer-based scheme trips the circuit breakers based on the magnitude of the detected disturbance without following any specific sequence. This approach enables the proposed scheme to shed the

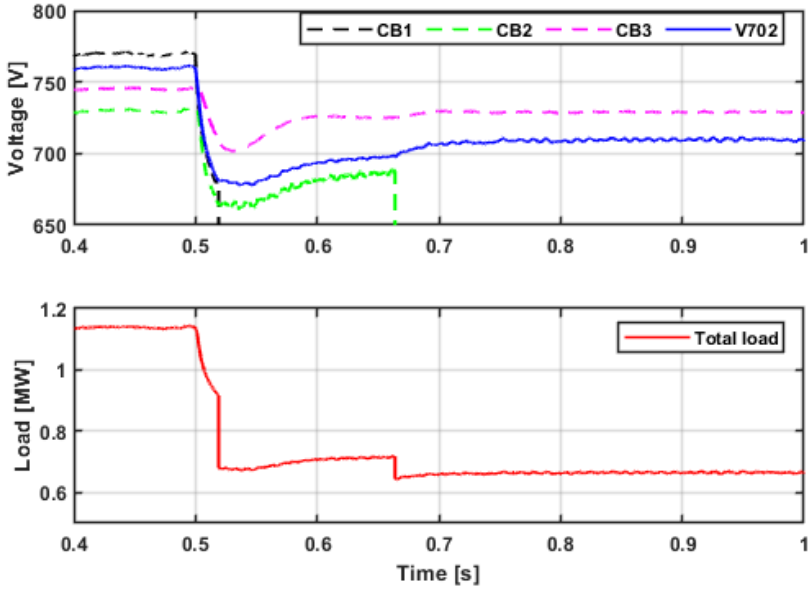

Figure 6.11: Case 3: Performance of Adaptive Scheme; **a)** DC Voltage measured at CB1, CB2, CB3 **b)** Load power

best combination of loads for optimal operation and reliability of the microgrid.

- The adaptive scheme results shown in Fig. 6.7 and in Fig. 6.11 regulate the system voltage at lower voltages, which could expose critical loads to lower voltages after load shedding. On the other hand, the proposed MILP timer-based scheme regulates the system voltage at higher voltages due to its faster response to any disturbance, as depicted in Fig. 9 and Fig. 13.

- The proposed technique can measure and predict power imbalance more accurately than the adaptive scheme. This is because it does not involve a derivative (dv/dt) component, sometimes slowing CBs' response by approximating the voltage measurement.

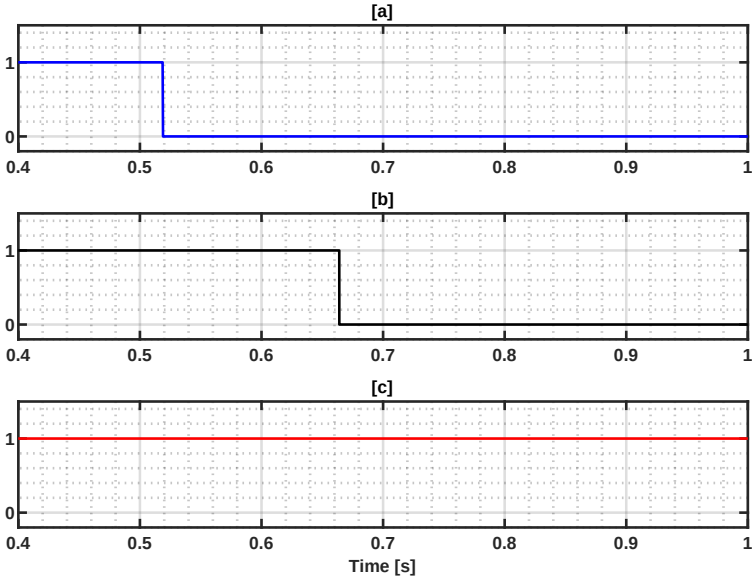

Figure 6.12: Case 3: Circuit breakers states of the non-critical loads under adaptive scheme

Table 6.2 summarizes the results of three case studies, comparing the performance metrics of an adaptive timer-based scheme with those of the proposed MILP timer-based scheme. The table displays the trip time of the circuit breakers, the minimum voltage experienced V_{min}, and the final regulated voltage V_{final} shared by the critical loads.

Table 6.2: Summary of Comparison of MILP and Adaptive timer based schemes

Disturbance	LS Scheme	Trip Time CB1 (s)	Trip Time CB2 (s)	Trip Time CB(s)	Vmin (V)	Recovery (V)
Small	Proposed Scheme	0	0.524	0	719	750
	Adaptive Timer	0.528	0	0	719	750
Large	Proposed Scheme	0.52	0.52	0.523	695	740
	Adaptive Timer	0.519	0.56	0	690	720
Islanded	Proposed Scheme	0	0.52	0.52	691	720
	Adaptive Timer	0.52	0.667	0	695	705

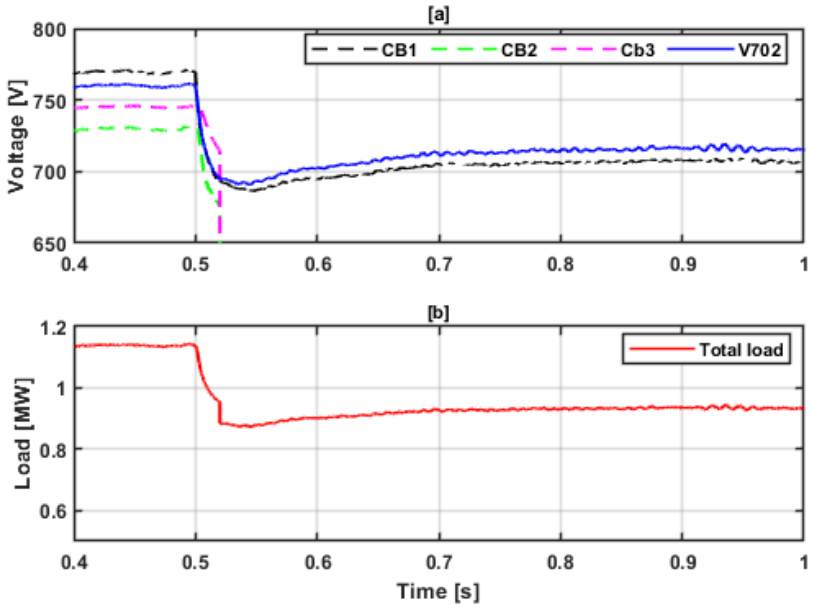

Figure 6.13: Case 3: Performance of MILP Scheme; **a)** DC Voltage measured at CB1, CB2, CB3 **b)** Load power

6.6 Summary

This chapter addressed the limitations of conventional and adaptive load-shedding schemes in DC microgrids by proposing a novel MILP timer-based load-shedding strategy. The proposed approach integrates a short delay timer mechanism for initiating load-shedding actions with a MILP algorithm to optimise load-shedding decisions based on locally measured bus voltages. This enables the scheme to dynamically determine the optimal amount of non-critical loads to disconnect in response to generation deficiencies, ensuring faster, more accurate, and proportionally controlled load-shedding actions.

Simulation results, conducted on a DC microgrid model adapted from the IEEE 37-bus system, demonstrated the effectiveness of the proposed scheme in enhancing system resilience and operational performance. Compared to the

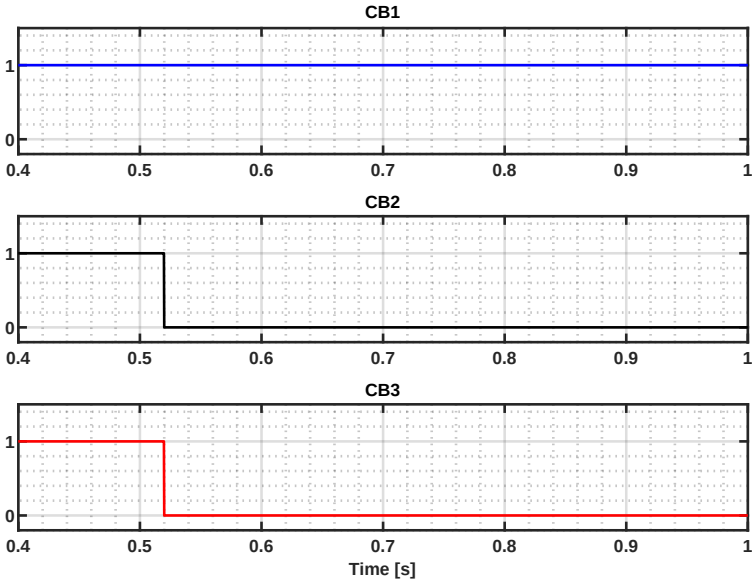

Figure 6.14: Case 3: Circuit breakers states of the non-critical loads under MILP scheme

adaptive load-shedding approach, the MILP timer-based scheme achieved faster response times, reduced system recovery durations during disturbances, and significantly minimised voltage sags. The scheme consistently maintained the DC bus voltage above the critical threshold, thereby ensuring the protection of critical loads from low-voltage conditions.

Moreover, the proposed scheme effectively reduced unnecessary load disconnections (over-shedding) and improved system reliability by coordinating multiple load-shedding steps in proportion to the magnitude of the disturbance. This dynamic and optimal shedding mechanism overcomes the limitations associated with conventional step-by-step load-shedding methods, ensuring better power balance, reduced voltage deviations, and enhanced system resilience during severe disturbance events.

Chapter 7

Conclusions and Future Work

In regions such as Sub-Saharan Africa, where nearly 1 billion people lack access to reliable electricity, the adoption of innovative and sustainable energy solutions is essential. DC microgrids have emerged as a viable solution to addressing these challenges, offering off-grid, flexible, and scalable energy access. Their growing relevance in this context is largely attributed to their ability to seamlessly integrate renewable energy resources and the adaptability provided by decentralised energy systems. These advantages are particularly significant in overcoming critical challenges such as energy poverty, high transmission costs, and infrastructural limitations, especially in remote and rural areas.

Beyond their regional significance, DC microgrids hold immense potential in driving the global energy transition. As power networks evolve towards achieving a net-zero carbon future, DC microgrids offer numerous advantages over conventional AC systems. These benefits include the optimal utilisation and integration of renewable energy resources, enhanced controllability, improved system flexibility, greater reliability, redundancy, security, and lower investment costs.

However, unlocking the full potential of DC microgrids requires addressing several technical challenges. Critical issues such as accurate disturbance detection, effective control of voltages at the DC buses, and the implementation of

efficient load-shedding strategies when the demand is more than capacity are fundamental to ensuring system reliability and resilience. In particular, the development of robust, non-communication-based control strategies is essential to minimise dependence on costly and potentially unreliable communication infrastructures. Existing methods often involve trade-offs between voltage regulation and power supply reliability, highlighting the need for more effective approaches to maintaining system integrity.

In response to these challenges, this thesis has made significant contributions toward enhancing the resilience, voltage stability, and operational efficiency of DC microgrids through the development of novel voltage control and load-shedding strategies. The research presented in this thesis addresses the adverse effects of unequal bus voltages caused by disturbances and provides effective mechanisms for managing non-critical load shedding when load demand exceeds power generation capacity. The key contributions of this research are summarised as follows:

- Development of a novel MILP timer-based load-shedding scheme, capable of optimising load-shedding decisions based on local voltage measurements, reducing unnecessary load disconnections, and improving system resilience during severe disturbances.

- A disturbance detection and location method utilising the voltage derivative approach for rapid disturbance identification and localisation.

- An improved DC Bus Signalling (DBS) control technique designed to mitigate the effects of unequal bus voltages, enhancing voltage regulation and system stability.

- A comprehensive review of existing DC load-shedding schemes, highlighting their operational principles, limitations, and areas for improvement.

This chapter concludes the thesis by summarising the key findings and contributions of the research while also outlining potential avenues for future investigations into DC microgrid control and load-shedding.

7.1 Conclusions

The contributions from the work undertaken throughout this thesis can be attributed to three distinct knowledge streams. The following three sub-sections present the contributions to each stream in detail.

7.1.1 A Novel Timer and Mixed Integer Linear Programming Load Shedding Scheme

Maintaining power balance in DC microgrids becomes a critical challenge when the power demand exceeds the generation capacity of the DERs. In such scenarios, voltage control actions alone are insufficient to restore system resilience, necessitating the implementation of load-shedding control to prevent system collapse and ensure reliable operation. The review of existing non-communication-based DC load-shedding strategies, presented in Chapter Three of this thesis, identified significant limitations in conventional approaches and highlighted the need for more advanced, efficient techniques to improve the resilience of future DC microgrids.

In response to these limitations, a novel MILP timer-based load-shedding scheme was developed. The proposed strategy integrates a short delay timer mechanism for initiating load-shedding actions with an MILP optimisation algorithm to determine the optimal amount of non-critical loads to disconnect based on locally measured voltages. By continuously assessing the power imbalance, defined as the difference between the microgrid's generation capacity and total load demand, the scheme ensures proportionally controlled load-shedding deci-

sions. The strategy manages load disconnection through circuit breakers controlling non-critical loads, thereby maintaining power balance while minimizing unnecessary load-shedding events and preserving critical loads during severe disturbances.

The proposed scheme operates by shedding non-critical loads when the measured voltage at the load remains below a predefined threshold voltage (V_{th}) for a specified duration (T_d). Each circuit breaker is assigned a short time delay (T_d) for subsequent triggers, ensuring a structured and proportional response to disturbances while preventing unnecessary load shedding.

Performance metrics used in the simulation included the circuit breaker trip time, the minimum voltage level experienced by critical loads during disturbances, and the final recovery voltage of critical loads after load shedding. These metrics were used to validate the effectiveness of the proposed MILP-based load-shedding scheme, demonstrating its capability to improve load-shedding performance in DC microgrids, resulting in improved resilience. The simulation results showed that the proposed scheme:

- Achieved faster shedding of non-critical loads compared to adaptive timer schemes due to the integration of power imbalance assessment within the MILP algorithm.

- restored power balance in the DC microgrid by coordinating load-shedding steps based on locally measured voltages, thereby reducing large voltage sags and mitigating over-shedding issues commonly experienced in conventional schemes with prolonged time delays.

- Dynamically coordinated multiple load-shedding steps by triggering circuit breakers and shedding non-critical loads proportional to the magnitude of the observed disturbance.

- Maintained the DC bus voltage above critical thresholds, ensuring that essential and critical loads remain protected from excessively low voltage conditions.

These findings highlight the potential of the proposed MILP timer-based load-shedding scheme as an effective solution for enhancing the resilience of DC microgrids. Its ability to operate without a communication infrastructure makes it particularly suitable for remote and communication-constrained environments.

7.1.2 Enhanced Disturbance Identification and Voltage Regulation Technique

7.1.2.1 Disturbance Identification Technique using Voltage Derivative

The accurate identification and localisation of disturbances within a microgrid are essential for enabling timely control actions and mitigating power imbalances at their source. A voltage derivative-based dv/dt technique was implemented for effective disturbance detection and localisation within a DC microgrid environment. This method was applied to a redesigned 37-bus system DC microgrid, providing a realistic platform for evaluating its performance.

The proposed approach enables rapid disturbance detection by calculating RoCoV based on observed voltage variations across different areas of the microgrid. By comparing the calculated RoCoV values against predefined minimum and maximum thresholds set within the control algorithm, the method effectively distinguishes between different disturbance scenarios, such as over-generation, under-generation, and large-scale faults. The technique accurately identifies the specific bus location where the disturbance has occurred by analysing the magnitude of voltage spikes resulting from the RoCoV response. When the disturbance magnitude exceeds the critical defined threshold of $-500V/s$, the control strategy

automatically triggers load-shedding to preserve voltage stability and maintain system integrity.

The proposed technique enables fast and accurate disturbance identification and can effectively locate the specific bus where the disturbance occurs within the DC microgrid. This capability is crucial in determining the disturbance magnitude and guiding the appropriate control actions required to mitigate its impact. By enabling targeted and timely responses, the technique enhances the system's responsiveness, reliability, and resilience, particularly in non-communication-based DC microgrids. It provides a practical and efficient solution for improving system stability, especially under dynamic and fault-prone operating conditions commonly encountered in remote or resource-constrained environments.

7.1.2.2 Enhanced DC Bus Signalling Voltage Control

The design and implementation of an adaptive DBS control strategy for improving voltage regulation and power-sharing efficiency in non-communication-based DC microgrids is proposed. The proposed DBS control strategy utilised an adaptive control technique to dynamically regulate DC bus voltages based on load demand and generation levels. Voltage thresholds are defined corresponding to four distinct operational states, with each state representing a specific voltage range that guides the control actions of the system. The operational state of each DER, such as PV and WT, is continuously compared with the DC bus voltage to determine the appropriate voltage regulation response. This approach enabled the system to manage disturbances effectively within the defined voltage thresholds without the immediate need for load shedding. By dynamically adjusting the DC bus voltage and selectively activating renewable energy sources only when necessary, the strategy ensures a more responsive system behaviour. Additionally, it minimises reliance on GTC units and BESS, thereby enhancing overall system efficiency and reducing operational costs.

Simulation results conducted under both grid-connected and islanded operating conditions confirmed the effectiveness of the proposed Adaptive DBS control strategy. The strategy demonstrated the capability to maintain power balance, minimise DC bus voltage deviations within acceptable limits, prevent voltage collapse, and facilitate smooth transitions between operational states among DERs. These results validate the proposed method's ability to effectively mitigate voltage fluctuations and improve voltage regulations within the DC microgrid.

The Adaptive DBS control strategy presented an efficient and non-communication-based alternative to conventional control methods. Its ability to dynamically regulate voltage and manage power-sharing without relying on communication infrastructure makes it particularly suitable for remote and resource-constrained environments.

7.1.3 Additional Contributions:

Further contributions of this work include the evaluation of existing DC load-shedding schemes. A detailed investigation was carried out into bus voltage control and load-shedding strategies used in non-communication-based DC microgrids, offering critical insights into current practices and their limitations. This analysis identified key areas where performance can be improved and underscored the growing need for advanced load-shedding solutions that can function effectively without reliance on communication infrastructure. Such capability is essential for ensuring reliable and resilient microgrid operation in remote, isolated, and resource-constrained environments.

To address this need, a comprehensive evaluation of existing load-shedding schemes was carried out, covering both conventional approaches, such as voltage-based, timer-based, and combined methods, and adaptive strategies, including adaptive voltage-based and adaptive timer-based techniques. Using state flow analysis, various disturbance scenarios were simulated and prioritised based on

critical operating conditions to assess system behaviour and evaluate the performance of each load-shedding scheme.

The evaluation considered key performance metrics, including the circuit breaker trip time, the minimum voltage level sustained by critical loads during disturbances, and the final recovery voltage of critical loads after system stabilisation. The results revealed notable limitations in all existing approaches. Adaptive schemes delivered faster and more reliable responses; however, their reliance on lower voltage thresholds for shedding lower-priority loads often exposed critical loads to undesirable low-voltage conditions. This makes adaptive schemes more appropriate for microgrids with fewer load-shedding steps. In contrast, conventional schemes, dependent on fixed voltage and time thresholds, suffered from delayed responses, which led to significant bus voltage deviations and, in many cases, unnecessary disconnection of non-critical loads.

The results demonstrate a clear need for the development of more advanced and robust load-shedding strategies that can enhance the operational resilience of future DC microgrids. These findings form a foundation for the advanced load-shedding strategies proposed in this thesis, aimed at addressing the identified limitations and ensuring improved system performance under practical and dynamic microgrid operating conditions.

7.2 Future Research

Building on the research conducted in this thesis, several promising areas for future investigation have been identified:

- Incorporation of Nonlinear Characteristics: Enhancing the model by incorporating nonlinear characteristics and applying nonlinear programming could improve the representation of system behaviours, offering a more accurate depiction of complex microgrid dynamics. For instance, this could in-

clude modelling the nonlinear voltage-current characteristics of power electronic converters, the nonlinear charging and discharging profiles of BESS, or the nonlinear power output curves of renewable energy sources such as PV systems and wind turbines under varying environmental conditions.

- Hybrid Optimisation for Load Shedding in DC Microgrids: Future research could explore the integration of hybrid optimisation techniques with the proposed MILP-based load-shedding strategy to further enhance decision-making accuracy, computational speed, and adaptability in complex microgrid environments. While such hybrid approaches—combining Mixed-Integer Linear Programming (MILP) with heuristic or metaheuristic algorithms like Genetic Algorithms (GA), Particle Swarm Optimisation (PSO), or Artificial Neural Networks (ANN)—have been widely studied in AC microgrids, their application in DC microgrids remains relatively underexplored.

  DC microgrids offer specific advantages for hybrid optimisation, as they eliminate the need for frequency and reactive power control, allowing algorithms to focus on voltage stability, load prioritisation, and energy balancing. Hybrid optimisation methods can address the computational complexity of MILP in large-scale or highly dynamic systems, improve real-time responsiveness, and better handle nonlinearities, uncertainties, and multi-objective trade-offs. These enhancements are particularly valuable in scenarios involving renewable variability, storage limitations, and multi-microgrid interconnections. Developing such hybrid schemes could significantly advance the resilience and scalability of DC microgrid control frameworks.

- Load Type Modelling and Impact on Load-Shedding Performance: The results in this thesis have shown that the type of load connected to the

DC microgrid significantly influences the system's dynamic response during disturbances and load-shedding events. In particular, constant power loads (CPLs) were observed to have destabilising effects—especially during mode transitions—due to their tendency to demand fixed power regardless of voltage fluctuations, potentially leading to unwanted power export from isolated DERs. To address this, future work could reconfigure the microgrid model to incorporate and systematically evaluate different load types, including CPLs, constant resistive loads (CRLs), and constant current loads (CCLs). Implementing these load models in a controlled manner would provide deeper insight into their individual and combined effects on voltage stability, power flow, and control response. Moreover, future research could explore hybrid load compositions that better represent real-world scenarios, such as those in data centres, hospitals, or industrial zones, where critical and non-critical loads coexist with different electrical characteristics. The integration of diverse load models would also enable the development of more robust and adaptive load-shedding algorithms, tailored to handle the nonlinear behaviour and sensitivities introduced by complex load dynamics. Additionally, analysing circuit breaker strategies—such as sectionalised zones or priority-based load grouping—could further improve protection coordination and microgrid resilience under such conditions.

- Future research may explore further refinements by integrating predictive models and machine learning techniques to optimise load-shedding decisions and enhance real-time adaptability.

Bibliography

[1] VerdeWatts. (2024, January 17) Shift to renewable power accelerates. [Online]. Available: https://www.verdewatts.com

[2] M. S. Kulkarni, S. Mishra, S. K. Sudabattula, N. K. Sharma, D. B. Basha, M. Bajaj, and M. B. Tuka, "Enhancing grid resiliency in distributed energy systems through a comprehensive review and comparative analysis of islanding detection methods," *Scientific Reports*, vol. 14, no. 1, p. 12124, 2024.

[3] M. Khodayar, S. Manshadi, and A. Vafamehr, "The short-term operation of microgrids in a transactive energy architecture," *The Electricity Journal*, vol. 29, no. 10, pp. 41–48, 2016.

[4] J. M. Abdullah and V. Sumathi, "An overview and minimum fault ramp rate analysis of impedance based circuit breaker topologies," *IEEE Access*, 2023.

[5] F. S. Al-Ismail, "Dc microgrid planning, operation, and control: A comprehensive review," *IEEE Access*, vol. 9, pp. 36 154–36 172, 2021.

[6] H. Lotfi and A. Khodaei, "Ac versus dc microgrid planning," *IEEE Transactions on Smart Grid*, vol. 8, no. 1, pp. 296–304, 2015.

[7] A. T. Elsayed, A. A. Mohamed, and O. A. Mohammed, "Dc microgrids and distribution systems: An overview," *Electric power systems research*, vol. 119, pp. 407–417, 2015.

[8] L. Richard, C. Boudinet, S. A. Ranaivoson, J. O. Rabarivao, A. E. Befeno, D. Frey, M.-C. Alvarez-Hérault, B. Raison, and N. Saincy, "Development of a dc microgrid with decentralized production and storage: From the lab to field deployment in rural africa," *energies*, vol. 15, no. 18, p. 6727, 2022.

[9] U. G. Onu, A. C. Z. de Souza, and B. D. Bonatto, "Drivers of microgrid projects in developed and developing economies," *Utilities Policy*, vol. 80, p. 101487, 2023.

[10] N. Zhi, K. Ding, L. Du, and H. Zhang, "An soc-based virtual dc machine control for distributed storage systems in dc microgrids," *IEEE Transactions on Energy Conversion*, vol. 35, no. 3, pp. 1411–1420, 2020.

[11] J. Liu, W. Zhang, and G. Rizzoni, "Robust stability analysis of dc microgrids with constant power loads," *IEEE Transactions on Power Systems*, vol. 33, no. 1, pp. 851–860, 2017.

[12] D. Kumar, F. Zare, and A. Ghosh, "Dc microgrid technology: system architectures, ac grid interfaces, grounding schemes, power quality, communication networks, applications, and standardizations aspects," *Ieee Access*, vol. 5, pp. 12 230–12 256, 2017.

[13] T. Dragičević, X. Lu, J. C. Vasquez, and J. M. Guerrero, "Dc microgrids—part i: A review of control strategies and stabilization techniques," *IEEE Transactions on power electronics*, vol. 31, no. 7, pp. 4876–4891, 2015.

[14] L. Zhang, W. Zhang, F. Zeng, and X. Yang, "A review of control strategies in dc microgrid," in *Journal of Physics: Conference Series*, vol. 1087, no. 4. IOP Publishing, 2018, p. 042035.

[15] E. E. Ojo, M. L. Zulu, and A. O. Akinrinde, "The modelling and simulation of power flow and fault analysis for a hybrid dc microgrid," in *2021 IEEE PES/IAS PowerAfrica*. IEEE, 2021, pp. 1–5.

[16] L. Meng, Q. Shafiee, G. F. Trecate, H. Karimi, D. Fulwani, X. Lu, and J. M. Guerrero, "Review on control of dc microgrids and multiple microgrid clusters," *IEEE journal of emerging and selected topics in power electronics*, vol. 5, no. 3, pp. 928–948, 2017.

[17] M. Kumar, S. C. Srivastava, and S. N. Singh, "Control strategies of a dc microgrid for grid connected and islanded operations," *IEEE Transactions on Smart Grid*, vol. 6, no. 4, pp. 1588–1601, 2015.

[18] S. K. Kollimalla, M. K. Mishra, A. Ukil, and H. Gooi, "Dc grid voltage regulation using new hess control strategy," *IEEE Transactions on Sustainable Energy*, vol. 8, no. 2, pp. 772–781, 2016.

[19] T. Zaman, Z. Feng, S. Mitra, M. Syed, S. Karanki, L. Villa, and G. Burt, "Ann driven fosmc based adaptive droop control for enhanced dc microgrid resilience," *IEEE Transactions on Industry Applications*, 2023.

[20] L. Gao, Y. Liu, H. Ren, and J. M. Guerrero, "A dc microgrid coordinated control strategy based on integrator current-sharing," *Energies*, vol. 10, no. 8, p. 1116, 2017.

[21] N. N. A. Bakar, M. Y. Hassan, M. F. Sulaima, M. Na'im Mohd Nasir, and A. Khamis, "Microgrid and load shedding scheme during islanded mode: A

review," *Renewable and Sustainable Energy Reviews*, vol. 71, pp. 161–169, 2017.

[22] N. Sapari, H. Mokhlis, J. A. Laghari, A. Bakar, and M. Dahalan, "Application of load shedding schemes for distribution network connected with distributed generation: A review," *Renewable and Sustainable Energy Reviews*, vol. 82, pp. 858–867, 2018.

[23] M. Sechilariu, B. C. Wang, F. Locment, and A. Jouglet, "Dc microgrid power flow optimization by multi-layer supervision control. design and experimental validation," *Energy conversion and management*, vol. 82, pp. 1–10, 2014.

[24] C. Wang, J. Duan, B. Fan, Q. Yang, and W. Liu, "Decentralized high-performance control of dc microgrids," *IEEE Transactions on Smart Grid*, vol. 10, no. 3, pp. 3355–3363, 2018.

[25] N. L. Diaz, A. C. Luna, J. C. Vasquez, and J. M. Guerrero, "Centralized control architecture for coordination of distributed renewable generation and energy storage in islanded ac microgrids," *IEEE Transactions on Power Electronics*, vol. 32, no. 7, pp. 5202–5213, 2016.

[26] J. Mohammadi and F. B. Ajaei, "Dc microgrid load shedding schemes," in *2019 IEEE/IAS 55th Industrial and Commercial Power Systems Technical Conference (I&CPS)*. IEEE, 2019, pp. 1–7.

[27] U. Energy, "Doe microgrid workshop report," 2018.

[28] N. Hatziargyriou, H. Asano, R. Iravani, and C. M. Marnay, "Ieee power energy mag," 2007.

[29] M. Shahbazitabar, H. Abdi, H. Nourianfar, A. Anvari-Moghaddam, B. Mohammadi-Ivatloo, and N. Hatziargyriou, "An introduction to mi-

crogrids, concepts, definition, and classifications," *Microgrids: Advances in Operation, Control, and Protection*, pp. 3–16, 2021.

[30] V. Adomavičius, G. Šimkonienė, and B. Azzopardi, "Advantages of the microgrids based on a small-scale hydropower plants," 2022.

[31] S. E. Eyimaya and N. Altin, "Microgrids: Definitions, architecture, and control strategies," in *Power Electronics Converters and their Control for Renewable Energy Applications*. Elsevier, 2023, pp. 167–186.

[32] N. Lidula and A. Rajapakse, "Microgrids research: A review of experimental microgrids and test systems," *Renewable and sustainable energy reviews*, vol. 15, no. 1, pp. 186–202, 2011.

[33] C. De MartiniP and N. Fromer, "Grid 2020: towards a policy of renewable and distributed energy resources. california institute of technology resnick institute," Tech. Rep., Pasadena, CA, Tech. Rep., 2012.

[34] H. Abdi and M. Shahbazitabar, "Smart city: A review on concepts, definitions, standards, experiments, and challenges," *Journal of Energy Management and Technology*, vol. 4, no. 3, pp. 1–6, 2020.

[35] R. Majumder, "Some aspects of stability in microgrids," *IEEE Transactions on power systems*, vol. 28, no. 3, pp. 3243–3252, 2013.

[36] R. Bayindir, E. Hossain, E. Kabalci, and R. Perez, "A comprehensive study on microgrid technology," *International Journal of Renewable Energy Research*, vol. 4, no. 4, pp. 1094–1107, 2014.

[37] N. Ertugrul, "Battery storage technologies, applications and trend in renewable energy," 2016, pp. 420–425.

[38] H. E. O. Farias and L. N. Canha, "Battery energy storage systems (bess) overview of key market technologies," in *2018 IEEE PES Transmission & Distribution Conference and Exhibition-Latin America (T&D-LA)*. IEEE, 2018, pp. 1–5.

[39] T. S. Ustun, C. Ozansoy, and A. Zayegh, "Recent developments in microgrids and example cases around the world—a review," *Renewable and Sustainable Energy Reviews*, vol. 15, no. 8, pp. 4030–4041, 2011.

[40] A. L. Dimeas and N. D. Hatziargyriou, "Operation of a multiagent system for microgrid control," *IEEE Transactions on Power systems*, vol. 20, no. 3, pp. 1447–1455, 2005.

[41] S. Li, T. A. Haskew, and L. Xu, "Conventional and novel control designs for direct driven pmsg wind turbines," *Electric Power Systems Research*, vol. 80, no. 3, pp. 328–338, 2010.

[42] J. P. Lopes, C. L. Moreira, and A. Madureira, "Defining control strategies for microgrids islanded operation," *IEEE Transactions on power systems*, vol. 21, no. 2, pp. 916–924, 2006.

[43] M. Y. Worku, M. A. Hassan, L. S. Maraaba, and M. A. Abido, "Islanding detection methods for microgrids: A comprehensive review," *Mathematics*, vol. 9, no. 24, p. 3174, 2021.

[44] H. Han, X. Hou, J. Yang, J. Wu, M. Su, and J. M. Guerrero, "Review of power sharing control strategies for islanding operation of ac microgrids," *IEEE Transactions on Smart Grid*, vol. 7, no. 1, pp. 200–215, 2015.

[45] A. Khodaei and A. Arabnya, "Dynamics of microgrids in distribution network flexibility," 2024.

[46] S. S. Rangarajan, R. Raman, A. Singh, C. K. Shiva, R. Kumar, P. K. Sadhu, E. R. Collins, and T. Senjyu, "Dc microgrids: A propitious smart grid paradigm for smart cities," *Smart Cities*, vol. 6, no. 4, pp. 1690–1718, 2023.

[47] B. Modu, M. P. Abdullah, M. A. Sanusi, and M. F. Hamza, "Dc-based microgrid: Topologies, control schemes, and implementations," *Alexandria Engineering Journal*, vol. 70, pp. 61–92, 2023.

[48] T. Dragičević, J. M. Guerrero, J. C. Vasquez, and D. Škrlec, "Supervisory control of an adaptive-droop regulated dc microgrid with battery management capability," *IEEE Transactions on power Electronics*, vol. 29, no. 2, pp. 695–706, 2013.

[49] G. Shahgholian, "A brief review on microgrids: Operation, applications, modeling, and control," *International Transactions on Electrical Energy Systems*, vol. 31, no. 6, p. e12885, 2021.

[50] D. between ac microgrid and dc microgrd, "Differences between ac microgrid and dc microgrd," *https://veckta.com/2021/05/27/the-differences-between-ac-microgrids-and-dc-microgrids/*, 2021.

[51] Z. Shuai, J. Fang, F. Ning, and Z. J. Shen, "Hierarchical structure and bus voltage control of dc microgrid," *Renewable and Sustainable Energy Reviews*, vol. 82, pp. 3670–3682, 2018.

[52] J. Hu, T. Zhang, S. Du, and Y. Zhao, "An overview on analysis and control of micro-grid system," *International Journal of Control and Automation*, vol. 8, no. 6, pp. 65–76, 2015.

[53] P. Xu, J. Xu, K. Wang, and G. Li, "Hierarchical control architecture for networked synchronization of multi-microgrids," in *2022 Power System and Green Energy Conference (PSGEC)*. IEEE, 2022, pp. 272–277.

[54] S. Gawande, P. S. Shete, and P. Chaturvedi, "Control architectures for low voltage dc (lvdc) microgrid," in *Planning of Hybrid Renewable Energy Systems, Electric Vehicles and Microgrid: Modeling, Control and Optimization*. Springer, 2022, pp. 629–647.

[55] L. Yan, M. Sheikholeslami, W. Gong, M. Shahidehpour, and Z. Li, "Architecture, control, and implementation of networked microgrids for future distribution systems," *Journal of Modern Power Systems and Clean Energy*, vol. 10, no. 2, pp. 286–299, 2022.

[56] H. Gu, Z. Jiao, and J. Liu, "Small-signal model and stability analysis of dc microgrids with master-slave control strategy," in *2019 IEEE Power & Energy Society General Meeting (PESGM)*. IEEE, 2019, pp. 1–5.

[57] Y. Hennane, Y. A. A. B. Hassi, A. Berdai, and V. Tytiuk, "Primary, secondary and tertiary controls of a mesh multi-pcc microgrid," in *2022 IEEE 4th International Conference on Modern Electrical and Energy System (MEES)*. IEEE, 2022, pp. 1–5.

[58] X. Li, Z. Ji, F. Yang, Z. Dou, C. Zhang, and L. Chen, "A distributed two-level control strategy for dc microgrid considering safety of charging equipment," *Energies*, vol. 15, no. 22, p. 8600, 2022.

[59] A. Hooshyar and R. Iravani, "Microgrid protection," *Proceedings of the IEEE*, vol. 105, no. 7, pp. 1332–1353, 2017.

[60] M. Mehmood, S. B. A. Bukhari, A. Altamimi, Z. A. Khan, S. A. A. Kazmi, M. Yousif, and D. R. Shin, "Microgrid protection using magneto-resistive

sensors and superimposed reactive energy," *Sustainability*, vol. 15, no. 1, p. 599, 2022.

[61] S. A. Hosseini, H. A. Abyaneh, S. H. H. Sadeghi, F. Razavi, and A. Nasiri, "An overview of microgrid protection methods and the factors involved," *Renewable and Sustainable Energy Reviews*, vol. 64, pp. 174–186, 2016.

[62] Z. Liang, H. Chen, X. Wang, S. Chen, and C. Zhang, "Risk-based uncertainty set optimization method for energy management of hybrid ac/dc microgrids with uncertain renewable generation," *IEEE Transactions on Smart Grid*, vol. 11, no. 2, pp. 1526–1542, 2019.

[63] B. Papari, C. Edrington, T. Vu, and F. Diaz-Franco, "A heuristic method for optimal energy management of dc microgrid," in *2017 IEEE Second International Conference on DC Microgrids (ICDCM)*. IEEE, 2017, pp. 337–343.

[64] N. Nikmehr and S. Najafi-Ravadanegh, "Probabilistic optimal power dispatch in multi-microgrids using heuristic algorithms," in *2014 Smart Grid Conference (SGC)*. IEEE, 2014, pp. 1–6.

[65] Q. Zhou, M. Shahidehpour, A. Paaso, S. Bahramirad, A. Alabdulwahab, and A. Abusorrah, "Distributed control and communication strategies in networked microgrids," *IEEE Communications Surveys & Tutorials*, vol. 22, no. 4, pp. 2586–2633, 2020.

[66] H. Jiang, Z. Wang, F. Zuo, Y. Yao, and P. Wang, "An information/power fusion coordinated control framework for bipolar dc microgrids," in *Journal of Physics: Conference Series*, vol. 2835, no. 1. IOP Publishing, 2024, p. 012031.

[67] K. T. Tan, X. Peng, P. L. So, Y. C. Chu, and M. Z. Chen, "Centralized control for parallel operation of distributed generation inverters in microgrids," *IEEE Transactions on Smart Grid*, vol. 3, no. 4, pp. 1977–1987, 2012.

[68] P. Tenti and T. Caldognetto, "Master/slave power-based control of low-voltage microgrids," in *Microgrid*. Elsevier, 2017, pp. 101–135.

[69] J. Rajagopalan, K. Xing, Y. Guo, F. Lee, and B. Manners, "Modeling and dynamic analysis of paralleled dc/dc converters with master-slave current sharing control," in *Proceedings of Applied Power Electronics Conference. APEC'96*, vol. 2. IEEE, 1996, pp. 678–684.

[70] T.-F. Wu, Y.-K. Chen, and Y.-H. Huang, "3c strategy for inverters in parallel operation achieving an equal current distribution," *IEEE Transactions on Industrial Electronics*, vol. 47, no. 2, pp. 273–281, 2000.

[71] T. Morstyn, B. Hredzak, G. D. Demetriades, and V. G. Agelidis, "Unified distributed control for dc microgrid operating modes," *IEEE Transactions on Power Systems*, vol. 31, no. 1, pp. 802–812, 2015.

[72] F. Guo, Q. Xu, C. Wen, L. Wang, and P. Wang, "Distributed secondary control for power allocation and voltage restoration in islanded dc microgrids," *IEEE Transactions on Sustainable Energy*, vol. 9, no. 4, pp. 1857–1869, 2018.

[73] A. Abhishek, A. Ranjan, S. Devassy, B. Kumar Verma, S. K. Ram, and A. K. Dhakar, "Review of hierarchical control strategies for dc microgrid," *IET Renewable Power Generation*, vol. 14, no. 10, pp. 1631–1640, 2020.

[74] R. Han, L. Meng, J. M. Guerrero, and J. C. Vasquez, "Distributed nonlinear control with event-triggered communication to achieve current-sharing

and voltage regulation in dc microgrids," *IEEE Transactions on Power Electronics*, vol. 33, no. 7, pp. 6416–6433, 2017.

[75] Q. Shafiee, J. M. Guerrero, and J. C. Vasquez, "Distributed secondary control for islanded microgrids—a novel approach," *IEEE Transactions on power electronics*, vol. 29, no. 2, pp. 1018–1031, 2013.

[76] J. P. Torreglosa, P. Garcia-Trivino, L. M. Fernández-Ramirez, and F. Jurado, "Control strategies for dc networks: A systematic literature review," *Renewable and Sustainable Energy Reviews*, vol. 58, pp. 319–330, 2016.

[77] S. K. Sahoo, A. K. Sinha, and N. Kishore, "Control techniques in ac, dc, and hybrid ac–dc microgrid: A review," *IEEE Journal of Emerging and Selected Topics in Power Electronics*, vol. 6, no. 2, pp. 738–759, 2017.

[78] J. Mohammadi and F. B. Ajaei, "Improved mode-adaptive droop control strategy for the dc microgrid," *IEEE Access*, vol. 7, pp. 86 421–86 435, 2019.

[79] S. Peyghami, H. Mokhtari, P. Davari, P. C. Loh, and F. Blaabjerg, "On secondary control approaches for voltage regulation in dc microgrids," *IEEE Transactions on Industry Applications*, vol. 53, no. 5, pp. 4855–4862, 2017.

[80] P. Sanjeev, N. P. Padhy, and P. Agarwal, "Autonomous power control and management between standalone dc microgrids," *IEEE Transactions on Industrial Informatics*, vol. 14, no. 7, pp. 2941–2950, 2017.

[81] P. Prabhakaran, Y. Goyal, and V. Agarwal, "Novel nonlinear droop control techniques to overcome the load sharing and voltage regulation issues in dc microgrid," *IEEE Transactions on power electronics*, vol. 33, no. 5, pp. 4477–4487, 2017.

[82] X. Lu, K. Sun, J. M. Guerrero, J. C. Vasquez, and L. Huang, "Double-quadrant state-of-charge-based droop control method for distributed en-

ergy storage systems in autonomous dc microgrids," *IEEE Transactions on Smart Grid*, vol. 6, no. 1, pp. 147–157, 2014.

[83] S. Augustine, M. K. Mishra, and N. Lakshminarasamma, "Adaptive droop control strategy for load sharing and circulating current minimization in low-voltage standalone dc microgrid," *IEEE Transactions on Sustainable Energy*, vol. 6, no. 1, pp. 132–141, 2014.

[84] J. Mohammadi and F. Badrkhani Ajaei, "Versatile decentralized control of the dc microgrid," *IET Smart Grid*, vol. 2, no. 1, pp. 77–88, 2019.

[85] K. Sun, L. Zhang, Y. Xing, and J. M. Guerrero, "A distributed control strategy based on dc bus signaling for modular photovoltaic generation systems with battery energy storage," *IEEE transactions on power electronics*, vol. 26, no. 10, pp. 3032–3045, 2011.

[86] N. Eghtedarpour and E. Farjah, "Control strategy for distributed integration of photovoltaic and energy storage systems in dc micro-grids," *Renewable energy*, vol. 45, pp. 96–110, 2012.

[87] Y. Gu, W. Li, and X. He, "Frequency-coordinating virtual impedance for autonomous power management of dc microgrid," *IEEE Transactions on Power Electronics*, vol. 30, no. 4, pp. 2328–2337, 2014.

[88] J. Meng, Y. Wang, C. Wang, and H. Wang, "Design and implementation of hardware-in-the-loop simulation system for testing control and operation of dc microgrid with multiple distributed generation units," *IET Generation, Transmission & Distribution*, vol. 11, no. 12, pp. 3065–3072, 2017.

[89] D. Chen, L. Xu, and L. Yao, "Dc voltage variation based autonomous control of dc microgrids," *IEEE transactions on power delivery*, vol. 28, no. 2, pp. 637–648, 2013.

[90] N. L. Diaz, T. Dragičević, J. C. Vasquez, and J. M. Guerrero, "Intelligent distributed generation and storage units for dc microgrids—a new concept on cooperative control without communications beyond droop control," *IEEE Transactions on Smart Grid*, vol. 5, no. 5, pp. 2476–2485, 2014.

[91] Q. Yang, L. Jiang, H. Zhao, and H. Zeng, "Autonomous voltage regulation and current sharing in islanded multi-inverter dc microgrid," *IEEE Transactions on Smart Grid*, vol. 9, no. 6, pp. 6429–6437, 2017.

[92] D. Chen and L. Xu, "Autonomous dc voltage control of a dc microgrid with multiple slack terminals," *IEEE Transactions on Power Systems*, vol. 27, no. 4, pp. 1897–1905, 2012.

[93] L. Xu and D. Chen, "Control and operation of a dc microgrid with variable generation and energy storage," *IEEE transactions on power delivery*, vol. 26, no. 4, pp. 2513–2522, 2011.

[94] A. Khorsandi, M. Ashourloo, and H. Mokhtari, "A decentralized control method for a low-voltage dc microgrid," *IEEE Transactions on Energy Conversion*, vol. 29, no. 4, pp. 793–801, 2014.

[95] T. D. Khoa, L. T. Dos Santos, M. Sechilariu, and F. Locment, "Load shedding and restoration real-time optimization for dc microgrid power balancing," in *2016 IEEE International Energy Conference (ENERGYCON)*. IEEE, 2016, pp. 1–6.

[96] F. Li, Z. Lin, H. Xu, and R. Wang, "A review of dc bus signalling control methods in dc microgrids," in *2022 IEEE International Power Electronics and Application Conference and Exposition (PEAC)*. IEEE, 2022, pp. 1286–1291.

[97] J. Mohammadi and F. B. Ajaei, "Adaptive voltage-based load shedding scheme for the dc microgrid," *Ieee Access*, vol. 7, pp. 106 002–106 010, 2019.

[98] M. Sechilariu, B. C. Wang, and F. Locment, "Supervision control for optimal energy cost management in dc microgrid: Design and simulation," *International Journal of Electrical Power & Energy Systems*, vol. 58, pp. 140–149, 2014.

[99] P. Sanjeev, N. P. Padhy, and P. Agarwal, "Peak energy management using renewable integrated dc microgrid," *IEEE Transactions on Smart Grid*, vol. 9, no. 5, pp. 4906–4917, 2017.

[100] L. Shun, L. Qingfen, and W. Jiali, "Dynamic optimization of adaptive under-frequency load shedding based on wams," in *2016 IEEE Information Technology, Networking, Electronic and Automation Control Conference*. IEEE, 2016, pp. 920–926.

[101] L. Trigueiro dos Santos, M. Sechilariu, and F. Locment, "Optimized load shedding approach for grid-connected dc microgrid systems under realistic constraints," *Buildings*, vol. 6, no. 4, p. 50, 2016.

[102] L. T. Dos Santos, M. Sechilariu, and F. Locment, "Day-ahead microgrid optimal self-scheduling: Comparison between three methods applied to isolated dc microgrid," in *IECON 2014-40th Annual Conference of the IEEE Industrial Electronics Society*. IEEE, 2014, pp. 2010–2016.

[103] ——, "Prediction-based economic dispatch and online optimization for grid-connected dc microgrid," in *2016 IEEE International Energy Conference (ENERGYCON)*. IEEE, 2016, pp. 1–6.

[104] C. Liu, S. S. Abdulkareem, A. Rezvani, S. Samad, N. Aljojo, L. K. Foong, and K. Nishihara, "Stochastic scheduling of a renewable-based microgrid in

the presence of electric vehicles using modified harmony search algorithm with control policies," *Sustainable cities and society*, vol. 59, p. 102183, 2020.

[105] D.-H. Dam and H.-H. Lee, "An adaptive power distributed control method to ensure proportional load power sharing in dc microgrid considering equivalent line impedances," in *2016 IEEE Energy Conversion Congress and Exposition (ECCE)*. IEEE, 2016, pp. 1–6.

[106] S. Mandal and K. K. Mandal, "Optimal energy management of microgrids under environmental constraints using chaos enhanced differential evolution," *Renewable Energy Focus*, vol. 34, pp. 129–141, 2020.

[107] D. Rwegasira, I. B. Dhaou, A. Anagnostou, A. Kondoro, N. Shililiandumi, A. Kelati, S. J. Taylor, N. Mvungi, and H. Tenhunen, "A framework for load shedding and demand response in dc microgrid using multi-agent system," in *2017 21st Conference of Open Innovations Association (FRUCT)*. IEEE, 2017, pp. 284–289.

[108] L. Zhang, Y. Wang, H. Li, and P. Sun, "Hierarchical coordinated control of dc microgrid with wind turbines," in *IECON 2012-38th Annual Conference on IEEE Industrial Electronics Society*. IEEE, 2012, pp. 3547–3552.

[109] H. Wen, K. Zheng, and Y. Du, "Hierarchical coordinated control for dc microgrid with crowbar and load shedding control," in *2017 IEEE 3rd International Future Energy Electronics Conference and ECCE Asia (IFEEC 2017-ECCE Asia)*. IEEE, 2017, pp. 2208–2212.

[110] S. Sahoo and S. Mishra, "A multi-objective adaptive control framework in autonomous dc microgrid," *IEEE Transactions on Smart Grid*, vol. 9, no. 5, pp. 4918–4929, 2017.

[111] A. Garg, B. M. Joshi, and R. Oruganti, "Modeling a dc microgrid with real-time power management using dc bus signalling," in *2018 IEEE Energy Conversion Congress and Exposition (ECCE)*. IEEE, 2018, pp. 46–53.

[112] J. Schonberger, S. Round, and R. Duke, "Autonomous load shedding in a nanogrid using dc bus signaling," in *IECON 2006-32nd Annual Conference on IEEE Industrial Electronics*. IEEE, 2006, pp. 5155–5160.

[113] D. Chen and L. Xu, "Dc microgrid with variable generations and energy storage," 2011.

[114] A. Babagana, T. Zaman, Y. Seferi, M. Syed, and G. Burt, "Comparison of non-communication based dc load shedding schemes," in *2022 57th International Universities Power Engineering Conference (UPEC)*. IEEE, 2022, pp. 1–6.

[115] J. Mohammadi and F. B. Ajaei, "Adaptive time delay strategy for reliable load shedding in the direct-current microgrid," *Ieee Access*, vol. 8, pp. 114 509–114 518, 2020.

[116] I. Kim, R. Regassa, and R. G. Harley, "The modeling of distribution feeders enhanced by distributed generation in digsilent," in *2015 IEEE 42nd Photovoltaic Specialist Conference (PVSC)*. IEEE, 2015, pp. 1–5.

[117] A. M. Stanisavljević, V. A. Katić, B. P. Dumnić, and B. P. Popadić, "A brief overview of the distribution test grids with a distributed generation inclusion case study," *Serbian Journal of Electrical Engineering*, vol. 15, no. 1, pp. 115–129, 2018.

[118] R. on IEEE Distribution Test Feeder Working Group, "Ieee 37 node test feeder," 1992.

[119] K. P. Schneider, B. Mather, B. C. Pal, C.-W. Ten, G. J. Shirek, H. Zhu, J. C. Fuller, J. L. R. Pereira, L. F. Ochoa, L. R. de Araujo *et al.*, "Analytic considerations and design basis for the ieee distribution test feeders," *IEEE Transactions on power systems*, vol. 33, no. 3, pp. 3181–3188, 2017.

[120] B. R. Ravada and N. R. Tummuru, "Control of a supercapacitor-battery-pv based stand-alone dc-microgrid," *IEEE Transactions on Energy Conversion*, vol. 35, no. 3, pp. 1268–1277, 2020.

[121] R. on IEEE Distribution Test Feeder Working Group, "Ieee 37 node test feeder," 1992.

[122] E. Rodriguez-Diaz, F. Chen, J. C. Vasquez, J. M. Guerrero, R. Burgos, and D. Boroyevich, "Voltage-level selection of future two-level lvdc distribution grids: A compromise between grid compatibility, safety, and efficiency," *IEEE Electrification Magazine*, vol. 4, no. 2, pp. 20–28, 2016.

[123] M. Borghei and M. Ghassemi, "A multi-objective optimization scheme for resilient, cost-effective planning of microgrids," *IEEE Access*, vol. 8, pp. 206 325–206 341, 2020.

[124] H. Kakigano, Y. Miura, and T. Ise, "Low-voltage bipolar-type dc microgrid for super high quality distribution," *IEEE transactions on power electronics*, vol. 25, no. 12, pp. 3066–3075, 2010.

[125] J. Mohammadi, F. B. Ajaei, and G. Stevens, "Grounding the dc microgrid," *IEEE Transactions on Industry Applications*, vol. 55, no. 5, pp. 4490–4499, 2019.

[126] P. Salonen, P. Nuutinen, P. Peltoniemi, and J. Partanen, "Lvdc distribution system protection—solutions, implementation and measurements," in *2009*

13th European Conference on Power Electronics and Applications. IEEE, 2009, pp. 1–10.

[127] A. Yazdani, A. R. Di Fazio, H. Ghoddami, M. Russo, M. Kazerani, J. Jatskevich, K. Strunz, S. Leva, and J. A. Martinez, "Modeling guidelines and a benchmark for power system simulation studies of three-phase single-stage photovoltaic systems," *IEEE transactions on power delivery*, vol. 26, no. 2, pp. 1247–1264, 2010.

[128] L. Ye, H. B. Sun, X. R. Song, and L. C. Li, "Dynamic modeling of a hybrid wind/solar/hydro microgrid in emtp/atp," *Renewable Energy*, vol. 39, no. 1, pp. 96–106, 2012.

[129] X. H. Nguyen and M. P. Nguyen, "Mathematical modeling of photovoltaic cell/module/arrays with tags in matlab/simulink," *Environmental Systems Research*, vol. 4, pp. 1–13, 2015.

[130] G. Michalke, A. D. Hansen, and T. Hartkopf, "Control strategy of a variable speed wind turbine with multipole permanent magnet synchronous generator," in *2007 European Wind Energy Conference and Exhibition*, vol. 160. Citeseer, 2007.

[131] M. Jahanpour-Dehkordi, S. Vaez-Zadeh, and J. Mohammadi, "Development of a combined control system to improve the performance of a pmsg-based wind energy conversion system under normal and grid fault conditions," *IEEE Transactions on Energy Conversion*, vol. 34, no. 3, pp. 1287–1295, 2019.

[132] K. E. Okedu, "Improving the performance of pmsg wind turbines during grid fault considering different strategies of fault current limiters," *Frontiers in Energy Research*, vol. 10, p. 909044, 2022.

[133] O. Tremblay, L.-A. Dessaint, and A.-I. Dekkiche, "A generic battery model for the dynamic simulation of hybrid electric vehicles," in *2007 IEEE Vehicle Power and propulsion conference*. Ieee, 2007, pp. 284–289.

[134] A. Yazdani and R. Iravani, *Voltage-sourced converters in power systems: modeling, control, and applications*. John Wiley & Sons, 2010.

[135] J. Mohammadi, S. Vaez-Zadeh, E. Ebrahimzadeh, and F. Blaabjerg, "Combined control method for grid-side converter of doubly fed induction generator-based wind energy conversion systems," *IET Renewable Power Generation*, vol. 12, no. 8, pp. 943–952, 2018.

[136] D. Nilsson and A. Sannino, "Load modelling for steady-state and transient analysis of low-voltage dc systems," in *Conference Record of the 2004 IEEE Industry Applications Conference, 2004. 39th IAS Annual Meeting.*, vol. 2. IEEE, 2004, pp. 774–780.

[137] A. Emadi, A. Khaligh, C. H. Rivetta, and G. A. Williamson, "Constant power loads and negative impedance instability in automotive systems: definition, modeling, stability, and control of power electronic converters and motor drives," *IEEE Transactions on vehicular technology*, vol. 55, no. 4, pp. 1112–1125, 2006.

[138] D. Salomonsson and A. Sannino, "Load modelling for steady-state and transient analysis of low-voltage dc systems," *IET Electric Power Applications*, vol. 1, no. 5, pp. 690–696, 2007.

[139] N. Bottrell, M. Prodanovic, and T. C. Green, "Dynamic stability of a microgrid with an active load," *IEEE Transactions on power electronics*, vol. 28, no. 11, pp. 5107–5119, 2013.

[140] F. Zhao, N. Li, Z. Yin, and X. Tang, "Small-signal modeling and stability analysis of dc microgrid with multiple type of loads," in *2014 International Conference on Power System Technology*. IEEE, 2014, pp. 3309–3315.

[141] T. M. Inc., "Matlab version: 9.13.0 (r2022b)," Natick, Massachusetts, United States, 2022. [Online]. Available: https://www.mathworks.com

[142] S. Liu, K. Yang, Y. Yang, Z. Liu, Y. Geng, and J. Wang, "Railway dc circuit breaker based on the superconducting fault current limiter," in *2016 27th International Symposium on Discharges and Electrical Insulation in Vacuum (ISDEIV)*, vol. 2. IEEE, 2016, pp. 1–4.

[143] M. Kempkes, I. Roth, and M. Gaudreau, "Solid-state circuit breakers for medium voltage dc power," in *2011 IEEE Electric Ship Technologies Symposium*. IEEE, 2011, pp. 254–257.

[144] W. Y. Kong, "Review of dc circuit breakers for submarine applications." 2012.

[145] Y. Kaya and S. Yamamura, "A self-adaptive system with a variable-parameter pid controller," *Transactions of the American Institute of Electrical Engineers, Part II: Applications and Industry*, vol. 80, no. 6, pp. 378–386, 1962.

[146] Q. Zhou, Z. Li, Q. Wu, and M. Shahidehpour, "Two-stage load shedding for secondary control in hierarchical operation of islanded microgrids," *IEEE Transactions on Smart Grid*, vol. 10, no. 3, pp. 3103–3111, 2018.

[147] X. Lu, K. Sun, J. M. Guerrero, J. C. Vasquez, and L. Huang, "State-of-charge balance using adaptive droop control for distributed energy storage systems in dc microgrid applications," *IEEE Transactions on Industrial electronics*, vol. 61, no. 6, pp. 2804–2815, 2013.

[148] A. Meghwani, S. Chakrabarti, and S. Srivastava, "A fast scheme for fault detection in dc microgrid based on voltage prediction," in *2016 National Power Systems Conference (NPSC)*. IEEE, 2016, pp. 1–6.

[149] M. H. Syed, E. Guillo-Sansano, S. M. Blair, A. J. Roscoe, and G. M. Burt, "A novel decentralized responsibilizing primary frequency control," *IEEE Transactions on Power Systems*, vol. 33, no. 3, pp. 3199–3201, 2018.

[150] S. Ferahtia, A. Djerioui, H. Rezk, A. Chouder, A. Houari, and M. Machmoum, "Adaptive droop based control strategy for dc microgrid including multiple batteries energy storage systems," *Journal of Energy Storage*, vol. 48, p. 103983, 2022.

[151] X. Lu, J. M. Guerrero, K. Sun, and J. C. Vasquez, "An improved droop control method for dc microgrids based on low bandwidth communication with dc bus voltage restoration and enhanced current sharing accuracy," *IEEE Transactions on Power Electronics*, vol. 29, no. 4, pp. 1800–1812, 2013.

[152] C. Papadimitriou, E. Zountouridou, and N. Hatziargyriou, "Review of hierarchical control in dc microgrids," *Electric Power Systems Research*, vol. 122, pp. 159–167, 2015.

[153] Y. Yang, X. Wang, C. Qi, C. Deng, L. Yu, and W. Yue, "A distributed event-triggered dynamic average consensus scheme with a time-varying threshold and its application in dc microgrid," *Asian Journal of Control*, vol. 25, no. 6, pp. 4551–4566, 2023.

[154] N. Muhammad, N. Z. Zakaria, S. Shaari, and A. M. Omar, "Threshold value of dc array current and dc string voltage for fault detection in grid-connected photovoltaic system," *Scientific Research Journal*, vol. 17, no. 1, pp. 1–13, 2020.

[155] P. G. Papageorgiou, K. O. Oureilidis, and G. C. Christoforidis, "Enhancing stability of dc microgrids employing smes-battery hybrid energy storage system," in *2022 Workshop on Blockchain for Renewables Integration (BLORIN)*. IEEE, 2022, pp. 85–90.

[156] P. Kou, D. Liang, J. Wang, and L. Gao, "Stable and optimal load sharing of multiple pmsgs in an islanded dc microgrid," *IEEE Transactions on Energy Conversion*, vol. 33, no. 1, pp. 260–271, 2017.

[157] A. Almousawi and A. A. Aldair, "Control strategy for a pv-bess-sc hybrid system in islanded microgrid," *Al-mağalla al-irāqiyya al-handasa al-kahrabāiyya wa-al-ilikttrūniyya*, vol. 19, no. 1, pp. 1–11, 2023.

[158] P. Kou, D. Liang, and L. Gao, "Distributed coordination of multiple pmsgs in an islanded dc microgrid for load sharing," *IEEE Transactions on Energy Conversion*, vol. 32, no. 2, pp. 471–485, 2017.

[159] A. A. Bazmi and G. Zahedi, "Sustainable energy systems: Role of optimization modeling techniques in power generation and supply—a review," *Renewable and sustainable energy reviews*, vol. 15, no. 8, pp. 3480–3500, 2011.

[160] D. P. Kothari, "Power system optimization," in *2012 2nd National conference on computational intelligence and signal processing (CISP)*. IEEE, 2012, pp. 18–21.

[161] A. M. Sasson and H. M. Merrill, "Some applications of optimization techniques to power systems problems," *Proceedings of the IEEE*, vol. 62, no. 7, pp. 959–972, 1974.

[162] M. Kaur and N. Narang, "An integrated optimization technique for optimal power flow solution," *Soft Computing*, vol. 24, pp. 10 865–10 882, 2020.

[163] D. Ananth and K. Vineela, "A review of different optimisation techniques for solving single and multi-objective optimisation problem in power system and mostly unit commitment problem," *International Journal of Ambient Energy*, vol. 42, no. 14, pp. 1676–1698, 2021.

[164] A. M. Haidar, A. Mohamed, and A. Hussain, "Vulnerability control of large scale interconnected power system using neuro-fuzzy load shedding approach," *Expert Systems with Applications*, vol. 37, no. 4, pp. 3171–3176, 2010.

[165] A. Vijay, W. Afzal, M. Tariq, A. Mustafa, and A. Shahzad, "Review of power generation optimization algorithms: Challenges and its applications," in *2022 International Conference on Augmented Intelligence and Sustainable Systems (ICAISS)*. IEEE, 2022, pp. 1391–1397.

[166] J. Sasikala and M. Ramaswamy, "Fuzzy based load shedding strategies for avoiding voltage collapse," *Applied Soft Computing*, vol. 11, no. 3, pp. 3179–3185, 2011.

[167] R. Kanimozhi, K. Selvi, and K. Balaji, "Multi-objective approach for load shedding based on voltage stability index consideration," *Alexandria Engineering Journal*, vol. 53, no. 4, pp. 817–825, 2014.

[168] M. Poshtan and S. Farinwata, "Intelligent undervoltage load curtailment," in *2006 IEEE International Conference on Fuzzy Systems*. IEEE, 2006, pp. 1721–1728.

[169] Y.-Y. Hong and S.-F. Wei, "Multiobjective underfrequency load shedding in an autonomous system using hierarchical genetic algorithms," *IEEE transactions on power delivery*, vol. 25, no. 3, pp. 1355–1362, 2010.

[170] H. Lu, P. Sriyanyong, Y. H. Song, and T. Dillon, "Experimental study of a new hybrid pso with mutation for economic dispatch with non-smooth cost function," *International Journal of Electrical Power & Energy Systems*, vol. 32, no. 9, pp. 921–935, 2010.

[171] I. J. Raglend, C. Raghuveer, G. R. Avinash, N. P. Padhy, and D. Kothari, "Solution to profit based unit commitment problem using particle swarm optimization," *Applied Soft Computing*, vol. 10, no. 4, pp. 1247–1256, 2010.

[172] J.-B. Park, K.-S. Lee, J.-R. Shin, and K. Y. Lee, "A particle swarm optimization for economic dispatch with nonsmooth cost functions," *IEEE Transactions on Power systems*, vol. 20, no. 1, pp. 34–42, 2005.

[173] S. K. Ghosh, T. K. Roy, M. A. H. Pramanik, and M. A. Mahmud, "A nonlinear double-integral sliding mode controller design for hybrid energy storage systems and solar photovoltaic units to enhance the power management in dc microgrids," *IET Generation, Transmission & Distribution*, vol. 16, no. 11, pp. 2228–2241, 2022.

[174] S. K. Ghosh, T. K. Roy, M. A. H. Pramanik, A. K. Sarkar, and M. A. Mahmud, "An energy management system-based control strategy for dc microgrids with dual energy storage systems," *Energies*, vol. 13, no. 11, p. 2992, 2020.

[175] M. F. Zia, E. Elbouchikhi, and M. Benbouzid, "Microgrids energy management systems: A critical review on methods, solutions, and prospects," *Applied energy*, vol. 222, pp. 1033–1055, 2018.

[176] L. Olatomiwa, S. Mekhilef, M. S. Ismail, and M. Moghavvemi, "Energy management strategies in hybrid renewable energy systems: A review," *Renewable and Sustainable Energy Reviews*, vol. 62, pp. 821–835, 2016.

[177] W. Jinhua and B. Yanyan, "An optimal adaptive under frequency load shedding using artificial neural networks," in *2022 IEEE International Conference on Electrical Engineering, Big Data and Algorithms (EEBDA)*. IEEE, 2022, pp. 249–253.

[178] S. Sarwar, H. Mokhlis, M. Othman, M. A. Muhammad, J. Laghari, N. N. Mansor, H. Mohamad, and A. Pourdaryaei, "A mixed integer linear programming based load shedding technique for improving the sustainability of islanded distribution systems," *Sustainability*, vol. 12, no. 15, p. 6234, 2020.

[179] M. Javadi and T. Amraee, "Mixed integer linear formulation for undervoltage load shedding to provide voltage stability," *IET Generation, Transmission & Distribution*, vol. 12, no. 9, pp. 2095–2104, 2018.

[180] L. Weimann, P. Gabrielli, A. Boldrini, G. J. Kramer, and M. Gazzani, "On the role of h2 storage and conversion for wind power production in the netherlands," in *Computer Aided Chemical Engineering*. Elsevier, 2019, vol. 46, pp. 1627–1632.

[181] P. Pourghasem, H. Seyedi, and K. Zare, "A new optimal under-voltage load shedding scheme for voltage collapse prevention in a multi-microgrid system," *Electric Power Systems Research*, vol. 203, p. 107629, 2022.

[182] C. A. Floudas and X. Lin, "Mixed integer linear programming in process scheduling: Modeling, algorithms, and applications," *Annals of Operations Research*, vol. 139, pp. 131–162, 2005.

[183] G. S. Thirunavukkarasu, M. Seyedmahmoudian, E. Jamei, B. Horan, S. Mekhilef, and A. Stojcevski, "Role of optimization techniques in microgrid energy management systems—a review," *Energy Strategy Reviews*, vol. 43, p. 100899, 2022.

Appendix A

Microgrid modelling Parameters

A.1 Underground Cable Parameters

Table A.1: Underground Cable Parameters Per-Unit Length

Type	**1**	**2**	**3**	**4**
Size	**1000 kcmil**	**250 kcmil**	**1 AWG**	**6 AWG**
R(mohm/m)	**0.075**	**0.232**	**0.599**	**1.701**
L(µH/m)	**0.118**	**0.181**	**0.262**	**0.366**
C (nF/m)	**0.402**	**0.216**	**0.152**	**0.120**

A.2 Cable and Lengths and Types

Table A.2: Cable and Lengths and Types

Node A	Node B	Length (m)	Type
701	702	292.6	1
702	705	121.9	1
702	713	109.7	1
702	703	402.3	1
703	727	73.2	4
703	730	182.9	1
704	714	24.4	4
704	720	243.8	1
705	742	97.5	4
705	712	73.2	2
706	725	85.2	4
707	724	231.4	4
707	722	36.6	2
708	733	97.5	2
708	732	97.5	4
709	731	182.9	4
709	708	97.5	2
710	735	61	4
710	736	390.1	4
711	741	121.9	4
711	740	61	4
713	704	158.5	1
714	718	158.5	4
720	707	280.4	1
720	706	182.9	4
727	744	85.3	4
730	709	61	1
733	734	170.7	2
734	737	195.1	2
734	710	158.5	3
737	738	122	3
738	711	122	3
744	728	61	4
744	729	85.3	4
775	709	0	XFM-1

A.3 Underground Cable Dimension

Table A.3: Underground Cable Dimension

Type	Size	Dimensions					
		r1	r2	r3	r4	r5	r6
1	1000 kcmil	12.7	14.99	18.1	19.62	24.08	25.54
2	250 kcmil	6.35	8.64	10.64	12.20	15.70	17.0
3	1 AWG	3.67	5.70	7.21	8.35	11.40	12.65
4	6 AWG	2.06	3.60	5.0	5.75	8.8	10.05

A.4 Parameters of the DC Microgrids

Table A.4: Parameters of the DC Microgrids

GTC	$S_Transformer$ = 1 MVA	Transformer: 0.75 kV/4.8 kV
	SGTC = 1 MVA	C_{dc} = 20 mF
	V_{rated} =750 VDC	F_{sw} = 2.7 kHz
WT	P_{WT} = 1 MW	V_{rated} = 690 V
	S_{PMSG} = 1.1 MVA	C_{dc} = 20 mF
	b = 377 rad/s	frated = 60 Hz
	Rs = 0.017 pu	Xl = 0.064 pu
	Rkd = 0.055 pu	Xq = 1.1 pu
	Xkd = 0.62 pu	Rkq = 0.183 pu
	Hg = 0.62 s	Xkq = 1.175 pu
	Cp-nom = 0.48 pu	Cdc = 20 mF
PV	P_{PV} = 5 x 0.1 MW	Max Irradiation= 1000 w/{m}2
	V_{OC} = 950.5 V	I_{SC} = 714 A
	C_{dc} = 10 mF	F_{sw}= 2.7 kHz
	T = 25 C	n = 1.42
	k = 1.38 *10-23 J/K	q =1.6*10-19 C
	Cells Ns = 72	Modules Ns = 21
	Cells Np = 1	Modules Np = 70
	Cin = 300 µF	Lin = 1 mH
BESS	P_{BESS} = 2×0.5 MW	V_{rated} = 700 V
	Capacity = 580Ah	C_{dc}= 10 mf
Load	Total Load	P_{load} = 1308 kW
	Non-Critical	P_{NCLoad} = 553 kW
	Critical	P_{cLoad} = 750 kW
	Constant Power	PCPL = 758.5 kW
	Constant Current	PCCL = 254 kW
	Constant Resistance	PCRL = 216 kW

A.5 DC Microgrid Load Data

Table A.5: DC Microgrid Load Data

Node	Type	Power (kW)
701	Constant Power	315
712	Constant Power	42
713	Constant Power	42
714	Constant Current	19
718	Constant Resistance	42
720	Constant Power	42
722	Constant Current	80
724	Constant Resistance	21
725	Constant Power	21
727	Constant Power	21
728	Constant Power	63
729	Constant Current	21
730	Constant Resistance	42
731	Constant Resistance	42
732	Constant Power	21
733	Constant Current	42
734	Constant Power	21
735	Constant Power	42
736	Constant Resistance	21
737	Constant Current	70
738	Constant Power	63
740	Constant Power	42
741	Constant Current	21
742	Constant Resistance	46.5
744	Constant Power	21

Appendix B

Load Shedding Simulations

B.1 State Flow Presentation of Conventional Load Shedding Schemes

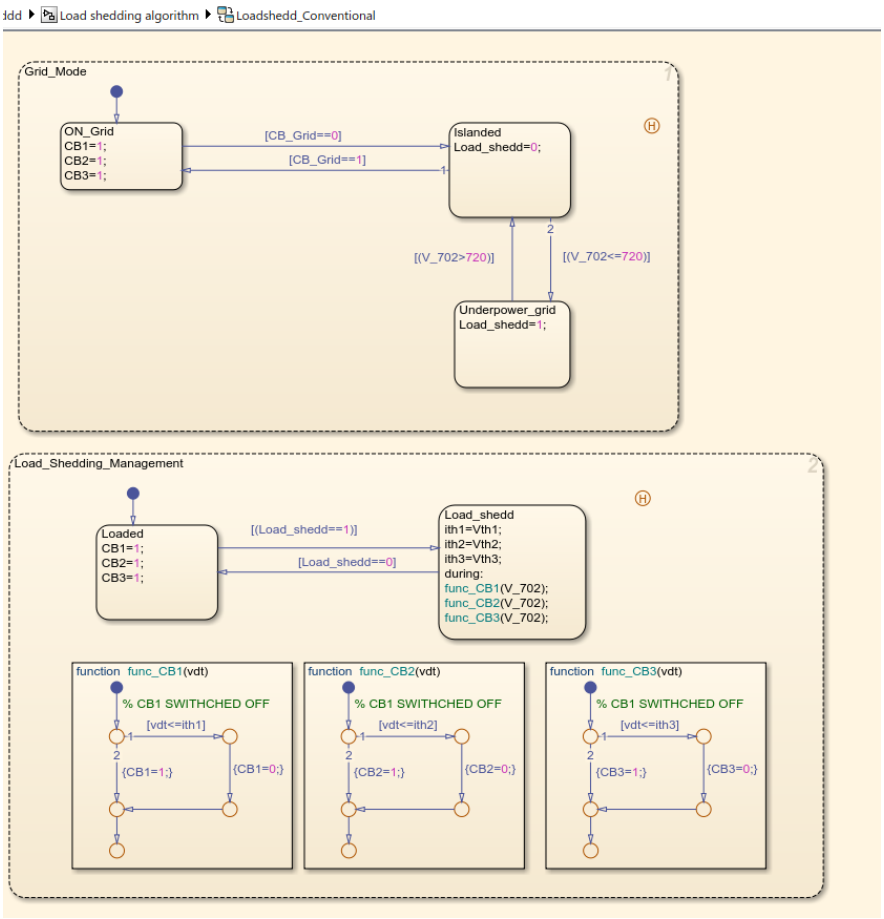

Figure B.1: State Flow Presentation of Conventional Load Shedding Schemes

B.2 State Flow Presentation of Adaptive Load shedding Schemes

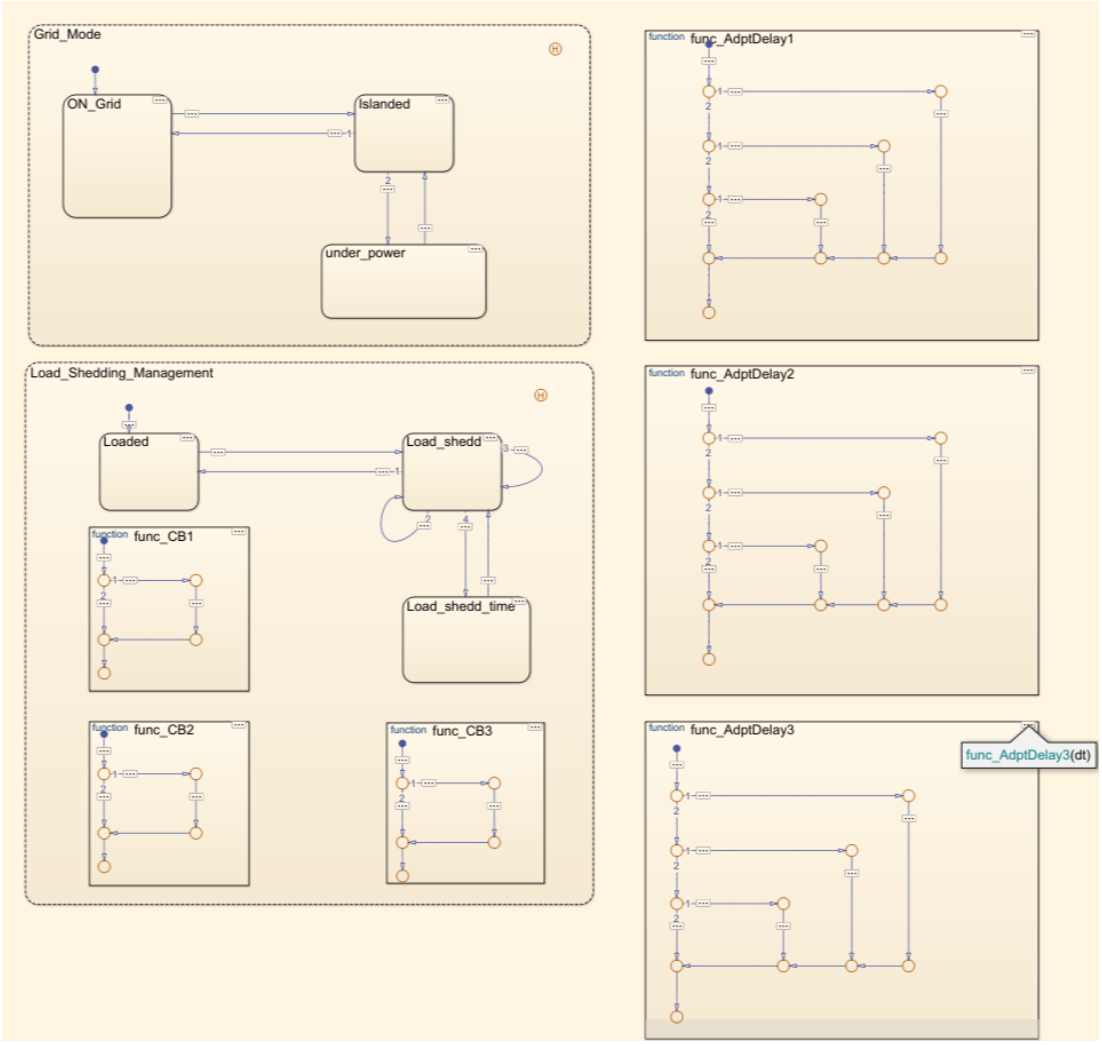

Figure B.2: State Flow Presentation of Adaptive Load shedding Schemes

B.3 GTC Model of IEEE 37 node converted to DC

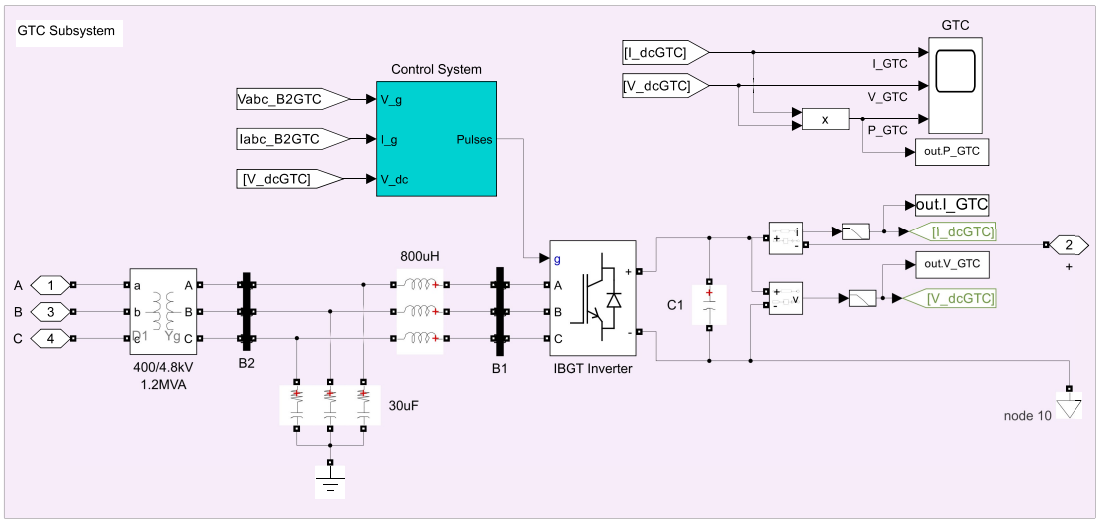

Figure B.3: GTC Model of IEEE 37 node converted to DC

B.4 PV Model of IEEE 37 node converted to DC

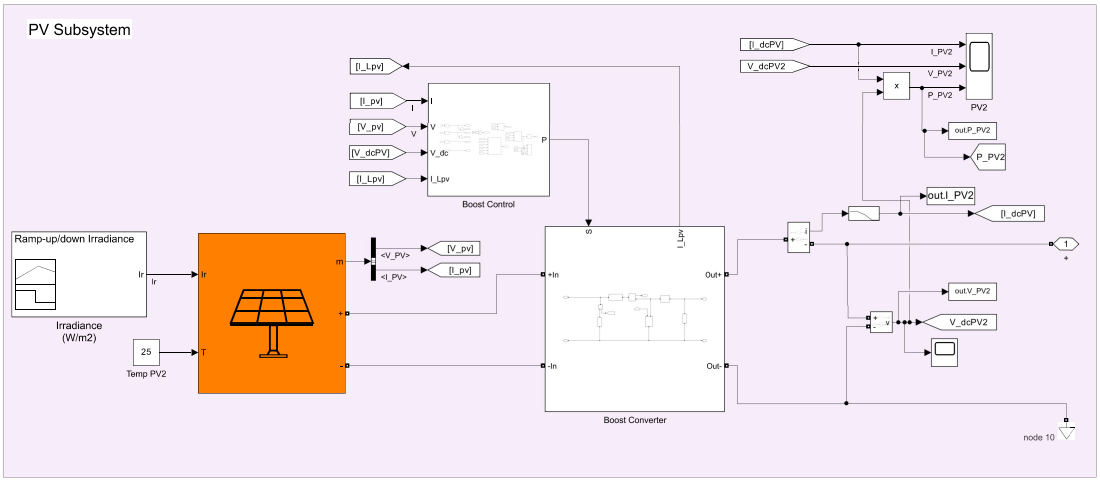

Figure B.4: PV Model of IEEE 37 node converted to DC

B.5 Wind Turbine Model of IEEE 37 node converted to DC

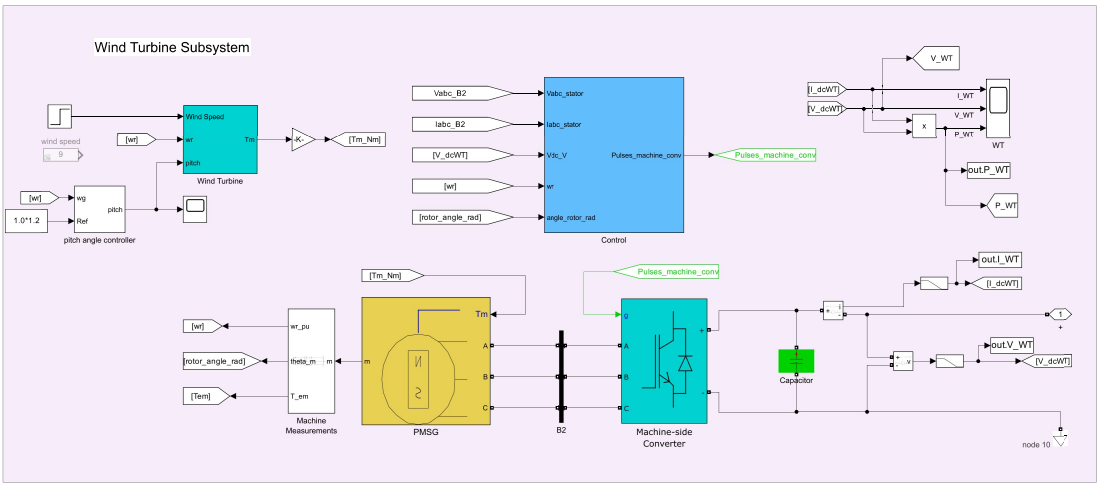

Figure B.5: Wind Turbine Model of IEEE 37 node converted to DC

B.6 BESS Model of IEEE 37 node converted to DC

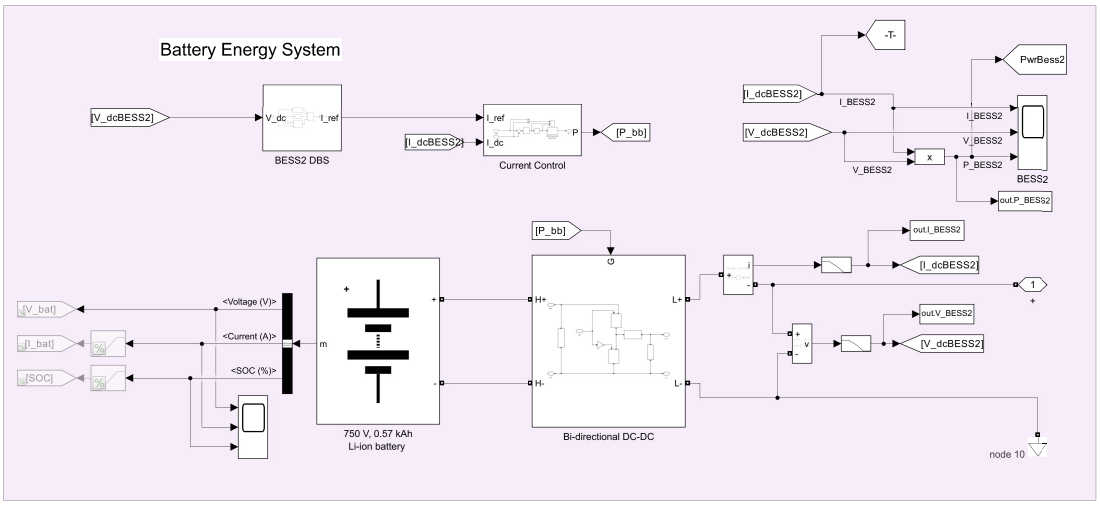

Figure B.6: BESS Model of IEEE 37 node converted to DC

B.7 Complete Model of IEEE 37 node converted to DC

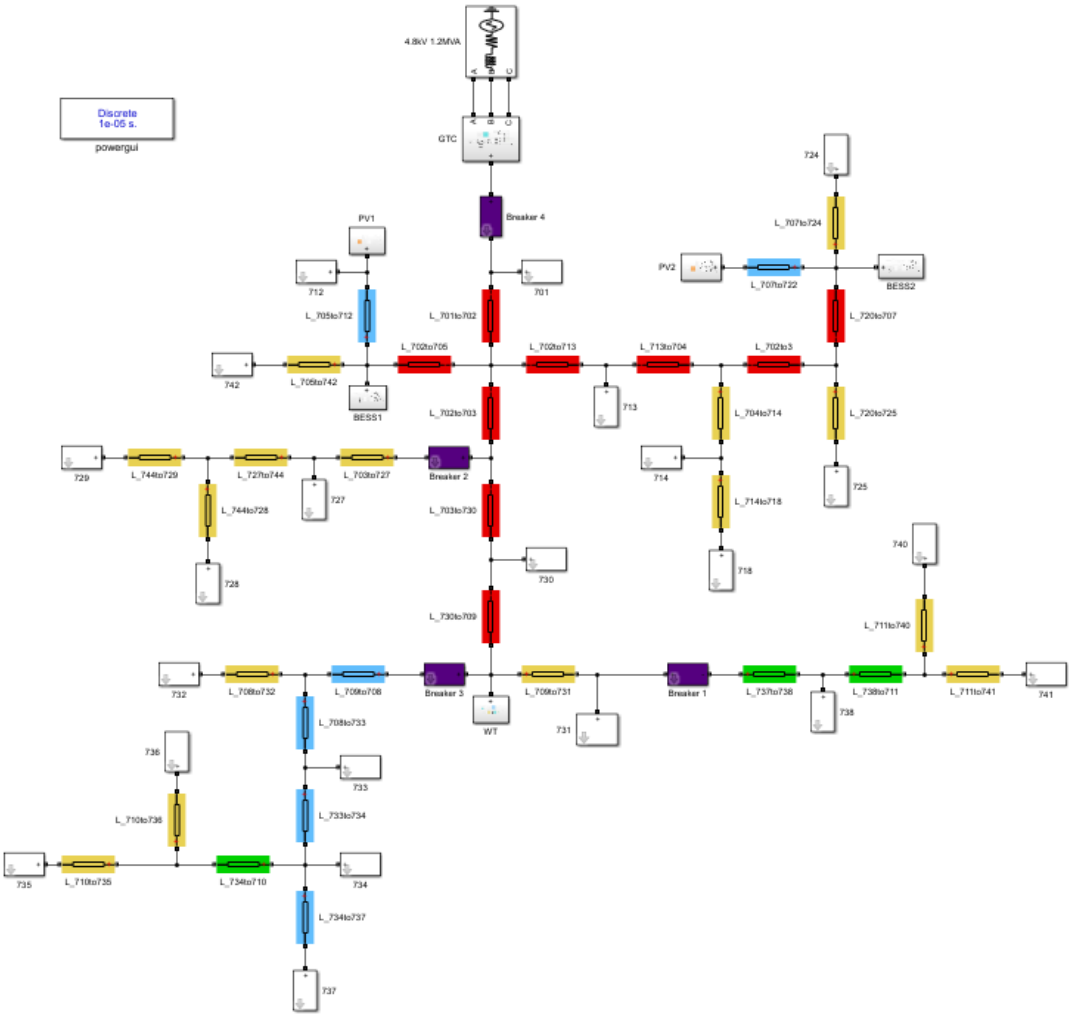

Figure B.7: Complete Model of IEEE 37 node converted to DC